ANALYTICAL STUDIES ON THE MECHANISM OF FIBRIN FORMATION

Carri Brodnax Geer

A dissertation submitted to the faculty of the University of North Carolina at Chapel Hill in partial fulfillment of the requirements for the degree of Doctor of Philosophy in the Department of Chemistry with Emphasis in Biophysics

Chapel Hill
2007

Approved By:

Dr. Susan T. Lord

Dr. Mark H. Schoenfisch

Dr. Roy R. Hantgan

Dr. James W. Jorgenson

Dr. Mark M. Wightman

ABSTRACT

Carri Brodnax Geer: Analytical Studies on the Mechanism of Fibrin Formation
(Under the direction of Dr. Susan Lord and Dr. Mark Schoenfisch)

Fibrinogen plays a crucial role in hemostasis, the regulation and maintenance of blood flow, and mediates surface-induced thrombosis at blood-contacting materials (e.g., implantable medical devices). Fibrinogen binds platelets and polymerizes to form fibrin, the structural scaffold of blood clots. The mechanisms by which fibrin formation is influenced by the surface properties of a material or therapeutic agents used to prevent platelet aggregation (e.g., *S*-nitrosothiols) are unclear. In addition, the exact mechanism of fibrin formation in solution remains controversial. Herein, the mechanism of fibrin formation in solution and at surfaces was investigated using surface-based analytical methods (surface plasmon resonance and atomic force microscopy). Additionally, the influence of *S*-nitrosoglutathione (a potent anti-platelet therapeutic) and its decomposition products on the mechanism of fibrin formation were examined by turbidity measurements.

The affinities of two fibrin fragments (desA-NDSK and desAB-NDSK) binding to fibrinogen were compared by SPR. The affinities of desA- and desAB-NDSK (5.8 ± 1.1 and 3.7 ± 0.7 μM, respectively) were not statistically different from one another. Peptide inhibition studies showed "B-b" interactions occurred between desAB-NDSK but not desA-NDSK and fibrinogen, indicating "B-b" interactions may occur simultaneously to "A-a" interactions and between the same to interacting molecules. An atomic force microscopy

method was developed to study the ruptures that occur upon the forced dissociation of desA-NDSK and desAB-NDSK from fibrinogen. The protein immobilization strategy and data collection procedures were varied to minimize multiple interactions and non-specific forces. Unlike the SPR experiments, "B-b" interactions were not detected in the forced dissociation of desAB-NDSK from fibrinogen.

The influence of *S*-nitrosoglutathione on the mechanism of fibrin formation was studied using turbidity measurements. *S*-nitrosogluathione (GSNO) and its decomposition products (reduced and oxidized glutathione, GSH and GSSG, respectively) each inhibited fibrin formation as evidenced by longer lag times, lower V_{max} values and lower final optical densities. GSH, GSSG and GSNO have numerous roles in physiology. However, the work presented herein is the first report of the inhibition of fibrin formation by GSH and GSSG.

Lastly, the role of surface properties on the mechanism of fibrin formation at surfaces was studied by SPR. Fibrinogen was adsorbed to a hydrophobic and negatively charged surface and the availability of fibrinopeptide A (FpA), a critical site for thrombin activation, were measured by antibody binding. Approximately 3 times more FpA was measured on fibrinogen adsorbed at the hydrophobic surface compared to the negatively charged surface, indicating surface properties strongly influence the availability of FpA on adsorbed fibrinogen. By better understanding the mechanism of fibrin formation in solution and at surfaces, researchers may be able design materials or therapies to improve the standard of care in hemostatic disorders and improve the blood-compatibility of currently available medical devices.

TABLE OF CONTENTS

LIST OF TABLES

LIST OF ABBREVIATIONS

~	approximately
^{o}C	degree(s) Celsius
%	percentage(s)
±	statistical margin of error
[...]	concentration
ε	extinction coefficient
µL	microliter(s)
µm	micrometer(s)
µmol	micromoles
µM	micromolar
AFM	atomic force microscope
AHRPY	alanine-histidine-arginine-proline-tyrosine amide
aq	aqueous
BSA	bovine serum albumin
Ca^{2+}	calcium ion
$CaCl_2$	calcium chloride
CNBr	cyanogen bromide
d	day(s)
e.g.	for example
ELISA	enzyme-linked immunosorbent assay
et al.	and others

etc.	and so forth
Fgn	fibrinogen
Fn	fibrin
FpA	Fibrinopeptide A
FpB	Fibrinopeptide B
g	gram(s)
GHRP	glycine-histidine-arginine-proline amide
GPRP	glycine-proline-arginine-proline amide
GSH	reduced glutathione
GSNO	*S*-nitroso-gluathione
GSSG	oxidized glutathione
GSX	glutathione derivatives
h	hour
HBSC	20 mM Hepes, 150 mM NaCl, 1 mM $CaCl_2$, pH 7.4
Hepes	(4-(2-hydroxyethyl)-1-piperazineethanesulfonic acid
HPLC-MS	high performance liquid chromatography-mass spectrometry
i.e.	that is
IgG	immunoglobulin G
kDa	kilodalton
mg	milligram
min	minute
mL	milliliter
mm	millimeter

mM	millimolar
NaCl	sodium chloride
NDSK	N-terminal disulfide knot
NO	nitric oxide
PAGE	polyacrylamide gel electrophoresis
pH	-log of proton concentration
pN	piconewton
nm	nanometer
NO	nitric oxide
QCM	quartz crystal microbalance
rpm	rotations per minute
RU	resonance units
s	second
S-	sulfur bound
SEM	scanning electron microscope
SPR	surface plasmon resonance
SDS	sodium dodecyl sulfate
SAM	self-assembled monolayer
U	unit of enzyme activity
UV	ultraviolet
Vh	volt•hour
Vis	visible
v:v	volume to volume ratio

LIST OF FIGURES

CHAPTER 1

INTRODUCTION

1.1 Physiological Significance of Fibrinogen

Synthesized predominantly in the liver, fibrinogen is a plasma protein present in blood at a concentration of approximately 2.5 mg/mL (1). Fibrinogen's primary role is in hemostasis, the regulation and maintenance of blood flow. During a vascular injury or bleeding event, fibrinogen bridges activated platelets to help form the initial platelet plug to stem the flow of blood (2, 3). Subsequently, the enzyme thrombin converts fibrinogen to fibrin polymer, the structural scaffolding of the blood clot that stabilizes the initial platelet plug to prevent further bleeding. Fibrin also localizes cells and proteins critical to wound healing and inflammation to the site of injury to promote vessel repair and regrowth. For example, fibrinogen and fibrin contain binding sites for fibroblast growth factor-2 and vascular endothelial growth factor, two proteins critical to wound healing and angiogenesis, respectively (4, 5). In addition to hemostasis, wound healing, and inflammation, fibrinogen has been shown to be an important indicator of cardiovascular health. Elevated fibrinogen levels in the blood may serve as a predicative marker for cardiovascular disease and/or stroke (6, 7).

Fibrinogen is also of great interest to the biomaterials community. Plasma protein adsorption is the first event to occur when blood contacts a surface. Research has shown the nature of the adsorbed protein layer dictates the body's subsequent response to the foreign

material (8-11). For example, albumin and immunoglobulin G (IgG) are present at much higher concentrations in plasma than fibrinogen, and thus among the first proteins to interact with the surface of a blood-contacting material. Because fibrinogen has a much higher affinity for surfaces, it quickly displaces albumin and IgG through a competitive adsorption process known as the Vroman effect (12, 13). Over the time scale of seconds to minutes, fibrinogen becomes the predominant protein at the surface. Eventually fibrinogen is displaced by high molecular weight kininogen at extended periods (e.g., minutes to hours) (13, 14). Regardless, fibrinogen is present at the surface at high concentrations during the time of surface-induced thrombosis and the initial stages of wound healing and inflammation. Each of these three processes have been shown to ultimately determine the biocompatibility of a blood-contacting material (8-10). Due to its importance in multiple critical biological functions, a deeper understanding of fibrinogen-surface interactions and fibrinogen's function at surfaces may lead to the design of more biocompatible materials.

1.2 Fibrinogen Structure

As with most large proteins, fibrinogen's structure and function are complex. A detailed schematic of fibrinogen's structure is shown in Figure 1.1. This 340 kDa hexameric glycoprotein is composed of two copies each of three polypeptide chains: Aα (610 amino acids), Bβ (461 amino acids) and γ (411 amino acids) and contains 29 disulfide bonds (15-19). The N-termini of all 6 chains are held together by 11 disulfide bonds in the center of the molecule, the E region. All three chains extend outward from the E region via a coiled-coil segment that terminates in a second, structurally important region of the molecule, the D region. The two distally located D regions are comprised of the C-termini of the Bβ and γ

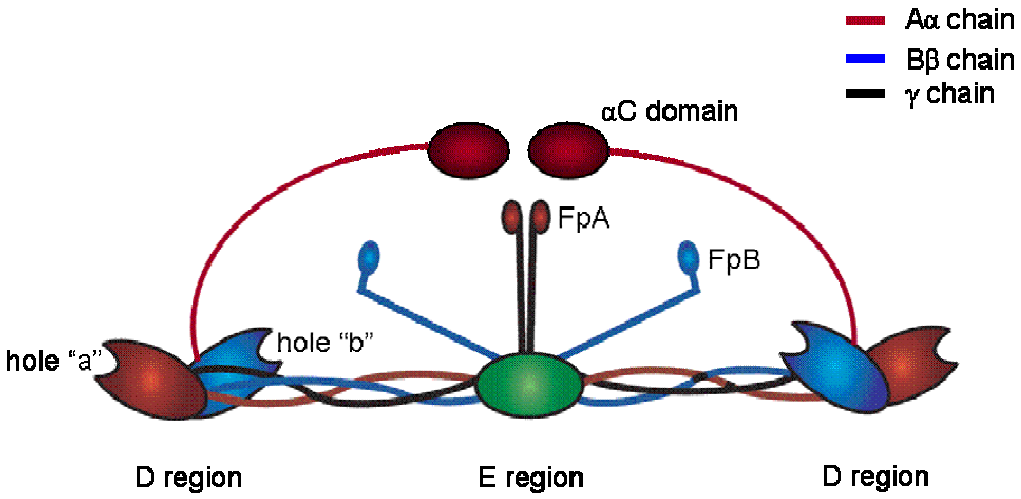

Figure 1.1 Schematic of fibrinogen.

chains that fold into two smaller structures, the βC and γC modules, respectively. The γC and βC module each contain a binding pocket critical to polymerization, hole "a" and "b", respectively. The C-termini of the α chains extend outward from the coiled-coils and terminate in small, globular structures, the αC regions. The two αC regions interact with each other and the N-termini of the Aα and Bβ chains in the E region (20). In addition to its role in fibrin formation and platelet aggregation, fibrinogen interacts with a host of other proteins and cells. For example, both fibrinogen and fibrin recruit neutrophils, monocytes and fibroblasts to the site of injury, localizing important cells to promote inflammation and wound healing (21). Fibrin(ogen)'s presence at the site of injury has also been exploited by *Staphylococcus aureus*, a deadly bacterial pathogen. *S. aureus* expresses fibrin(ogen)-specific receptors on its cell surface that help to localize the bacteria at the site of injury and facilitate infection (22, 23). Other proteins, such as albumin, von Willebrand factor and fibronectin have been shown to interact with fibrin(ogen), illustrating the wide-range of species that can interact with a single plasma protein (15).

1.3 Formation of Fibrin

1.3.1 The coagulation cascade. Fibrin formation *in vivo* is the result of a complex series of interactions collectively known as the coagulation cascade that are localized at specific cell surfaces (Fig. 1.2) (2, 3). Vascular injury interrupts the endothelium, the layer of cells lining blood vessel walls, to expose tissue factor-bearing cells such as fibroblasts to blood. The initial phase of coagulation occurs on the surface of the tissue factor-bearing cells. Circulating inactivated coagulation factor VII becomes activated and associates with membrane-bound tissue factor. The VIIa/tissue factor complex converts factor IX and X to

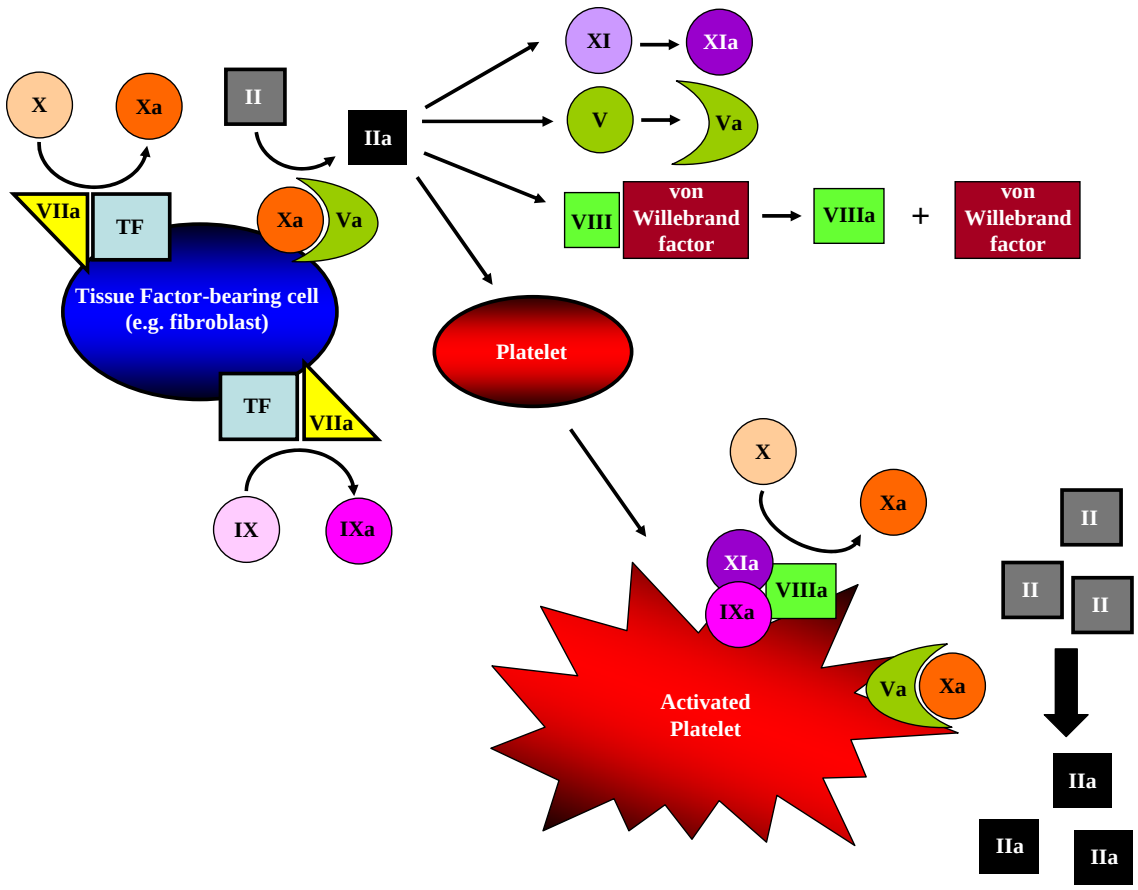

Figure 1.2 Schematic of the cell-based model of hemostasis adapted from (3).

IXa and Xa, respectively. Factor Xa in turn associates with Va on the cell surface. The Xa/Va complex converts a small amount of factor II (prothrombin) to IIa (active thrombin). The generation of the small, initial amount of thrombin at the surface of the tissue factor-bearing cells is responsible for the activation of additional coagulation factors such as XI, V and the VIII/von Willebrand factor complex. More importantly, initial thrombin generation serves to activate circulating platelets. The activated platelets aggregate to form a platelet plug that slows/stops the flow of blood at the wound. Once activated platelets are localized at the site of injury, large-scale thrombin generation occurs at the platelet surface. Factor IXa associates with VIIIa on the surface of the activated platelet to generate additional Xa. The same Xa/Va complex that forms on the surface of the tissue factor-bearing cell also forms on the surface of the platelet (Fig. 1.2). The coagulation cascade culminates in the generation of large amounts of thrombin on the surface of activated platelets. The large-scale thrombin generation is responsible for the conversion of soluble circulating fibrinogen into insoluble fibrin polymer shown in Figure 1.3.

1.3.2 Thrombin-catalyzed conversion of fibrinogen to fibrin. Thrombin is a 39 kDa serine protease that cleaves a peptide bond between arginine and glycine within fibrinogen (24, 25). Thrombin has a positively charged region on its surface that binds specific negatively charged regions of fibrinogen. The thrombin binding sites on fibrinogen are remote to the cleavage sites (26-28). Thrombin binding to fibrinogen properly aligns the polypeptide chain, allowing for efficient enzymatic cleavage. In the generally accepted mechanism of

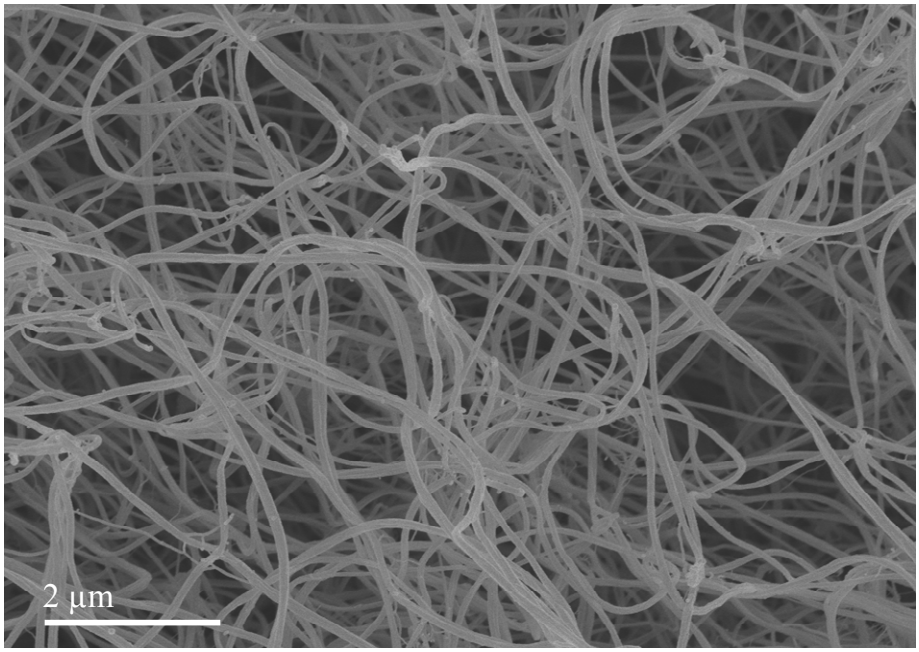

Figure 1.3 Scanning electron micrograph of insoluble fibrin polymer illustrating the mesh-like structure of the fibrin network.

fibrin formation (Fig. 1.4), thrombin first cleaves fibrinopeptide A (FpA), the first 16 amino acids of fibrinogen's Aα chain (29). Removal of FpA exposes Gly-Pro-Arg, the "A" knob, as the new N-terminal sequence of α chain (30). After FpA removal, the activated fibrinogen is referred to as desAA-fibrin monomer. The desAA-fibrin monomers spontaneously align to form half-staggered, double-stranded protofibrils held together by "A-a" knob-hole interactions between the "A" knobs and holes "a" located in the D regions of fibrinogen (Fig. 1.4) (31). Next, thrombin cleaves fibrinopeptide B (FpB), the first 14 amino acids of the Bβ chain. Removal of FpB occurs from the desAA-fibrin monomers within the protofibril structures, to expose Gly-His-Arg-Pro, termed the "B" knob, as the new sequence of the β chain. Analogous to "A-a" interactions, "B-b" interactions occur when the "B" knobs interact with holes "b" (Fig. 1.4). After FpB removal the protofibrils laterally aggregate and branch to form a dense fibrin network (30, 32).

While the importance of "A-a" interactions is well-understood, the role of "B-b" knob-hole interactions is surrounded by controversy. Many researchers believe "B-b" interactions are responsible for the lateral aggregation of protofibrils to form fibers. Studies have demonstrated that lateral aggregation is enhanced by FpB release, suggesting "B-b" interactions contribute to the lateral aggregation of protofibrils (33). Alternatively, clots can be formed in the absence of "B-b" interactions altogether. For example, certain snake venom enzymes cleave only FpA, and thereby no "B-b" interactions are possible(30). To further obscure the role of "B-b" interactions in fibrin formation, studies have shown clots can form when "B-b" interactions are the principle knob-hole interaction (34, 35). However, clots formed from "B-b" interactions were only observed at temperatures below physiological conditions (e.g., 15 ºC) and "A-a" interactions were not excluded entirely (36-41).

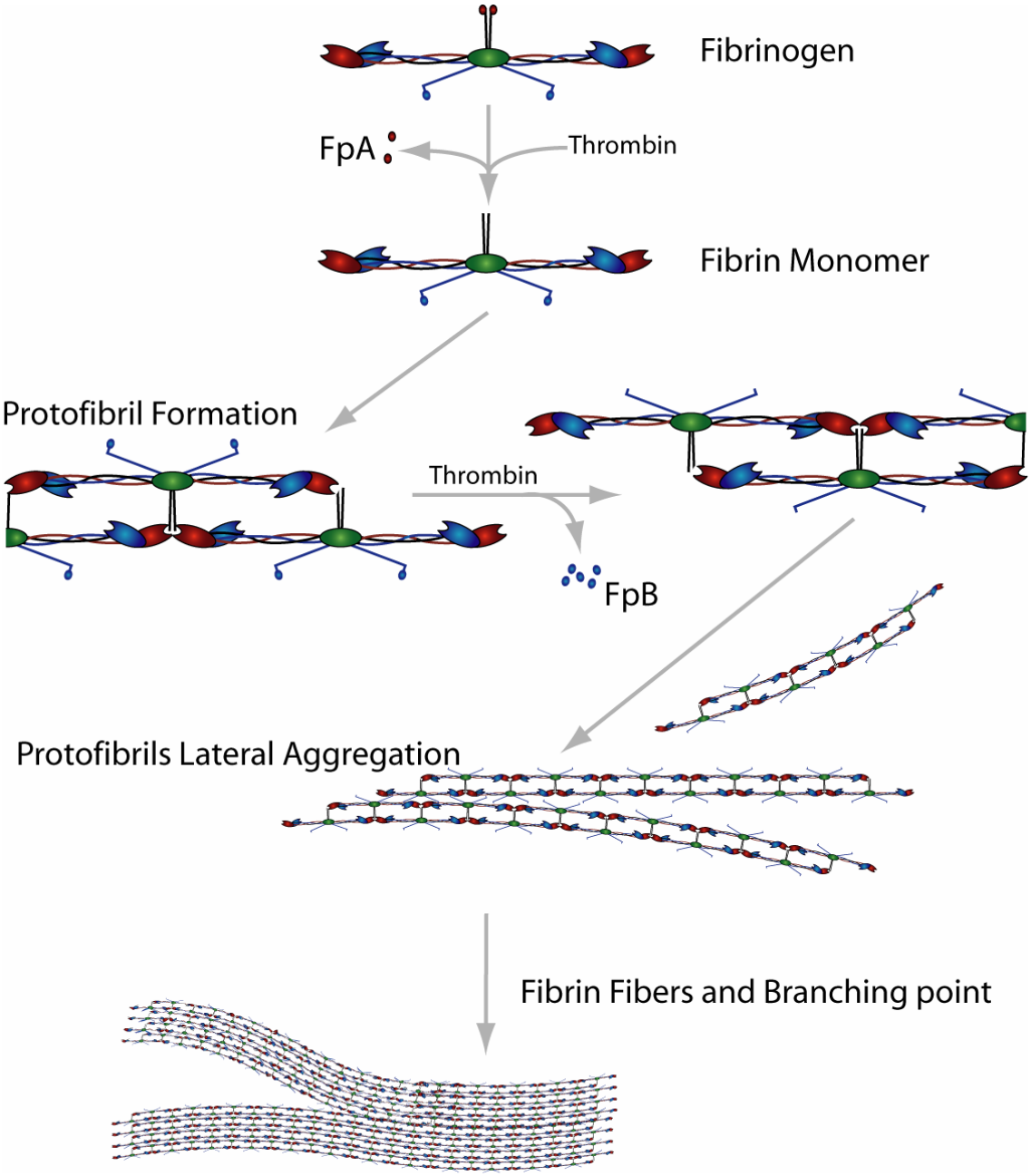

Figure 1.4 Proposed mechanism of thrombin-catalyzed fibrin formation.

1.3.3 Factors that influence fibrin formation. As discussed in Section 1.1, many proteins and cells interact with fibrinogen and fibrin during thrombosis, inflammation and wound-healing. Other parameters such as pH, chloride and calcium ion concentration, reducing agents and temperature may also affect the conversion of fibrinogen to fibrin (15, 18, 42). For example, calcium stabilizes fibrinogen's structure, accelerates fibrin formation and can partially protect fibrinogen from reduction and/or degradation (42-45). Some agents interact with fibrinogen directly to alter its function (e.g., pH, calcium and reducing agents), while others may interfere with fibrinogen and platelet activation to influence fibrin formation (25, 41, 46). For example, aspirin has been shown to inhibit platelet aggregation and acetylate lysine residues in fibrinogen leading to an altered, more permeable clot structure (46).

Endogenous and exogenous *S*-nitrosothiols (e.g., *S*-nitrosogluathione and *S*-nitrosopenacillamine) have emerged as a class of compounds with potent antiplatelet properties (47-49). *S*-nitrosothiols or RSNOs are considered nitric oxide (NO) donors because they readily transfer NO directly via transnitrosation reactions or decomposition to evolve NO, producing the thiol, thiyl radical or the disulfide (47-49). The reactive by-products of NO may interact with proteins via nitrosation of tyrosine or cyseine residues, leading to potential structural and/or functional alterations. *S*-nitrosoglutathione, an endogenous *S*-nitrosothiol, inhibits platelet aggregation and activation via two mechanisms, the transnitrosation of thiol residues in critical membrane proteins and the disruption of intracellular signaling via direct release of nitric oxide (36-41). Despite the abundance of research investigating the effects of *S*-nitrosothiols on platelets and numerous proteins, only one study to date has examined the effect of the *S*-nitrosothiols on fibrin formation, the physiological product of platelet aggregation/activation. Mutus and coworkers found both

endogenous and exogenous *S*-nitrosothiols, *S*-nitrosoglutathione and *S*-nitrosopenacillamine, respectively inhibit the initial rate of fibrin formation (50). Of note, reports on the effects of *S*-nitrosothiols and their decomposition products (e.g., *S*-nitrosoglutathione, oxidized and reduced glutathione) on the entire process of fibrin formation do not exist. In addition to its relevance as a decomposition product of *S*-nitrosoglutathione, glutathione is present in plasma at ~500 μM and may play a role in platelet function and/or fibrin formation (51). Glutathione and its disulfide are primarily responsible for maintaining the oxidative balance inside cells and blood (52). For example, glutathione levels change in patients with oxidative stress induced by cancer or smoking (53, 54). Given the dual importance of glutathione as a decomposition product of *S*-nitrosogluathione therapies for thrombosis and its presence in plasma as a reducing agent, understanding the effects of glutathione on fibrin formation may provide new and crucial insight into the role nitrosothiols and thiols in physiology.

1.4 Fibrin Formation at Surfaces

1.4.1 Surface-Induced Thrombosis. A consequence of poor biocompatibility is surface induced thrombosis, or the undesirable formation of a fibrin clot at the blood/material interface. Clots formed at the blood/material interface may occlude blood flow to/past the medical device, impair proper function of the device, and/or dislodge from the surface and cause thrombotic embolism. The initial event in the surface-induced thrombosis is plasma protein adsorption, a process that mediates subsequent cellular interactions between platelets, immune and inflammatory cells and the adsorbed proteins at the surface of the material (11). Of all plasma proteins, fibrinogen is of particular importance in surface-induced thrombosis

because of its dual role in modulating platelet adhesion and fibrin polymer formation. Much research has been devoted to understanding fibrinogen's role in surface-induced thrombosis and the influence of surface properties (9, 10, 55). For example, Tang and co-workers examined biomaterial-associated inflammation and found fibrinogen adsorption was required for phagocyte-material interactions that mediated subsequent inflammation (8, 56).

1.4.2 Fibrinogen Adsorption to Surfaces. Specific adsorption characteristics of fibrinogen including surface coverage, orientation and conformation have been widely studied at numerous surfaces and are well-documented in the literature (13, 57-64). Previous work from the Schoenfisch laboratory has demonstrated equivalent amounts of fibrinogen adsorbed to model hydrophobic, positively and negatively charged self-assembled monolayers (SAMs), yet a reduced amount of fibrinogen adsorbed to the hydrophilic surface (65). Other research has focused on understanding how surface properties influence the function of adsorbed fibrinogen as it relates to platelet adhesion (14, 66-72). Fibrinogen in solution does not interact with platelets, yet fibrinogen adsorbed at a surface undergoes conformational changes to expose the platelet binding site (66, 73, 74). Platelets readily bind to adsorbed fibrinogen, leading to their activation and the initiation of the coagulation cascade. Platelet adhesion to surfaces via interactions with adsorbed fibrinogen is of particular interest to biomaterial investigators because preventing the initiation of the coagulation cascade and subsequent thrombus formation may lead to more thromboresistant materials (55, 67, 68, 71, 72). To date, no known surface has demonstrated complete resistance to protein adsorption and even as little as 1% of a fibrinogen monolayer is sufficient to lead to significant platelet interactions with the surface (75).

1.4.3. Fibrin Formation at Surfaces. While a wealth of information exists regarding fibrinogen adsorption to a variety of materials and subsequent platelet interactions with immobilized fibrinogen, comparatively little research has focused on the influence of surface properties on fibrinogen's primary function: fibrin formation. Sit and Marchant visualized differences in fibrin assembly on hydrophobic graphite versus negatively charged mica surfaces using atomic force microscopy (76). Fibrinogen was adsorbed to the substrate, treated with thrombin and imaged as activated fibrin monomers were titrated into the AFM fluid cell. At the hydrophobic surface short fibrin strands formed first, followed by the formation of longer, branched fibrin strands. The final result was the formation of a full fibrin network. However, at the negatively charged surface the fibrin monomers aggregated and fibrin network formation was not observed. The authors hypothesized that fibrin formation at the negatively charged substrate was impaired due to several possibilities. First, the electrostatic interactions of fibrin assembly were abrogated due to the overwhelming interference of the electrostatic interactions between the proteins and the negatively charged mica. For example, fibrinogen has a net negative charge due in part to the highly negatively charged fibrinopeptides. Upon thrombin's removal of the fibrinopeptides, the E region of fibrinogen becomes positively charged. Interactions between the positively charged E region and the mica could render the positively charged polymerization "knobs" unavailable to interact with the negatively charged "holes" located in D regions of fibrin(ogen) molecules. Another explanation offered for the impaired fibrin formation at negatively charged substrates was potential interference with thrombin's activity. Thrombin binds to a negatively charged region in fibrinogen via a positively charged site on its exterior (26).

Interactions between the positively charged region on thrombin and the negatively-charged mica could prevent thrombin from cleaving fibrinopeptides from fibrinogen and thereby prevent fibrin formation.

While the studies by Sit and Marchant represent the first examination of the surface-dependence of fibrin formation, subsequent work in the Schoenfisch laboratory expanded the investigation to include not only hydrophobic and negatively charged surfaces, but hydrophilic and positively charged surfaces as well. Using quartz crystal microbalance (QCM) and scanning electron microscopy, Evans-Nguyen and Schoenfisch found that surface properties influence the amount and morphology of the fibrin clots (65). The surfaces of the quartz mass sensors were modified with alkanethiol self-assembled monolayers terminating in methyl (hydrophobic), hydroxyl (hydrophilic), amine (positively charged) or carboxylate (negatively charged) groups. The crystals were exposed to fibrinogen to initiate adsorption and the mass of adsorbed fibrinogen measured for each surface. Next, thrombin was added to the fibrinogen solution to initiate clot formation and the mass of fibrin at each surface was monitored in real time.

Of note, equivalent amounts of fibrinogen adsorbed to the hydrophobic, positively and negatively charged QCM crystals, yet significantly different fibrin structures were formed at each surface after thrombin addition. Similar to the findings reported by Sit and Marchant (76), Evans-Nguyen and Schoenfisch observed a stark contrast in the morphology and amount of fibrin formed at the hydrophobic versus negatively charged surface (65). Fibrin fibers appeared dense and branched on the hydrophobic surface, and closely resembled fibrin formed in solution. Fibrin fibers formed at the negatively charged surface were sparse and thin with noticeably fewer branch points. The amount of fibrin formed at the positively

charged surface was intermediary to the fibrin at the hydrophobic and negatively charged surfaces.

Collectively, the studies by Sit and Marchant and Evans-Nguyen and Schoenfisch clearly demonstrate fibrin formation at surfaces is influenced by the underlying substrate. More specifically, charge and wettability significantly influence the amount and architecture of fibrin fibers formed at surfaces.

1.4.4 Thrombin Interactions with Adsorbed Fibrinogen. To better understand how surface properties may influence fibrin formation, Evans-Nguyen et al. examined the initial phase of fibrin formation (i.e., the interaction between thrombin and fibrinogen) (65). Fibrinogen adsorbed to model hydrophobic, hydrophilic, positively and negatively charged substrates was treated with thrombin and the amount of FpA and FpB released from the adsorbed fibrinogen was monitored using HPLC-MS. The amount and rate of FpA and FpB release correlated well with the extent of fibrin formation observed in earlier studies. The fibrinogen adsorbed at the hydrophobic and positively charged surfaces exhibited the greatest amount and rate of fibrinopeptide release, suggesting thrombin was able to interact effectively with the adsorbed fibrinogen. The hydrophilic surface showed slightly less effective fibrinopeptide release compared to the hydrophobic and positively charged surfaces. Not surprising, the amount and rate of fibrinopeptide release was significantly reduced for fibrinogen adsorbed at the negatively charged surface, indicating severe impediments to the interaction between thrombin and fibrinogen. In addition to electrostatic interferences between the positively charged regions on thrombin responsible for fibrinogen recognition, the authors hypothesized that conformational changes resulting from adsorption could

explain the surface-dependent fibrinopeptide release properties. For example, Sit and Marchant used AFM to observe that fibrinogen adsorbed on hydrophobic and positively charged substrates underwent significantly more spreading compared to fibrinogen adsorbed at a negatively charged substrate (77). Therefore, the observed surface-dependent interactions between thrombin and adsorbed fibrinogen may be the result of surface-dependent conformational changes in addition to electrostatic interferences.

1.4.5 Study of Forces Involved in Fibrin Formation. As described above, several surface-based analytical methods have proven useful for studying various phases of fibrin formation. In addition to imaging adsorbed fibrinogen and fibrin structures, the atomic force microscope (AFM) has been used to probe the mechanical properties of fibrin fibers and fibrinogen oligomers. Guthold and co-workers used the AFM tip to stretch individual fibrin fibers and found that they could be extended up to 330% of their original length, making fibrin the most extensible known biopolymer (78). Weisel and co-workers used AFM to study the stretching of fibrinogen oligomers between the AFM tip and substrate (79). The authors observed a characteristic force pattern corresponding to the unfolding of individual domains within the fibrinogen polymers and they hypothesized the forces were related to the unfolding of the coiled-coil region in fibrinogen (80).

In other work, Weisel and co-workers examined the individual forces between fibrin(ogen) and its fragments using laser tweezers. The rupture force of "A-a" and "B-b" knob-hole interactions were measured in addition to αC-αC and αC-N-terminus of the Bβ chains. By understanding the individual bonds responsible for holding two fibrin molecules together and the magnitudes of those interactions, a better understanding of the physical properties of

fibrin may be possible. However, laser tweezers technology has several limitations. For example, the optical trap controlling the modified beads has a maximum strength of 200 pN, limiting the range of detectable interactions. Also, the spatial resolution is only accurate to within several nanometers (80-84). Consequently, mechanical behaviors of molecules (e.g., unfolding or stretching) occurring on the Å to nm scale immediately preceding bond rupture are not resolved from the bond rupture itself using laser tweezers. In this regard, the AFM has superior capabilities compared to laser tweezers. The AFM can measure both the magnitude and distance of bonds being ruptured, allowing researchers to study molecular deformations occurring within individual molecules (80, 82-84).

1.5 Significance and Goals of this Work

To date, studies have shown how small molecules, surfaces and other proteins interact with fibrinogen and ultimately influence fibrin formation. However, the mechanisms by which fibrin formation is influenced by certain parameters are unclear. In addition, the exact mechanism of fibrin formation in solution remains controversial. Due to the complications associated with the phase change of soluble fibrinogen to insoluble fibrin, the literature is void on the intermediate interactions of fibrin formation under physiological conditions, such as those between fibrin monomers and fibrinogen. By further elucidating the mechanism of fibrin formation in solution and understanding how different materials influence fibrin formation, researchers may be able design materials or therapies to improve the standard of care in hemostatic disorders as well as improve currently available biomaterials. The goals of my dissertation research were thus three-fold: 1) utilize surface-based analytical methods to further the current understanding of the mechanism of fibrin formation in solution by

clarifying the role of "B-b" knob-hole interactions; 2) characterize the influence of *S*-nitrosoglutathione, reduced glutathione, and oxidized glutathione on the mechanism of fibrin formation; and, 3) investigate the mechanism by which surface properties influence fibrin formation.

The goal of Chapter 1 was to provide a brief overview of the biological significance of fibrinogen and its role in surface-induced thrombosis. Chapter 2 focused on using surface plasmon resonance to measure the affinity of knob-hole interactions and determine whether "B-b" interactions occur alongside "A-a" interactions during protofibril formation and has been published previously (85). Chapter 3 describes the development of an atomic force microscopy method to investigate the physical/mechanical properties of knob-hole interactions. In Chapter 4, the effects of *S*-nitrosoglutathione and its decomposition products on the mechanism of fibrin formation were explored. Finally, Chapter 5 examines the influence of surface properties on fibrinopeptide A accessibility and has been published previously (86).

REFERENCES

(1) Redman, C. M.; Xia, H. "Fibrinogen biosynthesis. Assembly, intracellular degradation, and association with lipid synthesis and secretion." *Ann N Y Acad Sci* 2001**,** *936*, 480-495.

(2) Hoffman, M. "A cell-based model of coagulation and the role of factor VIIa." *Blood Rev* 2003**,** *17 Suppl 1*, S1-5.

(3) Wolberg, A. S. "Thrombin generation and fibrin clot structure." *Blood Rev* 2007**,** *21*, 131-142.

(4) Sahni, A.; Francis, C. W. "Vascular endothelial growth factor binds to fibrinogen and fibrin and stimulates endothelial cell proliferation." *Blood* 2000**,** *96*, 3772-3778.

(5) Sahni, A.; Odrljin, T.; Francis, C. W. "Binding of basic fibroblast growth factor to fibrinogen and fibrin." *J Biol Chem* 1998**,** *273*, 7554-7559.

(6) Meade, T. W.; Mellows, S.; Brozovic, M.; Miller, G. J.; Chakrabarti, R. R.; North, W. R.; Haines, A. P.; Stirling, Y.; Imeson, J. D.; Thompson, S. G. "Haemostatic function and ischaemic heart disease: principal results of the Northwick Park Heart Study." *Lancet* 1986**,** *2*, 533-537.

(7) Meade, T. W.; North, W. R.; Chakrabarti, R.; Stirling, Y.; Haines, A. P.; Thompson, S. G.; Brozovie, M. "Haemostatic function and cardiovascular death: early results of a prospective study." *Lancet* 1980**,** *1*, 1050-1054.

(8) Tang, L.; Eaton, J. W. "Fibrin(ogen) mediates acute inflammatory responses to biomaterials." *J Exp Med* 1993**,** *178*, 2147-2156.

(9) Tang, L.; Hu, W.-J. "Molecular determinants of biocompatibility." *Expert Rev. Med. Devices* 2005**,** *2*, 493-500.

(10) Tang, L.; Ugarova, T. P.; Plow, E. F.; Eaton, J. W. "Molecular determinants of acute inflammatory responses to biomaterials." *J Clin Invest* 1996**,** *97*, 1329-1334.

(11) Brash, J.; Horbett, T. *Proteins at Interfaces II:fundamentals and applications*. American Chemical Society: 1995; p 1-23.

(12) Andrade, J.; Hlady, V. *Blood in contact with natural and artificial surfaces*. The New York Academy of Sciences: New York, 1987; Vol. 516, p 158-172.

(13) Jung, S.-Y.; Lim, S.-M.; Albertorio, F.; Kim, G.; Gurau, M. C.; Yang, R. D.; Holden, M. A.; Cremer, P. S. "The Vroman effect: A molecular level description of fibrinogen displacement." *J. Am. Chem. Soc.* 2003**,** *125*, 12782-12786.

(14) Horbett, T. A. "Principles underlying the role of adsorbed plasma proteins in blood interactions with foreign materials." *Cardiovascular Pathology* 1993**,** *2*, 137S-148S.

(15) Weisel, J. W. "Fibrinogen and fibrin." *Adv Protein Chem* 2005**,** *70*, 247-299.

(16) Mosesson, M.; Siebenlist, K. R.; Meh, D. A. "The structure and biological features of fibrinogen and fibrin." *Ann. N.Y. Acad. Sci.* 2001**,** *936*, 11-30.

(17) Mosesson, M. W. "Fibrinogen and fibrin polymerization and functions." *Blood Coagulation and Fibrinolysis* 1999**,** *10*, S45-S48.

(18) Henschen, A. "On the structure of functional sites in fibrinogen." *Thromb. Res.* 1983**,** *Supplement V*, 27-39.

(19) Blomback, B. "Fibrinogen: Evolution of the structure-function concept." *Ann. N.Y. Acad. Sci.* 2001**,** *936*, 1-10.

(20) Litvinov, R. I.; Yakovlev, S.; Tsurupa, G.; Gorkun, O. V.; Medved, L.; Weisel, J. W. "Direct evidence for specific interactions of the fibrinogen alphaC-domains with the central E region and with each other." *Biochemistry* 2007**,** *46*, 9133-9142.

(21) Laurens, N.; Koolwijk, P.; de Maat, M. P. "Fibrin structure and wound healing." *J Thromb Haemost* 2006**,** *4*, 932-939.

(22) Hartford, O. M.; Wann, E. R.; Hook, M.; Foster, T. J. "Identification of residues in the *Staphylococcus aureus* fibrinogen-binding MSCRAMM clumping factor A (ClfA) that are important for ligand binding." *J Biol Chem* 2001**,** *276*, 2466-2473.

(23) Hawiger, J.; Kloczewiak, M.; Timmons, S.; Strong, D.; Doolittle, R. F. "Interaction of fibrinogen with staphylococcal clumping factor and with platelets." *Ann N Y Acad Sci* 1983**,** *408*, 521-535.

(24) Lundblad, R. L.; Kingdon, H. S.; Mann, K. G. "Thrombin." *Methods in Enzymology* 1976**,** *45*, 156-176.

(25) Goldsack, N. R.; Chambers, R. C.; Dabbagh, K.; Laurent, G. J. "Thrombin." *Int J Biochem Cell Biol* 1998**,** *30*, 641-646.

(26) Pechik, I.; Madrazo, J.; Mosesson, M. W.; Hernandez, I.; Gilliland, G. L.; Medved, L. "Crystal structure of the complex between thrombin and the central "E" region of fibrin." *Proc Natl Acad Sci U S A* 2004**,** *101*, 2718-2723.

(27) Rose, T.; Cera, E. D. "Three-dimensional modeling of thrombin-fibrinogen interaction." *J. Biol. Chem.* 2002**,** *277*, 18875-18880.

(28) Binnie, C. G.; Lord, S. T. "The fibrinogen sequences that interact with thrombin." *Blood* 1993**,** *81*, 3186-3192.

(29) Blomback, B. "Fibrin formation in whole blood." *Thromb Res* 2000**,** *99*, 307-310.

(30) Weisel, J. W. "Fibrin assembly. Lateral aggregation and the role of the two pairs of fibrinopeptides." *Biophys J* 1986**,** *50*, 1079-1093.

(31) Veklich, Y.; Ang, E. K.; Lorand, L.; Weisel, J. W. "The complementary aggregation sites of fibrin investigated through examination of polymers of fibrinogen with fragment E." *Proc. Natl, Acad. Sci.* 1998**,** *95*, 1438-1442.

(32) Weisel, J. W.; Nagaswami, C. "Computer modeling of fibrin polymerization kinetics correlated with electron microscope and turbidity observations: clot structure and assembly are kinetically controlled." *Biophys J* 1992**,** *63*, 111-128.

(33) Weisel, J. W.; Veklich, Y.; Gorkun, O. "The sequence of cleavage of fibrinopeptides from fibrinogen is important for protofibril formation and enhancement of lateral aggregation in fibrin clots." *J Mol Biol* 1993**,** *232*, 285-297.

(34) Shainoff, J. R.; Dardik, B. N. "Fibrinopeptide B in fibrin assembly and metabolism: physiologic significance in delayed release of the peptide." *Ann N Y Acad Sci* 1983**,** *408*, 254-268.

(35) Mosesson, M. W.; DiOrio, J. P.; Muller, M. F.; Shainoff, J. R.; Siebenlist, K. R.; Amrani, D. L.; Homandberg, G. A.; Soria, J.; Soria, C.; Samama, M. "Studies on the ultrastructure of fibrin lacking fibrinopeptide B (beta-fibrin)." *Blood* 1987**,** *69*, 1073-1081.

(36) Bell, S. E.; Shah, C. M.; Gordge, M. P. "Protein disulfide-isomerase mediates delivery of nitric oxide redox derivatives into platelets." *Biochem J* 2007**,** *403*, 283-288.

(37) Hothersall, J. S.; Noronha-Dutra, A. A. "Nitrosothiol processing by platelets." *Methods Enzymol* 2002**,** *359*, 238-244.

(38) Gordge, M. P.; Hothersall, J. S.; Noronha-Dutra, A. A. "Evidence for a cyclic GMP-independent mechanism in the anti-platelet action of S-nitrosoglutathione." *Br J Pharmacol* 1998**,** *124*, 141-148.

(39) Simon, D. I.; Stamler, J. S.; Jaraki, O.; Keaney, J. F.; Osborne, J. A.; Francis, S. A.; Singel, D. J.; Loscalzo, J. "Antiplatelet properties of protein *S*-nitrosothiols derived

from nitric oxide and endothelium-derived relaxing factor." *Arterioscler Thromb* 1993**,** *13*, 791-799.

(40) Radomski, M. W.; Rees, D. D.; Dutra, A.; Moncada, S. "*S*-nitroso-glutathione inhibits platelet activation in vitro and in vivo." *Br J Pharmacol* 1992**,** *107*, 745-749.

(41) Mellion, B. T.; Ignarro, L. J.; Myers, C. B.; Ohlstein, E. H.; Ballot, B. A.; Hyman, A. L.; Kadowitz, P. J. "Inhibition of human platelet aggregation by *S*-nitrosothiols. Heme-dependent activation of soluble guanylate cyclase and stimulation of cyclic GMP accumulation." *Mol Pharmacol* 1983**,** *23*, 653-664.

(42) Mihalyi, E. "Clotting of bovine fibrinogen. Calcium binding to fibrin during clotting and its dependence on release of fibrinopeptide B." *Biochemistry* 1988**,** *27*, 967-976.

(43) Procyk, R.; Blomback, B. "Disulfide bond reduction in fibrinogen: calcium protection and effect on clottability." *Biochemistry* 1990**,** *29*, 1501-1507.

(44) Hardy, J. J.; Carrell, N. A.; McDonagh, J. "Calcium ion functions in fibrinogen conversion to fibrin." *Ann N Y Acad Sci* 1983**,** *408*, 279-287.

(45) Griaznukhina, E. A. "Effect of calcium, ionic strength and temperature on the enzymatic phase of fibrinogen conversion to fibrin." *Ukr Biokhim Zh* 1964**,** *36*, 898-906.

(46) Undas, A.; Brummel-Ziedins, K. E.; Mann, K. G. "Antithrombotic properties of aspirin and resistance to aspirin: beyond strictly antiplatelet actions." *Blood* 2007**,** *109*, 2285-2292.

(47) Al-Sa'doni, H. H.; Ferro, A. "*S*-nitrosothiols as nitric oxide-donors: chemistry, biology and possible future therapeutic applications." *Curr Med Chem* 2004**,** *11*, 2679-2690.

(48) Hogg, N. "Biological chemistry and clinical potential of *S*-nitrosothiols." *Free Radic Biol Med* 2000**,** *28*, 1478-1486.

(49) Williams, D. L. H. "The Chemistry of *S*-Nitrosothiols." *Acc. Chem. Res.* 1999**,** *32*, 869-876.

(50) Akhter, S.; Vignini, A.; Wen, Z.; English, A.; Wang, P. G.; Mutus, B. "Evidence for *S*-nitrosothiol-dependent changes in fibrinogen that do not involve transnitrosation or thiolation." *Proc Natl Acad Sci U S A* 2002**,** *99*, 9172-9177.

(51) Wring, S. A.; Hart, J. P.; Birch, B. J. "Determination of glutathione in human plasma using high-performance liquid chromatography with electrochemical detection with a carbon-epoxy resin composite electrode chemically modified with cobalt phthalocyanine." *Analyst* 1989**,** *114*, 1571-1573.

(52) Anderson, M. E.; Meister, A. "Dynamic state of glutathione in blood plasma." *J Biol Chem* 1980**,** *255*, 9530-9533.

(53) Dogru-Abbasoglu, S.; Mutlu-Turkoglu, U.; Turkoglu, S.; Erbil, Y.; Barbaros, U.; Uysal, M.; Aykac-Toker, G. "Glutathione S-transferase-pi in malignant tissues and plasma of human colorectal and gastric cancers." *J Cancer Res Clin Oncol* 2002**,** *128*, 91-95.

(54) Lane, J. D.; Opara, E. C.; Rose, J. E.; Behm, F. "Quitting smoking raises whole blood glutathione." *Physiol Behav* 1996**,** *60*, 1379-1381.

(55) Gorbet, M. B.; Sefton, M. V. "Biomaterial-associated thrombosis: roles of coagulation factors, complement, platelets and leukocytes." *Biomaterials* 2004**,** *25*, 5681-5703.

(56) Tang, L.; Eaton, J. W. "Inflammatory responses to biomaterials." *Am J Clin Pathol* 1995**,** *103*, 466-471.

(57) Agnihotri, A.; Christopher A, S. "Time-dependent conformational changes in fibrinogen measured by atomic force microscopy." *Langmuir* 2004**,** *20*, 8864-8852.

(58) Cacciafesta, P.; Hallam, K. R.; Watkinson, A. C.; Allen, G. C.; Miles, M. J.; Jandt, K. D. "Visualization of human plasma fibrinogen adsorped on titanium implant surfaces with different roughness." *Surf. Sci.* 2001**,** *491*, 405-420.

(59) Cacciafesta, P.; Humphris, A. D. L.; Jandt, K. D.; Miles, M. J. "Human plasma fibrinogen adsorption on ultraflat titanium oxide surfaces studied with atomic force microscopy." *Langmuir* 2000**,** *16*, 8167-8175.

(60) Dyr, J. E.; Tichy, I.; Jirouskova, M.; Tobiska, P.; Slavik, R.; Homola, J.; Brynda, E.; Houska, M.; Suttnar, J. "Molecular arrangement of adsorbed fibrinogen molecules characterized by specific monoclonal antibodies and a surface plasmon resonance sensor." *Sens, Acutators, B* 1998**,** *51*, 268-272.

(61) Hemmerle, J.; Altmann, S. M.; Maaloum, M.; Horber, J. K. H.; Heinrich, L.; Voegel, J. C.; Schaaf, P. "Direct observation of the anchoring process during the adsorption of fibrinogen on a solid surface by force-spectroscopy mode atomic force microscopy." *Proc. Natl, Acad. Sci.* 1999**,** *96*, 6705-6710.

(62) Holland, N. B.; Marchant, R. E. "Individual plasma proteins detected on rough biomaterials by phase imaging AFM." *J. Biomed. Mater. Res.* 2000**,** *51*, 307-315.

(63) Marchin, K. L.; Berrie, C. L. "Conformational changes in the plasma protein fibrinogen upon adsorption to graphite and mica investigated by atomic force microscopy." *Langmuir* 2003**,** *19*, 9883-9888.

(64) Retzinger, G. S.; Cook, B. C.; DeAnglis, A. P. "The binding of fibrinogen to surfaces and the identification of two distinct surface-bound species of the protein." *Journal of Colloid and Interface Science* 1994**,** *168*, 514-521.

(65) Evans-Nguyen, K. M.; Schoenfisch, M. H. "Fibrin proliferation at model surfaces: influence of surface properties." *Langmuir* 2005**,** *21*, 1691-1694.

(66) Cook, B. C. "Reactivity of human platelets with immobilized fibrinogen is dictated by the chemical character of the surface." *Thromb. Res.* 2001**,** *104*, 39-48.

(67) Lindon, J. N.; McManama, G.; Kushner, L.; Merrill, E. W.; Salzman, E. W. "Does the conformation of adsorbed fibrinogen dictate platelet interactions with artificial surfaces?" *Blood* 1986**,** *68*, 355-362.

(68) Rysava, J.; Dyr, J. E.; Homola, J.; Dostalek, J.; Krizova, P.; Masova, L.; Suttnar, J.; Briestensky, J.; Santar, I.; Myska, K.; Pecka, M. "Surface interactions of oxidized cellulose with fibrin(ogen) and blood platelets." *Sensors and Actuators, B: Chemical* 2003**,** *B90*, 243-249.

(69) Radomski, M. W.; Palmer, R. M. J.; Moncada, S. "The role of nitric oxide and cGMP in platelet adhesion to vascular endothelium." *Biochem. Biophys. Res. Commun.* 1987**,** *148*, 1482-1489.

(70) Shahbazi, T.; Jones, N.; Radomski, M. W.; Moro, M. A.; Gingell, D. "Nitric oxide donors inhibit platelet spreading on surfaces coated with fibrinogen but not with fibronectin." *Thrombosis Research* 1994**,** *75*, 631-642.

(71) Salzman, E. W.; Lindon, J.; McManama, G.; Ware, A. J. Role of fibrinogen in activation of platelets by artificial surfaces. In *Blood in Contact with Natural and Artificial Surfaces*, Leonard, E. F.;Turitto, V. T.;Vroman, L., Eds. The New York Academy of Sciences: New York, 1987; Vol. 516, pp 184-195.

(72) Anderson, J. M.; Kottke-Marchant, K. "Platelet interactions with biomaterials and artificial devices." *CRC Crit. Rev. Biocompat.* 1985**,** *1*, 111-204.

(73) Tomikawa, M.; Iwamoto, M.; Olsson, P.; Soederman, S.; Blombaeck, B. "On the platelet-fibrinogen interaction." *Thrombosis Research* 1980**,** *19*, 869-876.

(74) Endenburg, S. C.; Hantgan, R. R.; Sixma, J. J.; de Groot, P. G.; Zwaginga, J. J. "Platelet adhesion to fibrin(ogen)." *Blood Coagul Fibrinolysis* 1993**,** *4*, 139-142.

(75) Tsai, W. B.; Grunkemeier, J. M.; Horbett, T. A. "Human plasma fibrinogen adsorption and platelet adhesion to polystyrene." *J Biomed Mater Res* 1999**,** *44*, 130-139.

(76) Sit, P. S.; Marchant, R. E. "Surface-dependent differences in fibrin assembly visualized by atomic force microscopy." *Surf. Sci.* 2001**,** *491*, 421-432.

(77) Sit, P. S.; Marchant, R. E. "Surface-dependent conformations of human fibrinogen observed by atomic force microscopy under aqueous conditions." *Thromb. Haemostasis* 1999**,** *82*, 1053-1060.

(78) Liu, W. J., L.M.; Sparks, E.A.; Falvo, M.R.; Hantgan, R.R.; Superfine, R.; Lord, S.T.; Guthold, M. "Fibrin fibers have extraordinary extensibility and elasticity." *Science* 2006**,** *313*, 634.

(79) Brown, A. E.; Litvinov, R. I.; Discher, D. E.; Weisel, J. W. "Forced unfolding of coiled-coils in fibrinogen by single-molecule AFM." *Biophys J* 2007**,** *92*, L39-41.

(80) Fisher, T. E.; Oberhauser, A. F.; Carrion-Vazquez, M.; Marszalek, P. E.; Fernandez, J. M. "The study of protein mechanics with the atomic force microscope." *Trends in Biochemical Sciences* 1999**,** *24*, 379-384.

(81) Levy, R.; Maaloum, M. "Specific molecular interactions by force spectroscopy: From single bonds to collective properties." *Biophysical Chemistry* 2005**,** *117*, 233-237.

(82) Clausen-Schaumann, H.; Seitz, M.; Krautbauer, R.; Gaub, H. E. "Force spectroscopy with single bio-molecules." *Current Opinion in Chemical Biology* 2000**,** *4*, 524-530.

(83) Heinz, W. F.; Hoh, J. H. "Spatially resolved force spectroscopy of biological surfaces using the atomic force microscope." *Trends in Biotechnology* 1999**,** *17*, 143-150.

(84) Zlatanova, J.; Lindsay, S. M.; Leuba, S. H. "Single molecule force spectroscopy in biology using the atomic force microscope." *Progress in Biophysics and Molecular Biology* 2000**,** *74*, 37-61.

(85) Geer, C. B.; Tripathy, A.; Schoenfisch, M. H.; Lord, S. T.; Gorkun, O. V. "Role of "B-b" knob-hole interactions in fibrin binding to adsorbed fibrinogen." *J Thromb Haemost* 2007.

(86) Geer, C. B.; Rus, I. A.; Lord, S. T.; Schoenfisch, M. H. "Surface-dependent fibrinopeptide A accessibility to thrombin." *Acta Biomater* 2007**,** *3*, 663-668.

CHAPTER 2

ROLE OF "B-b" KNOB-HOLE INTERACTIONS IN FIBRIN BINDING TO ADSORBED FIBRINOGEN

2.1 Introduction

One of the most abundant proteins in blood, fibrinogen plays a pivotal role in hemostasis by sealing vessel ruptures and promoting wound healing (1). Following vessel injury, soluble fibrinogen is converted to an insoluble fibrin polymer matrix. This conversion occurs in three steps: thrombin catalysis leading to the formation of fibrin monomers; assembly of fibrin monomers into half-staggered, double-stranded protofibrils; and, assembly of multiple protofibrils into branched, thick fibers [for review see (2)]. The fibrinogen molecule consists of three pairs of non-identical polypeptide chains Aα, Bβ, and γ linked together by 29 disulfide bonds (3). Fibrinogen chains are folded into three distinct structural regions, two distal D regions linked by coiled-coil connectors to one central E region (Fig. 2.1A). Each D region contains polymerization holes "a" and "b" located in the C terminus of the γ and Bβ chains, respectively (4-6). The central E region contains two sets of "A" and "B" polymerization knobs that are hidden in fibrinogen (7). The knobs become exposed only when fibrinogen is transformed into fibrin monomer by the serine protease thrombin. Thrombin cleaves fibrinopeptides A (FpA) and B (FpB) from the N-terminus of fibrinogen's Aα and Bβ chains, respectively (8). The newly exposed polymerization knobs of one fibrin monomer interact with corresponding holes of another fibrin monomer or fibrinogen through "A-a" and "B-b" knob-hole interactions (9-12).

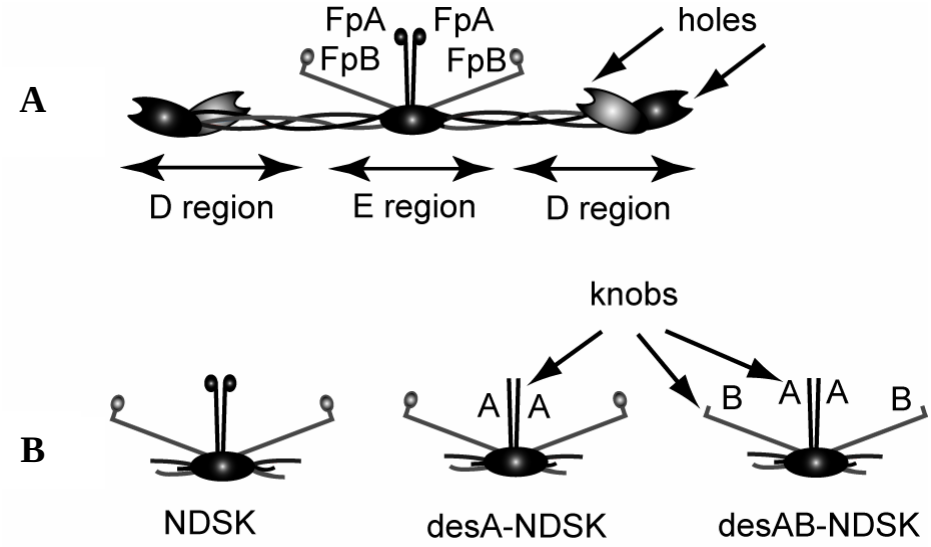

Figure 2.1 **A.** Schematic representation of fibrinogen; the E and D structural regions and polymerization holes are indicated by arrows, fibrinopeptides A and B (FpA and FpB) are depicted as spheres. **B.** Fibrin fragments without (NDSK) and with exposure of polymerization knobs A (desA-NDSK) or A and B (desAB-NDSK).

Thrombin cleaves FpA faster than FpB, so thrombin-catalyzed protofibrils are formed predominantly via “A-a” interactions (13-15). Nevertheless, studies with snake venom enzymes that remove either FpA or FpB have demonstrated that fibrin clots can be formed by either “A-a” or “B-b” interactions, indicating both interactions can mediate protofibril formation (15-20). Experiments with a variant recombinant fibrinogen showed that “B-b” interactions may play a substantial role in protofibril formation when “A-a” interactions are weakened (21). On the other hand, non-equilibrium based laser tweezers studies by Weisel and co-workers demonstrated only “A-a” interactions occur during the binding of fibrin fragments to fibrinogen molecules even when both “B” knobs and holes “b” are available (22). In similar experiments, “B-b” knob-hole interactions were apparent only when “A-a” interactions were excluded by experimental design (23). While it was shown that “B-b” interactions contribute to overall fibrin clot stability (17, 24), the question remains whether “B-b” interactions occur within protofibrils alongside “A-a” interactions or between protofibrils.

The work presented in this chapter was designed to measure the strength of “A-a” interactions under equilibrium conditions and clarify the role of “B-b” interactions. Surface plasmon resonance (SPR) was used to determine the affinity constants of individual knob-hole interactions without interference from other parts of the fibrin molecule that may contribute to polymerization, notably the αC domain and D-D interface (12, 25-27). The binding of fibrin fragments containing either “A” or “A” and “B” knobs (desA-NDSK or desAB-NDSK) was measured to the holes in fibrinogen adsorbed on a hydrophobic surface. Inhibition experiments were also performed by specifically blocking the holes “a” and/or “b”

with peptides to determine whether "B-b" interactions occur simultaneously to "A-a" interactions within the same pair of interacting molecules.

2.2 Experimental Methods

2.2.1 Materials. All reagents were of analytical grade and purchased from Sigma (St. Louis, MO) unless noted otherwise. Human plasma fibrinogen (FIB 1) and α-thrombin (HT 2970PA) were purchased from Enzyme Research Laboratories (Southbend, IN). Batroxobin (*batroxobin moojeni*) was obtained from CenterChem (Stamford, CT). Peptides GPRP amide and GHRP amide were purchased from Bachem USA (Torrance, CA) and Biopeptide Co. (San Diego, CA). Peptide AHRPY amide (28) was synthesized by the Protein Chemistry Core Facility at the University of North Carolina at Chapel Hill.

2.2.2 Fibrinogen and NDSK preparation. Fibrinogen was dialyzed against 20 mM HEPES, pH 7.4, 150 mM NaCl, 1 mM $CaCl_2$ buffer (HBSC), stored at -80 °C, thawed at 37 °C for 10 min and maintained at ambient temperature. Fibrinogen concentration was determined using an extinction coefficient of 1.51 at 280 nm for a 1 mg/mL solution (13). We prepared three different forms of NDSK fragments (Fig. 2.1B) based on described procedures (29, 30). Fibrin clots were formed by adding thrombin (1 U/ml) or batroxobin (1 BU/mL) to fibrinogen (10 mg/mL) and incubating for 24 h. The fibrin clot or fibrinogen (10 mg/ml) was dissolved in 70% formic acid and reacted with CNBr (1/1.5, w/w, protein/CNBr ratio). The reaction continued for 24 h at ambient temperature under nitrogen. Following dialysis against 5% acetic acid and 100 mM NaCl, NDSK was purified from the fibrinogen, desA-NDSK batroxobin-generated fibrin, and desAB-NDSK thrombin-generated fibrin. Each

fragment was purified by size-exclusion chromatography using two sequentially connected Superdex 200 prep grade HR16/50 columns (Pharmacia, Uppsala, Sweden), equilibrated with 5% acetic acid and 100 mM NaCl. Fragment fractions were pooled, concentrated using a 30 kDa molecular mass cutoff centrifugal filter device (Millipore, Bedford, MA), dialyzed against 20 mM HEPES, pH 7.4, 150 mM NaCl buffer (HBS) and stored at -80 °C. The fragment concentrations were determined from the absorbance at 280 nm using the theoretical extinction coefficients for 1 mg/mL solutions, 0.74 for NDSK (Mr = 59 kDa), 0.78 for desA-NDSK (Mr = 56 kDa), and 0.82 for desAB-NDSK (Mr = 53 kDa).

2.2.3 Polyacrylamide gel electrophoresis (PAGE). Native and SDS electrophoresis was performed with an automated PHAST system (Pharmacia, Uppsala, Sweden), using the same 8-25% gradient polyacrylamide gels. Native gels were run using 0.25 M Tris, 0.88 M L-alanine pH 8.8 buffer for 280 Vh. SDS gels were run using 0.20 M Tricine, 0.20 M Tris, pH 8.1, 0.55% SDS buffer system for 76 Vh. Protein bands were visualized with Coomassie R250.

2.2.4 Analytical ultracentrifugation. Sedimentation equilibrium experiments were performed using a Beckman Optima XL-I analytical ultracentrifuge with a Ti50 8-hole rotor and six-sectored centerpieces. Samples of NDSK, desA-NDSK and desAB-NDSK (three different concentrations of each fragment at 0.25, 0.50, and 0.75 ABS_{280}) were spun at 10,000 rpm or at 13,000 rpm for 18 h at 25 °C. Absorbance scans at 280 nm were recorded every 2 h. Equilibrium was assumed when the difference between two consecutive absorbance profiles became zero. The meniscus-depletion method was employed to

determine the absorbance offsets after over-speeding the samples at 25,000 rpm for 6 h. Equilibrium absorbance profiles were analyzed using Beckman XL-A/XL-I Analysis Software Version 4.0 and fit using both a single-species and a monomer-dimer model based on the Lamm equation (31). Experiments with NDSK and desA-NDSK were performed twice, and the equilibrium constants averaged. The desAB-NDSK experiment was performed once.

2.2.5 Surface plasmon resonance (SPR). SPR sensorchips were prepared in house for use with a Biacore X (Biacore, Inc., Uppsala, Sweden) instrument using glass cover slips (Electron Microscopy Sciences, Washington, PA) modified with hydrophobic self-assembled monolayers (SAMs), as described previously (32). The HBSC flow rate was a constant 10 μL/min and a continuous flow of 25 °C buffer was maintained through the instrument at all times. After reaching a stable baseline (drift < 1 response unit/min), 1 mg/mL fibrinogen in HBSC was flowed over the sensorchip surface for 600 s, the chip rinsed with HBSC for 300 s and then washed three times using the manufacturer's "wash" command over an additional 300 s. The NDSK, desA-NDSK or desAB-NDSK samples were injected over the thoroughly rinsed adsorbed fibrinogen and the association/dissociation profiles were monitored for 600 s. Notably, we used 1 mg/mL fibrinogen to generate a closely-spaced monolayer of protein, minimizing conformational changes observed with monolayers formed from dilute solutions (33, 34)). The desA- and desAB-NDSK binding was measured 600 s after completion of the fragment injection to avoid the complications associated with measuring and subtracting bulk refractive index shifts. Thus, steady-state measurements rather than kinetic analyses were used to determine equilibrium binding constants.

To obtain binding curves, fibrinogen deposition and fragment binding were repeated for a range of concentrations of desA-NDSK or desAB-NDSK fragments using a new sensorchip for each experiment. Profiles were normalized with respect to the amount of fibrinogen deposited during each binding experiment, correcting the SPR signal for the molecular mass difference of the fragments compared to fibrinogen. Experiments were designed to be independent of the concentration of fibrinogen molecules capable of binding fragments, which we assumed to be reproducible from sensorchip to sensorchip. The reproducibility of our data supported this assumption. The resulting normalized signal was expressed in units of binding ratios, representing an average number of fragment molecules bound per fibrinogen molecule. For desAB-NDSK, the normalized binding response was plotted against fragment concentration to generate a binding curve. For desA-NDSK, which exists in a monomer-dimer equilibrium in solution, the ratio of monomers to dimers was calculated at each desA-NDSK concentration using the centrifugation data and adjusted the total SPR signal for the binding of dimers to the adsorbed fibrinogen. The mass contribution of the second molecule in the dimer, which we assumed does not directly interact with adsorbed fibrinogen and therefore does not contribute to the affinity of desA-NDSK for fibrinogen, was subtracted from the total fragment binding. The resulting signal was the mass response of the monomers and one molecule of the dimer pair that was interacting directly with adsorbed fibrinogen. The final corrected signal from desA-NDSK molecules directly interacting with fibrinogen was plotted against fragment concentration to generate a binding curve. Peptide competition experiments were performed in triplicate using GPRP, GHRP and AHRPY by incubating 25 μM desA-NDSK or desAB-NDSK with 4 mM of one or two peptides prior to injection over adsorbed fibrinogen.

2.3 Results

2.3.1 Purification of NDSK, desA-NDSK, and desAB-NDSK fragments. The NDSK fragment of fibrinogen is composed of two copies each of Aα1-51, Bβ1-118, and γ1-78, all joined by 11 disulfide bonds. NDSK, containing intact FpA and FpB and thus no exposed polymerization knobs, was purified from a CNBr digest of fibrinogen. The fragments desA-NDSK containing polymerization knobs "A" and desAB-NDSK containing polymerization knobs "A" and "B" were purified from the CNBr digest of desA- and desAB-fibrin, respectively. The ligand fragments, depicted in Figure 2.1B, were generated and purified as described in methods. A representative chromatogram of NDSK fragment purification is shown in Figure 2.2. The reaction conditions generated two products, which appeared as a closely spaced doublet in SDS-PAGE (for NDSK, the two top-most bands in Fig. 2.2 insert, indicated by the arrow in CNBr digest lane). Increasing the digest time (up to 48 h) or concentration of CNBr (up to 1/5, w/w, protein/CNBr ratio) did not change the appearance or yield of the NDSK species. Notably, doublets were present in the CNBr digests of fibrinogen, desA- and desAB-fibrin clots. The two products (Fig. 2.2 insert, NDSK lane) were resolved using size exclusion chromatography and, for all experiments, we used the form with the lower apparent molecular mass. These fragments ran as single bands in SDS with an apparent molecular mass of ~ 67 kDa (Fig. 2.2, insert and Fig. 2.3B).

2.3.2 Characterization of NDSK fragments. The NDSK fragments were analyzed by both native and denatured polyacrylamide gel electrophoresis (PAGE). While both NDSK and desAB-NDSK appeared as single bands on the native gel, the desA-NDSK fragment appeared as two bands suggesting the presence of a higher molecular mass species (Fig. 2.3).

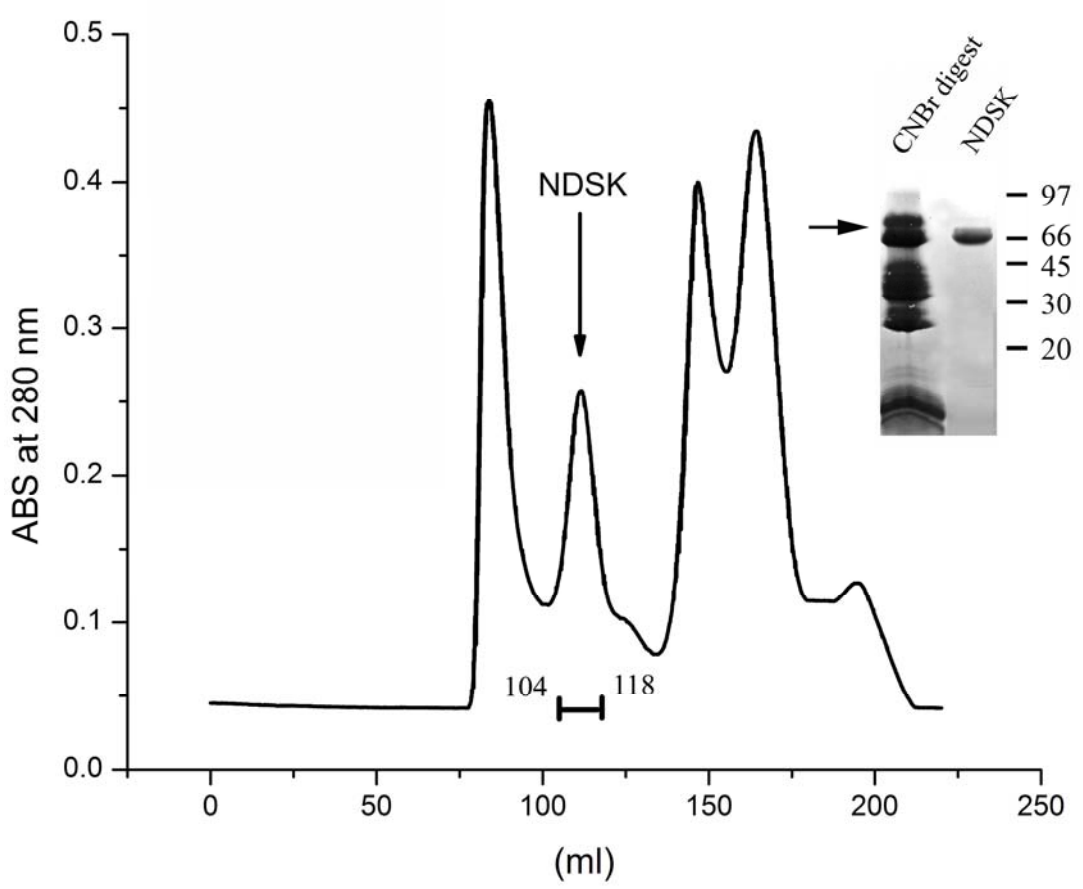

Figure 2.2 Representative chromatogram of NDSK fragment purification using two sequentially connected Superdex 200 prep grade HR16/50columns. The position of the NDSK peak and the volume (mL) over which fragments were collected is identified by the horizontal bracket underneath the peak. The insert shows an 8-25% gradient SDS PAGE of the CNBr digest of fibrinogen with the NDSK bands denoted by an arrow and final purified NDSK fragment from the CNBr digest. The position of molecular mass markers (in kDa) is indicated on the right.

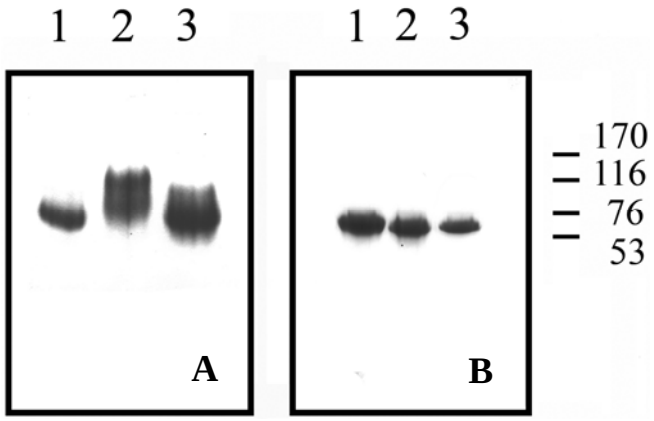

Figure 2.3 Polyacrylamide gel electrophoresis analysis of 2 µg NDSK (1), desA-NDSK (2), and desAB-NDSK (3) in a native 8-25% gradient polyacrylamide gel **A.** and in a denatured (SDS) 8-25% gradient polyacrylamide gel. **B.** The position of the molecular mass markers (in kDa) for the denatured SDS gel is indicated at the side of panel B.

In contrast, all three fragments ran as single bands during SDS-PAGE, (Fig. 2.3B). To characterize the fragments in solution, analytical ultracentrifugation experiments of NDSK, desA-NDSK, and desAB-NDSK in HBSC (Fig. 2.4), were performed as described in Experimental Methods. The equilibrium absorbance profiles were analyzed using both a single-species and a monomer-dimer model based on the Lamm equation (31). The best fit was obtained with a monomer-dimer model using the calculated molecular weights of 59 kDa for NDSK, 56 kDa for desA-NDSK, and 53 kDa for desAB-NDSK monomers. From this fit, the equilibrium dissociation constants of complex formation were determined to be 25 μM for NDSK, 12 μM for desA-NDSK, and 46 μM for desAB-NDSK. Thus, under the conditions of our SPR experiments up to 60% of the desA-NDSK molecules were dimers, while essentially all NDSK and desAB-NDSK molecules were monomers.

2.3.3 NDSK binding experiments. Fragment binding to adsorbed fibrinogen was measured by surface plasmon resonance (SPR); a representative sensorgram is shown in Figure 2.5. Fibrinogen was adsorbed at the hydrophobic surface of the methyl-terminated SAM upon flowing 1 mg/mL fibrinogen over the SPR sensor chip surface (Fig. 2.5A). The adsorption of fibrinogen resulted in monolayer coverage of the surface with a protein density of $6.0 \pm 0.9 \times 10^{-9}$ $\mu g/\mu m^2$ calculated assuming 1 SPR response unit is equivalent to 1 pg/mm^2 of protein surface coverage as described by Biacore. Because exposure of the adsorbed fibrinogen to an additional injection of 1 mg/mL fibrinogen did not result in additional adsorption (data not shown), the chip surface was assumed to be completely covered. Fibrinogen desorption from the surface during subsequent buffer flow was minimal (Fig. 2.5B), indicating fibrinogen molecules adhered to the SAM rather than to one another.

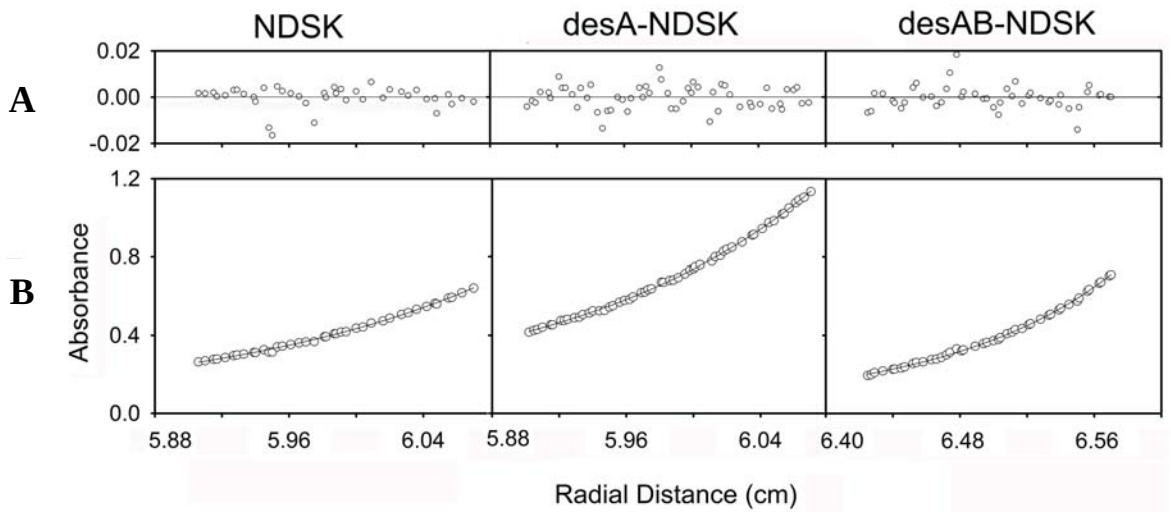

Figure 2.4 Analytical ultracentrifugation sedimentation data for NDSK, desA- and desAB-NDSK. **A.** curve-fitting residuals and **B.** equilibrium absorbance profiles.

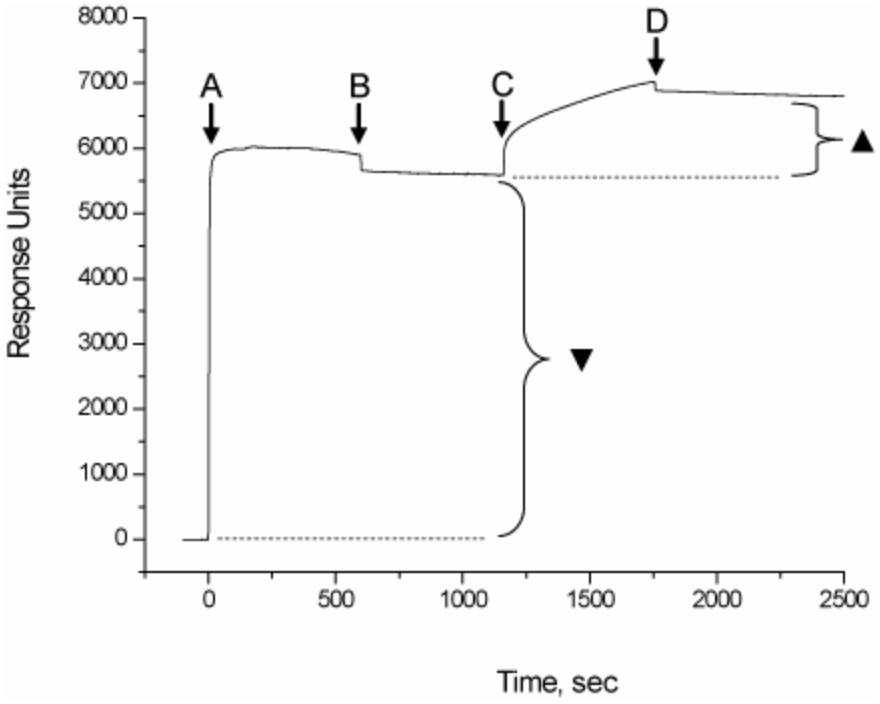

Figure 2.5 Representative SPR sensorgram of response unit changes observed during **A.** injection of 1 mg/mL fibrinogen, **B.** restoration of buffer flow, **C.** injection of 25 μM desAB-NDSK and **D.** restoration of buffer flow. The maximum SPR response change for fibrinogen is identified by (▼) and for desAB-NDSK fragment by (▲).

To determine the affinity constants for knob-hole interactions, two different knob-containing fragments were employed: desA-NDSK and desAB-NDSK. The desA-NDSK fragment contained only the "A" knob, while the desAB-NDSK fragment contained both the "A" and "B" knobs. The binding of both knob containing fragments in solution to holes in immobilized fibrinogen was studied. Upon introduction of desAB-NDSK into the SPR flow cell, the fragment associated with the adsorbed fibrinogen as indicated by the increase in SPR response (Fig. 2.5C). After restoration of buffer flow (Fig. 2.5D) a continual, very small change in SPR response consistent with the slow dissociation of desAB-NDSK was observed. A similar profile for desA-NDSK binding to fibrinogen was observed. Fragment binding profiles were obtained over a concentration range of 0.1 to 22 μM for desAB-NDSK and 0.1 to 43 μM for desA-NDSK. The SPR responses were converted to binding ratios (average number of fragment molecules bound per fibrinogen molecule on the surface) using equation 2.1,

$$\text{Binding Ratio} = \frac{\text{Fragment SPR response}}{\text{Fibrinogen SPR response}} \times \frac{\text{Mr (fibrinogen)}}{\text{Mr (fragment)}} \qquad [2.1]$$

where fragment SPR response is that generated by the fragment bound to fibrinogen (▲ in Fig. 2.5); fibrinogen SPR response is that generated by the adsorption of fibrinogen (▼ in Fig. 2.5); Mr (fibrinogen) is the mass of fibrinogen (340 kDa); and, Mr (fragment) is the mass of each corresponding fragment (desA-NDSK = 56 kDa and desAB-NDSK = 53 kDa). Because the ultracentrifugation and native PAGE data showed the desA-NDSK fragment self-associates, a correction was applied to account for the mass contribution of desA-NDSK dimers. The binding ratios obtained from equation 1 were adjusted using equation 2.2.

$$\text{Adjusted desA-NDSK Binding Ratio} = \text{desA-NDSK Binding Ratio} - \frac{\text{desA-NDSK Binding Ratio} \times \text{\% desA-NDSK dimer}}{2} \quad [2.2]$$

The % desA-NDSK dimer was calculated for each desA-NDSK concentration using a dimer equilibrium dissociation constant of 12 μM. Finally, the desAB-NDSK binding ratios and desA-NDSK adjusted binding ratios were plotted as a function of desA- or desAB-NDSK concentration. The resulting binding curve for each NDSK fragment is shown in Figure 2.6. The plotted data were fit using a single-site interaction binding model, equation 2.3,

$$\text{Binding Ratio} = \frac{B_{max}[\text{NDSK fragment}]}{K_d + [\text{NDSK fragment}]} \quad [2.3]$$

where B_{max} is the maximum binding signal, K_d is the equilibrium dissociation constant, and [NDSK fragment] is the concentration of the injected fragment in μM. Equilibrium dissociation constant values of 3.7 ± 0.7 μM for desAB-NDSK and 5.8 ± 1.1 μM for desA-NDSK binding to fibrinogen were determined, which were not statistically different at the 95% confidence level according to a two-sided unpaired t-test ($p = 0.14$). The maximum binding was 2.3 ± 0.1 for desA-NDSK and 1.6 ± 0.1 for desAB-NDSK (Fig. 2.6).

Additional SPR experiments were conducted to verify the specificity and evaluate the individual contributions of "A-a" and "B-b" interactions. First, the binding of the NDSK fragment with no active knobs was examined. At 50 μM the binding of NDSK was less than 15% of the desA-NDSK binding at 43 μM (Fig. 2.7), demonstrating no significant binding in the absence of knobs. Peptide inhibitors of polymerization were employed to selectively inhibit either "A-a" (GPRP) or "B-b" (GHRP and AHRPY) interactions. DesA- or

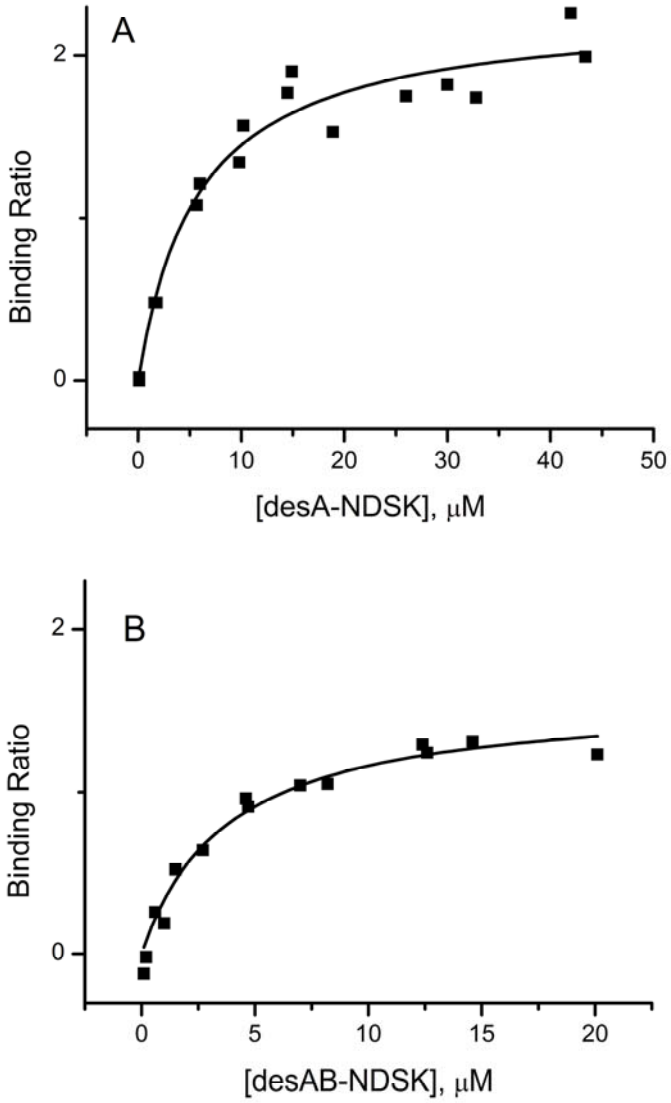

Figure 2.6 Binding curves for **A.** desA-NDSK and **B.** desAB-NDSK binding to 1 mg/mL fibrinogen adsorbed to a hydrophobic-terminated self-assembled monolayer as determined by SPR. The solid curves are the best fits obtained using eq. 2.3.

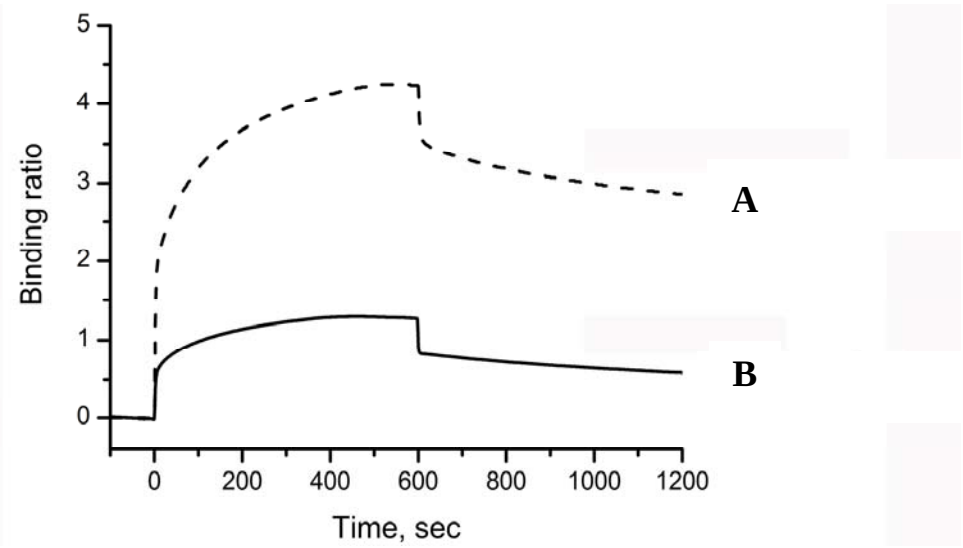

Figure 2.7 Representative SPR sensorgrams showing the binding of **A.** 43 μM desA-NDSK (dashed line) and **B.** 50 μM NDSK (solid line) to adsorbed fibrinogen.

desAB-NDSK (25 μM) was incubated with the peptides, the mixture exposed to adsorbed fibrinogen, and the SPR signal assessed 1200 s after injection. When desAB-NDSK was incubated with GHRP and GPRP individually, the binding was decreased by 48 and 89%, respectively, compared to desAB-NDSK alone (Fig. 2.8A). Because crystallography studies showed GHRP can bind in both holes "a" and "b" (35), inhibition with AHRPY was also examined, which binds exclusively in hole "b" (36). The results with AHRPY were the same as with GHRP; desAB-NDSK binding decreased 52% compared to desAB-NDSK alone (Fig. 2.9). When the equimolar mixture of GHRP and GPRP was incubated with desAB-NDSK the binding ratio fell below zero, likely due to both the loss of desAB-NDSK binding and a slight desorption of fibrinogen. The small decrease in SPR signal resulting from fibrinogen desorption was determined to be less than 2% over the course of each experiment and was not detectable for any of the other fragment/peptide mixtures because the increase in signal due to fragment binding obscured the decrease in signal due to fibrinogen desorption. Similar to desAB-NDSK with GPRP, an 84% decrease in binding was observed when desA-NDSK was incubated with GPRP (Fig. 2.8B). Incubation of desA-NDSK with GHRP or AHRPY did not result in inhibition, but rather a slight increase in binding compared to desA-NDSK alone. Finally, the addition of an equimolar mixture of GHRP and GPRP to desA-NDSK resulted in an 89% decrease in desA-NDSK binding. Collectively, these results demonstrate that the binding of desA- and desAB-NDSK to fibrinogen is promoted by specific knob-hole interactions and that "B-b" knob-hole interactions contribute to the binding of desAB-NDSK to surface-bound fibrinogen.

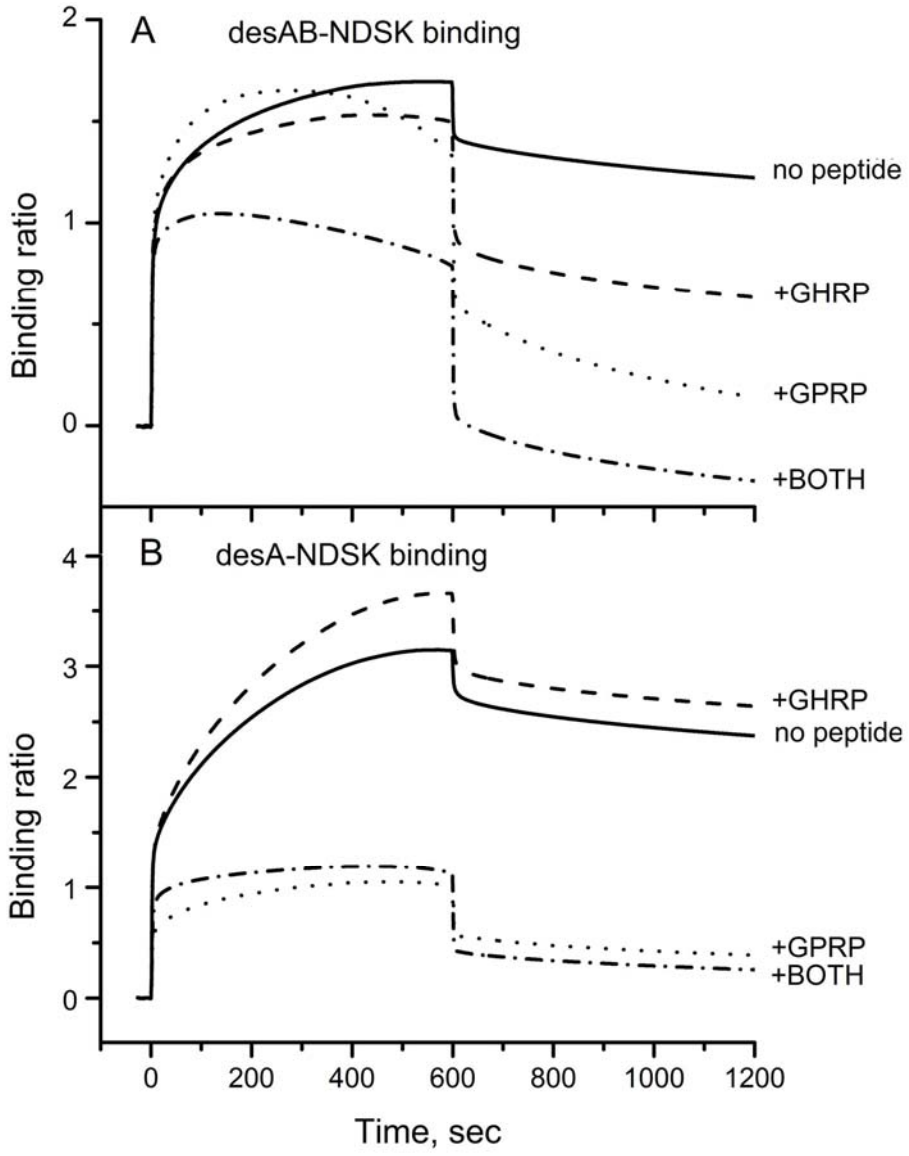

Figure 2.8 Representative SPR sensorgrams showing the binding of **A.** 25 μM desAB-NDSK (solid line) and **B.** 25 μM desA-NDSK (solid line), in the presence of 4 mM GHRP (dashed line), 4 mM GPRP (dotted line), and equimolar mixture (BOTH) of GHRP and GPRP (dashed and dotted line) to adsorbed fibrinogen.

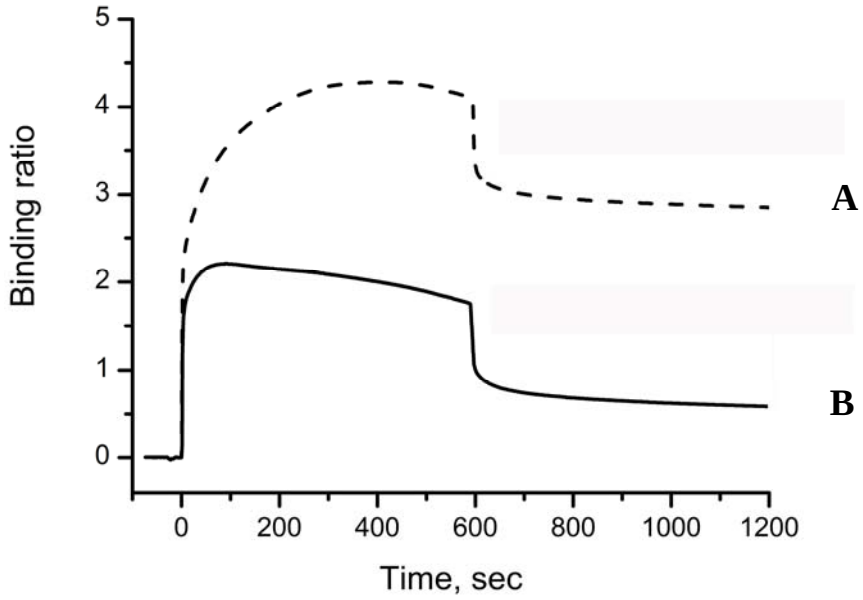

Figure 2.9 Representative SPR sensorgrams showing the binding of **A.** 25 μM desA-NDSK and 4 mM AHRPY (dotted line) and **B.** 25 μM desAB-NDSK and 4 mM AHRPY (solid line) to adsorbed fibrinogen.

2.4 Discussion

The design of these experiments allowed measurement of the affinities for knob-hole interactions between two molecules ("A-a" alone or "A-a" and "B-b" together) in the absence of other interactions that occur during polymerization. Although the affinities determined herein (5.8 ± 1.1 μM and 3.7 ± 0.7 μM) were not significantly different from one another, the higher affinity for the desAB-NDSK suggests both "A-a" and "B-b" interactions contribute to the binding. This suggestion was confirmed by the peptide inhibition studies, which showed both knob-hole pairs participate in desAB-NDSK binding to immobilized fibrinogen. At least an 84% decrease in both desA- and desAB-NDSK binding to fibrinogen was observed in the presence of GPRP, demonstrating "A-a" interactions are important to the binding of both fragments. Moreover, GHRP and AHRPY competed solely with desAB-NDSK, indicating that "B-b" interactions participate in desAB-NDSK but not desA-NDSK binding to immobilized fibrinogen. Finally, the GHRP/GPRP mixture decreased desAB-NDSK binding more than GPRP alone, as would be expected if "B-b" interactions contributed to this interaction. Taken together these data strongly support the conclusion that "B-b" interactions participate in the binding of desAB-NDSK to immobilized fibrinogen. This finding differs from that obtained in recent laser tweezers studies where GPRP, but not GHRP, inhibited interactions between desAB-NDSK and fibrinogen (22). "B-b" interactions were detected in laser tweezers experiments only under conditions where "A-a" interactions were impaired or excluded (23). The difference between the SPR results herein and the laser tweezers data likely reflects the inherent differences between the methods. For example, "B-b" interactions may occur subsequent to "A-a" interactions and thus are not detected in the forced dissociations of the laser tweezers binding studies. Alternatively, the nature of the

immobilized species, directly adsorbed fibrinogen in the SPR experiments or covalently immobilized fibrinogen in the laser tweezers experiments, may alter the availability of hole "b".

The affinities determined in this chapter (5.8 ± 1.1 μM and 3.7 ± 0.7 μM for desA- and desAB-NDSK, respectively) are remarkably similar to those determined for fragment D binding to suspended desAB-fibrin fragments that were produced by sonication, 2.4 μM (37). This similarity suggests that the affinities determined by SPR are analogous to those found in solution. Interactions between fibrinogen and suspended desAB-fibrin fragments were even stronger (e.g., 56 nM), as anticipated if one fibrinogen molecule binds to fibrin through multiple sites (i.e., the two D regions) (37). Recently, Ugarova and colleagues determined a similar affinity (1.47 ± 0.26 μM) using SPR to measure soluble fibrinogen binding to covalently immobilized fibrin molecules (38). The similarity of these measurements suggests that the studies described in this chapter measure the interactions that mediate fibrin monomer binding to a single D region of intact fibrinogen. Other investigations have examined the individual "A-a" and "B-b" interactions using peptides that mimic the "A" and "B" knobs (i.e., GPRP and GHRP, respectively). In the presence of 2 mM calcium, K_d's of 20 μM for GPRP and 16 μM for GHRP were found (39). These affinities are somewhat weaker than the affinities determined for the larger desA- and desAB-NDSK fragments, which likely reflects the entropy costs associated with restraining the conformations of the smaller molecules. The values determined by SPR are rational when compared with the published data (19, 37, 39, 40), indicating the data reflect the affinities of the "A-a" and "B-b" interactions as they occur in fibrin polymers.

The observation that desAB-NDSK binds fibrinogen through both "A-a" and "B-b" interactions infers that both sets of interactions may occur between the same two fibrin molecules in a polymer. In other words, "A-a" and "B-b" interactions may both support protofibril formation. A model where "B-b" interactions occur within protofibrils was also inferred from previous studies using recombinant fibrinogens with substitutions in the high-affinity calcium binding site in γC (21, 41). Thrombin-catalyzed polymerization of these fibrinogens was severely impaired and this polymerization was abolished by GHRP. Furthermore, the batroxobin-catalyzed polymerization was undetectable. Similarly, Okumura and co-workers have recently found that substitutions in hole "a" markedly impair thrombin-catalyzed polymerization and that this polymerization is abolished by GHRP. Also, the anchrod-catalyzed polymerization of these variants was undetectable (Okumura et al, personal communication). Consideration of the SPR binding studies together with the polymerization of these variant fibrinogens indicates that 1) both "A-a" and "B-b" interactions can support protofibril formation; 2) "A-a" interactions are higher affinity than "B-b" and on their own can support nearly normal polymerization; and, 3) "B-b" interactions are lower affinity than "A-a" but are sufficient to support delayed polymerization.

This work also revealed that desA-NDSK, and to a much lower degree NDSK and desAB-NDSK, form dimers in solution. However, the dimerization of fragments does not preclude their binding to fibrinogen. This observation suggests that the desA-NDSK monomers comprising the dimer are connected via regions of the molecule that do not interfere with the "A" knob and subsequent "A-a" interactions. A recent laser tweezers study which examined interactions between pairs of NDSK fragments indicated that FpB mediates desA-NDSK

dimerization. These studies showed interactions between two desA-NDSK molecules. The interactions were lost when FpB was removed from one of the molecules, indicating a dependence on fibrinopeptide B (30). The biological significance of desA-NDSK dimerization is currently unknown.

In conclusion, SPR binding studies showed that both "A-a" and "B-b" interactions participate in the binding of desAB-NDSK to fibrinogen, and that the affinity of desA-NDSK binding was not markedly different from desAB-NDSK binding. As such, the "A-a" interactions are particularly strong. Furthermore, the "B-b" interactions can occur alongside "A-a" interactions when both the "B" knob and "b" hole are available. The SPR studies in this chapter were designed to model the very early stages of polymerization (i.e., interactions occurring between two molecules). The detection of both "A-a" and "B-b" interactions occurring between the fibrin (desAB-NDSK) and fibrinogen molecule demonstrates "B-b" interactions may have a role in protofibril formation.

REFERENCES

(1) Laurens, N.; Koolwijk, P.; de Maat, M. P. "Fibrin structure and wound healing." *J Thromb Haemost* 2006**,** *4*, 932-9.

(2) Weisel, J. W. "Fibrinogen and fibrin." *Adv Protein Chem* 2005**,** *70*, 247-99.

(3) Henschen, A. "On the Structure of Functional Sites in Fibrinogen." *Thromb. Res.* 1983**,** *Supplement V*, 27-39.

(4) Spraggon, G.; Everse, S. J.; Doolittle, R. F. "Crystal structures of fragment D from human fibrinogen and its crosslinked counterpart from fibrin." *Nature* 1997**,** *389*, 455-62.

(5) Pratt, K. P.; Cote, H. C.; Chung, D. W.; Stenkamp, R. E.; Davie, E. W. "The primary fibrin polymerization pocket: three-dimensional structure of a 30-kDa C-terminal gamma chain fragment complexed with the peptide Gly-Pro-Arg-Pro." *Proc Natl Acad Sci U S A* 1997**,** *94*, 7176-81.

(6) Doolittle, R. F.; Spraggon, G.; Everse, S. J. "Three-dimensional structural studies on fragments of fibrinogen and fibrin." *Curr Opin Struct Biol* 1998**,** *8*, 792-8.

(7) Goldsack, N. R.; Chambers, R. C.; Dabbagh, K.; Laurent, G. J. "Thrombin." *Int J Biochem Cell Biol* 1998**,** *30*, 641-6.

(8) Blomback, B. "The fibrinopeptides." *Thromb Diath Haemorrh Suppl* 1966**,** *20*, 201-10.

(9) Laudano, A. P.; Doolittle, R. F. "Synthetic peptide derivatives that bind to fibrinogen and prevent the polymerization of fibrin monomers." *Proc. Natl, Acad. Sci.* 1978**,** *75*, 3085-3089.

(10) Hantgan, R. R.; Hermans, J. "Assembly of Fibrin." *J. Biol. Chem.* 1979**,** *254*, 11272-11281.

(11) Olexa, S. A.; Budzynski, A. Z. "Effects of fibrinopeptide cleavage on the plasmic degradation pathways of human cross-linked fibrin." *Biochemistry* 1980**,** *19*, 647-651.

(12) Yang, Z.; Mochalkin, I.; Doolittle, R. F. "A model of fibrin formation based on crystal structures of fibrinogen and fibrin fragments complexed with synthetic peptides." *Proc Natl Acad Sci U S A* 2000**,** *97*, 14156-61.

(13) Mihalyi, E. "Clotting of bovine fibrinogen. Calcium binding to fibrin during clotting and its dependence on release of fibrinopeptide B." *Biochemistry* 1988**,** *27*, 967-76.

(14) Higgins, D. L.; Lewis, S. D.; Shafer, J. A. "Steady state kinetic parameters for the thrombin-catalyzed conversion of human fibrinogen to fibrin." *J Biol Chem* 1983**,** *258*, 9276-82.

(15) Ruf, W.; Bender, A.; Lane, D. A.; Preissner, K. T.; Selmayr, E.; Muller-Berghaus, G. "Thrombin-induced fibrinopeptide B release from normal and variant fibrinogens: influence of inhibitors of fibrin polymerization." *Biochim Biophys Acta* 1988**,** *965*, 169-75.

(16) Weisel, J. W.; Veklich, Y.; Gorkun, O. "The sequence of cleavage of fibrinopeptides from fibrinogen is important for protofibril formation and enhancement of lateral aggregation in fibrin clots." *J Mol Biol* 1993**,** *232*, 285-97.

(17) Shimizu, A.; Ferry, J. D. "Clots of beta-fibrin. Viscoelastic properties, temperature dependence of elasticity, and interaction with fibrinogen-binding tetrapeptides." *Biophys J* 1988**,** *53*, 311-8.

(18) Shen, L. L.; Hermans, J.; McDonagh, J.; McDonagh, R. P. "Role of fibrinopeptide B release: comparison of fibrins produced by thrombin and Ancrod." *Am J Physiol* 1977**,** *232*, H629-33.

(19) Shainoff, J. R.; Dardik, B. N. "Fibrinopeptide B in fibrin assembly and metabolism: physiologic significance in delayed release of the peptide." *Ann N Y Acad Sci* 1983**,** *408*, 254-68.

(20) Mosesson, M. W.; DiOrio, J. P.; Muller, M. F.; Shainoff, J. R.; Siebenlist, K. R.; Amrani, D. L.; Homandberg, G. A.; Soria, J.; Soria, C.; Samama, M. "Studies on the ultrastructure of fibrin lacking fibrinopeptide B (beta-fibrin)." *Blood* 1987**,** *69*, 1073-81.

(21) Lounes, K. C.; Ping, L.; Gorkun, O. V.; Lord, S. T. "Analysis of engineered fibrinogen variants suggests that an additional site mediates platelet aggregation and that "B-b" interactions have a role in protofibril formation." *Biochemistry* 2002**,** *41*, 5291-5299.

(22) Litvinov, R. I.; Gorkun, O. V.; Owen, S. F.; Shuman, H.; Weisel, J. W. "Polymerization of fibrin: specificity, strength, and stability of knob-hole interactions studied at the single-molecule level." *Blood* 2005**,** *106*, 2944-2951.

(23) Litvinov, R. I.; Gorkun, O. V.; Galanakis, D. K.; Yakovlev, S.; Medved, L.; Shuman, H.; Weisel, J. W. "Polymerization of fibrin: Direct observation and quantification of individual B:b knob-hole interactions." *Blood* 2007**,** *109*, 130-8.

(24) Bale, M. D.; Muller, M. F.; Ferry, J. D. "Effects of fibrinogen-binding tetrapeptides on mechanical properties of fine fibrin clots." *Proc Natl Acad Sci U S A* 1985**,** *82*, 1410-3.

(25) Okumura, N.; Gorkun, O. V.; Terasawa, F.; Lord, S. T. "Substitution of the gamma chain Asn 308 disturbs the D:D interface affecting fibrin polymerization, fibrinopeptide B release, and FXIIIa-catalyzed cross-linking." *Blood* 2004**,** *103*, 4157-4163.

(26) Matsuda, M.; Baba, M.; Morimoto, K.; Nakamikawa, C. ""Fibrinogen Tokyo II". An abnormal fibrinogen with an impaired polymerization site on the aligned DD domain of fibrin molecules." *J Clin Invest* 1983**,** *72*, 1034-41.

(27) Gorkun, O. V.; Veklich, Y. I.; Medved, L. V.; Henschen, A. H.; Weisel, J. W. "Role of the alpha C domains of fibrin in clot formation." *Biochemistry* 1994**,** *33*, 6986-97.

(28) Doolittle, R. F.; Pandi, L. "Binding of synthetic B knobs to fibrinogen changes the character of fibrin and inhibits its ability to activate tissue plasminogen activator and its destruction by plasmin." *Biochemistry* 2006**,** *45*, 2657-67.

(29) Blomback, B.; Hessel, B.; Iwanaga, S.; Reuterby, J.; Blomback, M. "Primary structure of human fibrinogen and fibrin. I. Cleavage of fibrinogen with cyanogen bromide. Isolation and characterization of NH 2 -terminal fragments of the ("A") chain." *J Biol Chem* 1972**,** *247*, 1496-512.

(30) Gorkun, O. V.; Litvinov, R. I.; Veklich, Y. I.; Weisel, J. W. "Interactions mediated by the N-terminus of fibrinogen's Bbeta chain." *Biochemistry* 2006**,** *45*, 14843-52.

(31) McRorie, D.; PJ, V. *Self-associating systems in the analytical ultracentrifuge*. Beckman Instruments, Inc., Palo Alto, California, 1993.

(32) Evans-Nguyen, K.; Schoenfisch, M. H. "Fibrin proliferation at model surfaces: Influence of surface properties." *Langmuir* 2005**,** *21*, 1691-1694.

(33) Sit, P. S.; Marchant, R. E. "Surface-dependent conformations of human fibrinogen observed by atomic force microscopy under aqueous conditions." *Thromb. Haemostasis* 1999**,** *82*, 1053-1060.

(34) Agnihotri, A.; Christopher A, S. "Time-Dependent conformational changes in fibrinogen measured by atomic force microscopy." *Langmuir* 2004**,** *20*, 8864-8852.

(35) Kostelansky, M. S.; Bolliger-Stucki, B.; Betts, L.; Gorkun, O. V.; Lord, S. T. "Bβ Glu397 and BβAsp398 but not BβAsp 432 Are Required for "B:b" Interactions." *Biochemistry* 2004**,** *43*, 2465-2474.

(36) Doolittle, R. F.; Chen, A.; Pandi, L. "Differences in binding specificity for the homologous gamma- and beta-chain "holes" on fibrinogen: exclusive binding of Ala-His-Arg-Pro-amide by the beta-chain hole." *Biochemistry* 2006**,** *45*, 13962-9.

(37) Husain, S. S.; Weisel, J. W.; Budzynski, A. Z. "Interaction of fibrinogen and its derivatives with fibrin." *J. Biol. Chem.* 1989**,** *264*, 11414-11420.

(38) Lishko, V. K.; Burke, T.; Ugarova, T. "Antiadhesive effect of fibrinogen: a safeguard for thrombus stability." *Blood* 2007**,** *109*, 1541-9.

(39) Laudano, A. P.; Doolittle, R. F. "Influence of calcium ion on the binding of fibrin amino terminal peptides to fibrinogen." *Science* 1981**,** *212*, 457-9.

(40) Chtcheglova, L. A.; Vogel, M.; Gruber, H. J.; Dietler, G.; Haeberli, A. "Kinetics of the interaction of desAABB-fibrin monomer with immobilized fibrinogen." *Biopolymers* 2006**,** *83*, 69-82.

(41) Lord, S. T.; Gorkun, O. V. "Insight from studies with recombinant fibrinogens." *Ann N Y Acad Sci* 2001**,** *936*, 101-16.

CHAPTER 3

DEVELOPMENT OF AN ATOMIC FORCE MICROSCOPY METHOD TO INVESTIGATE FIBRIN-FIBRIN INTERACTIONS

3.1 Introduction

Weisel and co-workers reported the use of laser tweezers force spectroscopy to investigate specific fibrin(ogen) interactions (1-3). Individual "A-a" knob-hole interactions were detected between pedestals modified with desA- or desAB-fibrin and fibrinogen- or D fragment-modified latex beads. In addition to a low-force population attributed to non-specific interactions, the forced dissociation of these interactions showed a single rupture event of ~125 pN in magnitude (1). In subsequent work, the same investigators employed variant fibrinogens and their fragments to reveal both "B-b" and "A-b" knob-hole interactions (2) and specific interactions between the *N*-terminus of the Bβ chain and the D, E, and αC regions of fibrinogen (3). Notably weaker than "A-a" binding, these interactions exhibited a more complex pattern that was attributed to the rupture of multiple parallel interactions (e.g., two simultaneous "B-b" bond ruptures). Therefore, the rupture force distribution displayed several force populations. The absolute magnitude of the observed forces was highly dependent on experimental conditions, including the loading rate (force per unit time) applied to the bond during rupture.

Despite its use in the investigation of many of the specific interactions involved in fibrin formation, laser tweezers technology has several limitations. First, the optical trap controlling the modified beads has a maximum strength of 200 pN, limiting the range of

detectable interactions. Second, spatial resolution is only accurate to within a few nanometers, unlike the sub-nanometer resolution possible with AFM (4-8). Consequently, mechanical behaviors of molecules such as molecular unfolding or stretching occuring on the Å to nm scale immediately preceding bond rupture are not resolved from the bond rupture itself using laser tweezers. The primary motivation for using AFM to study fibrin interactions is to exploit the superior capabilities of the instrument to gain deeper insight into knob-hole interactions beyond the information provided by laser tweezers.

In this chapter, a method to study the rupture forces of specific fibrin-fibrin interactions was developed using AFM combined with fibrin(ogen) and some of its fragments. The method allowed for the accurate measurement of specific fibrin(ogen) forces while eliminating nonspecific interactions. The unrivalled capabilities of the AFM enabled an in depth analysis of knob-hole interactions, providing crucial insight into the complexity of these interactions unobservable with laser tweezers.

3.2 Experimental Methods

3.2.1 Materials. All reagents were of analytical grade and purchased from Sigma (St. Louis, MO) unless noted otherwise. Human plasma fibrinogen (FIB 1) and α-thrombin (HT 2970PA) were purchased from Enzyme Research Laboratories (Southbend, IN). Batroxobin (*batroxobin moojeni*) was obtained from Center Chem (Stamford, CT). The amide peptide GPRP was synthesized by the Protein Chemistry Laboratory at the University of North Carolina at Chapel Hill (Chapel Hill, NC).

3.2.2 Recombinant fibrinogen preparation. Normal (wild type) was obtained as described previously (9, 10). Briefly, fibrinogen was expressed in Chinese Hamster Ovary cells (CHO) and purified using immunoaffinity chromatography on a column covalently modified with IF-1 monoclonal antibodies. After purification, fibrinogen was dialyzed against 20 mM HEPES pH 7.4, 150 mM NaCl buffer (HBS) and stored at -80 ^{0}C.

3.2.3 NDSK fibrin(ogen) fragments preparation. NDSK fragments represent the central region of fibrinogen (Fig. 3.1A) or fibrin and contain polymerization knobs. Three types of fragments were purified from CNBr digests and are illustrated in Figure 3.1B: NDSK retaining both FpA and FpB (no knobs exposed) isolated from human plasma fibrinogen, desA-NDSK lacking FpA ("A" knobs exposed) isolated from fibrin polymerized by batroxobin, and desAB-NDSK lacking both FpA and FpB ("A" and "B" knobs exposed) isolated from fibrin polymerized by thrombin. Briefly, CNBr digests of fibrinogen or fibrin were separated using size-exclusion chromatography on Superdex 200 column, (Amersham Biosciences, Piscataway, NJ) as described (3). Purified NDSK fragments were characterized by SDS-PAGE, dialyzed extensively against HBS and stored at -80 °C.

3.2.4 DD fragment preparation. The DD fragment of fibrinogen represents the cross-linked dimer of two D fragments from the D regions of fibrin molecules (Fig. 3.1C). Each D fragment contains both polymerization holes "a" and "b". The DD fragment was purified from a FXIII ligated fibrin clot as described previously (11). Briefly, the clot was digested by trypsin covalently coupled to agarose beads (Pierce, Rockford, IL). Fragments were purified using affinity chromatography on an NH_2-GPRPAA affinity column. After elution from the

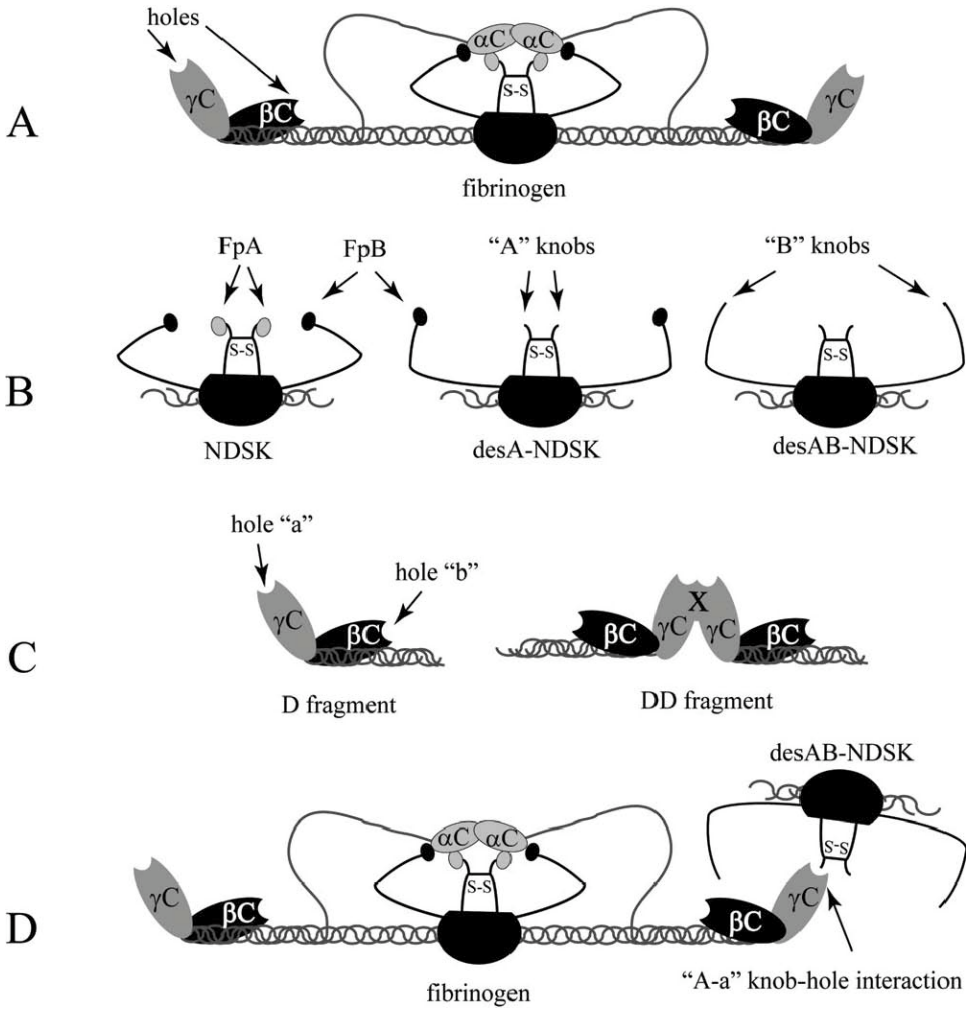

Figure 3.1 Schematic representation of all proteins used in AFM measurements, not to scale. **A.** Fibrinogen molecule depicted with αC domains interacting with fibrinopeptide A and fibrinopeptide B. Disulfide bond connecting the N terminus of the Aα chains denoted as S-S. Locations of polymerization holes "a" in γC module and "b" in the βC module indicated by arrows. **B.** Fragments consisting of the central part of fibrinogen (NDSK) and fibrin (desA- and desAB-NDSK) shown with both fibrinopeptides present (NDSK), fibrinopeptide A cleaved (desA-NDSK), and both fibrinopeptides cleaved (desAB-NDSK). **C.** Polymerization holes-containing fragments D and DD. The location of the DD interface containing interacting surfaces inaccessible to solvent is depicted by X in DD fragment. **D.** Schematic representation of "A-a" knob-hole interaction between desAB-NDSK (knob-containing molecule) and fibrinogen (hole-containing molecule).

column, the DD fragment was washed with HBS, concentrated using a 50 kDa cut-off centrifugal filter device (Millipore, Bedford, MA) and stored at -80 °C.

3.2.5 Substrate surface preparation: gold-coating and SAM generation. Two surfaces were modified for use throughout these experiments: glass microscope slides (Electron Microscopy Sciences, Washington, PA) for AFM substrates and DNP-S (Veeco Probes, Camarillo, CA) AFM cantilevers. The cantilevers were rinsed with chloroform, dried with a gentle stream of nitrogen and ozone cleaned for 30 min using a BioForce TipCleaner (Ames, IA). Microscope slides were cleaned as described previously (12). Both tips and slides were then coated with 3 nm of chromium and 45 nm of gold as described previously (12). For covalent attachment of protein, a carboxylic acid terminated self-assembled monolayer (SAM) was formed by immersing the gold-coated tips and substrates in 11-mercaptoundecanoic acid solution (2 mM in absolute ethanol) overnight immediately prior to use. All substrates were rinsed with absolute ethanol and ultra-pure water, and dried with nitrogen prior to use.

3.2.6 Sample Preparation and Force Curve Collection: Strategy 1. The ultimate designs of the specific methods in Strategy 1 were the result of several months of troubleshooting by Dr. Ryan Fuierer and Dr. Oleg Gorkun prior to my involvement in this project. To initiate covalent attachment of the proteins, the carboxylic acid-terminated surfaces were activated using a standard amine coupling method. The AFM tip and substrate were exposed to equal volumes of 0.1 M *N*-hydroxysuccinimide (NHS) and 0.4 M 1-Ethyl-3-(3dimethylaminopropyl) carbodiimide (EDC) (Pierce; Rockford, Il) in water for 30 min and

then rinsed with water. Next, 0.15 mg/mL of protein was incubated with the tip and the substrate. DesA-NDSK, desAB-NDSK or recombinant fibrinogen was attached to the tip and D fragment, DD fragment, BSA or recombinant fibrinogen was immobilized on the substrate. After the 10 min protein incubation, both surfaces were rinsed with AFM buffer (20 mM HEPES, 150 mM NaCl, 3 mM $CaCl_2$, 2 mg/ml BSA, 0.1% Triton X-100, pH 7.4) to block any remaining activated surface groups with BSA and to remove loosely adhered protein.

All force measurements were made in AFM buffer using a Molecular Force Probe 3D from Asylum Research (Santa Barbara, CA) controlled with Igor Pro 5.03B (Wavemetrics; Lake Oswego, OR). The substrate and tip were placed in the instrument and equilibrated in AFM buffer for ~2 h or until the signal deflection was stable. The laser spot was positioned just slightly off center from the apex of the "D" triangular cantilever (nominal spring constant of 60 pN/nm) prior to equilibration. Force curves were collected at no less than 3 randomly chosen spots for each substrate, and 500 to 1000 curves were collected at each spot. The approach/retract velocity was constant at 1800 nm/s and the initial trigger was set to 3 nm with a 500 nm force distance. The spring constant of the cantilever was measured via the thermal method after the signal deflection stabilized. The spring constant was measured at least 3 times per cantilever and the average value used in the force calculations and data analyses.

3.2.7 Sample Preparation and Force Curve Collection: Strategy 2. Based on numerous discussions with expert force spectroscopists at Duke University and preliminary data generated by Laurel Averett, several modifications were implemented to the protein immobilization methods and force curve collection procedure described in section 3.2.6. The

tip protein concentration was decreased from 0.15 mg/mL to 0.075 mg/mL for the desA-NDSK, desAB-NDSK and fibrinogen. The protein concentrations for the substrate were decreased from 0.15 mg/mL to 0.075 mg/mL, but D fragment, DD fragment or fibrinogen was mixed with an equal volume of 0.075 mg/mL BSA prior to immobilization. Therefore, the final protein concentrations were 0.038 mg/mL of D fragment, DD fragment or fibrinogen and 0.038 mg/mL BSA, hereafter referred to as 50% solutions of active protein. Also, the salt concentration was increased to 35 mM HEPES, 225 mM NaCl, 7.5 mM $CaCl_2$ during the substrate protein immobilization step. As with strategy 1, the proteins were incubated with the NHS/EDC-activated tip and substrate for 10 min and remaining active sites were blocked with BSA by rinsing the surfaces with AFM buffer. However, an additional 10 min incubation step with AFM buffer was included. Furthermore, a stringent washing procedure was developed to remove non-covalently attached proteins. The protein-modified surfaces were rinsed alternately and incubated for 1 min each with a high salt (50 mM HEPES, 1 M NaCl, pH 7.4) and low pH buffer (50 mM NaOAc, 300 mM NaCl, pH 4.0). The alternating wash procedure was repeated 5 times. Finally, the surfaces were rinsed copiously with AFM buffer and loaded into the AFM.

In addition to the protein immobilization protocol, significant modifications were made to the data collection methods. Force curves were collected in a 32 × 32 array over a 5 μm scan area using custom software written by Dr. Chad Ray, instead of 1000 curves at a single location. At least 3 scan areas were examined per substrate with a 5 nm trigger during force curve collection. Additionally, the spring constant was determined at the start of each scan area using a 30 nm trigger instead of the 3 nm trigger used in strategy 1. The average spring constant value was used in the force calculations and data analyses.

3.2.8 Custom Analysis Software. The force versus distance curves collected via both strategies were analyzed using custom software written by Dr. Russell Taylor, Department of Computer Science at the University of North Carolina at Chapel Hill. The program first converted cantilever deflection (raw data) versus tip-substrate separation distance to force versus separation distance curves using the average spring constant measured for the cantilever. Interactions (events) were identified as changes in force exceeding a user-defined threshold, typically 20 pN. Only the forces corresponding to events that occurred between 20 and 500 nm from the surface were used to generate histograms. For force curves collected via strategy 1, the histograms were generated by plotting the force of each event in 20 pN bins. For force curves collected via strategy 2, the number of events in each bin was divided by the total number of events to generate histograms showing probability versus force in 20 pN bins.

3.3 Results and Discussion

3.3.1 Data Analysis. The software written by Dr. Taylor calculated the rupture force and distance from the surface for each event in the force versus distance curves. Two filters were applied to the data based on observations made by Dr. Ryan Fuierer and Dr. Oleg Gorkun. First, the observed baseline noise in the force curves was typically ~5 pN, therefore 20 pN was selected as the force threshold. An additional filter based on the dimensions of fibrinogen was applied to the data to further ensure only specific fibrin-fibrin interactions were included in the analyses. Only events occurring between 20 and 500 nm from the substrate were included in the histograms.

Figure 3.2 shows a representative force versus distance curve containing several interactions (events) corresponding to bond ruptures between the desAB-NDSK on the tip and fibrinogen on the substrate. A schematic of the desAB-NDSK interaction with fibrinogen is shown in Figure 3.1D. While most of the force versus distance curves in a data set did not contain any interactions, the majority of the curves with interactions contained more than one event that satisfied the magnitude and distance criteria (Fig 3.2, *). The appearance of multiple interactions rupturing in a single force versus distance curve presents numerous challenges to the identification of the specific bonds responsible. Furthermore, multiple interactions occurring at different magnitudes such as those observed in this system led to multiple force populations in the resulting histograms. A common cause of multiple events has previously been attributed to the formation of a single bond (e.g., an "A-a" knob-hole interaction) between multiple pairs of interacting molecules on the tip and the substrate. Alternatively, multiple events could represent the formation of multiple bonds (e.g., "A-a" and "B-b" knob-hole interactions or αC-Bβ chain interactions) occurring between a single interacting pair of molecules containing multiple interaction sites. At the advice of Dr. Boris Akhremitichev and Dr. Chad Ray at Duke University, several modifications were made to the protein immobilization method and data collection protocols to minimize the potential for multiple interacting pairs of molecules. A detailed discussion of the changes implemented and the rationale is discussed below.

3.3.2 Comparison of Protein Immobilization Strategy 1 and 2. Due to the complications of multiple interactions occurring within a single force versus distance curve, the majority of the modifications in protein immobilization were designed to reduce the possibility of protein

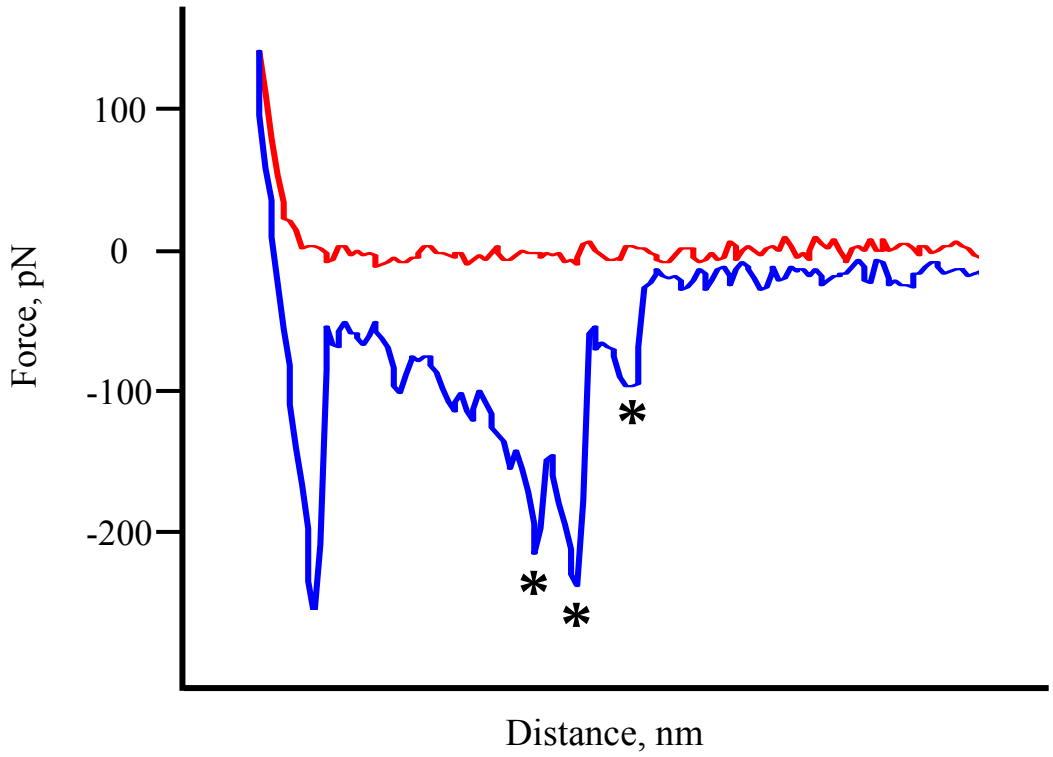

Figure 3.2 Representative force versus distance curve illustrating the observed signal as the desAB-NDSK modified AFM tip approaches (red) and retracts (blue) from the fibrinogen-modified substrate. The events denoted by the asterisks illustrate the events that exceeded the 20 pN force threshold and occurred between 20 and 500 nm from the surface; the user-defined criteria for an event.

aggregates or clusters on the surface. For example, decreasing the protein concentrations and co-immobilizing fibrinogen, D fragment or DD fragment with BSA ensured the active protein molecules were distributed far enough apart to prevent a single protein on the tip from interacting with two adjacent molecules on the surface. Stringent washing protocols alternating between high salt and low pH were also designed to promote electrostatic repulsion between the proteins on the surface and dislodge any non-covalently attached fibrinogen, D fragment or DD fragment to reduce aggregates at the surface.

The changes in force curve collection and spring constant determination were designed to more accurately determine the spring constant and better sample the proteins on the substrate. The increase in the trigger to 30 nm during spring constant determination caused the cantilever to undergo a more significant deflection, generating a wider linear deflection region used during curve fitting. The wider linear deflection range resulted in a more reliably measured spring constant. Additionally, taking force curves in a 32 × 32 array over a 5 μm scan area provided a more accurate assessment of the interactions between different molecules on the substrate and the molecules on the tip, rather than interrogating a small population of molecules repeatedly as in Strategy 1. The force curve collection in Strategy 1 only examined 3 locations per substrate, whereas Strategy 2 examined 3072 locations per substrate.

The reproducibility of force curves acquired via Strategy 2 was significantly improved between 5 μm scans within a single surface, surface to surface, and day to day. Figure 3.3 shows histograms generated from the interactions between desAB-NDSK and fibrinogen using both strategies. Despite the reproducibility improvements, the resulting histogram was

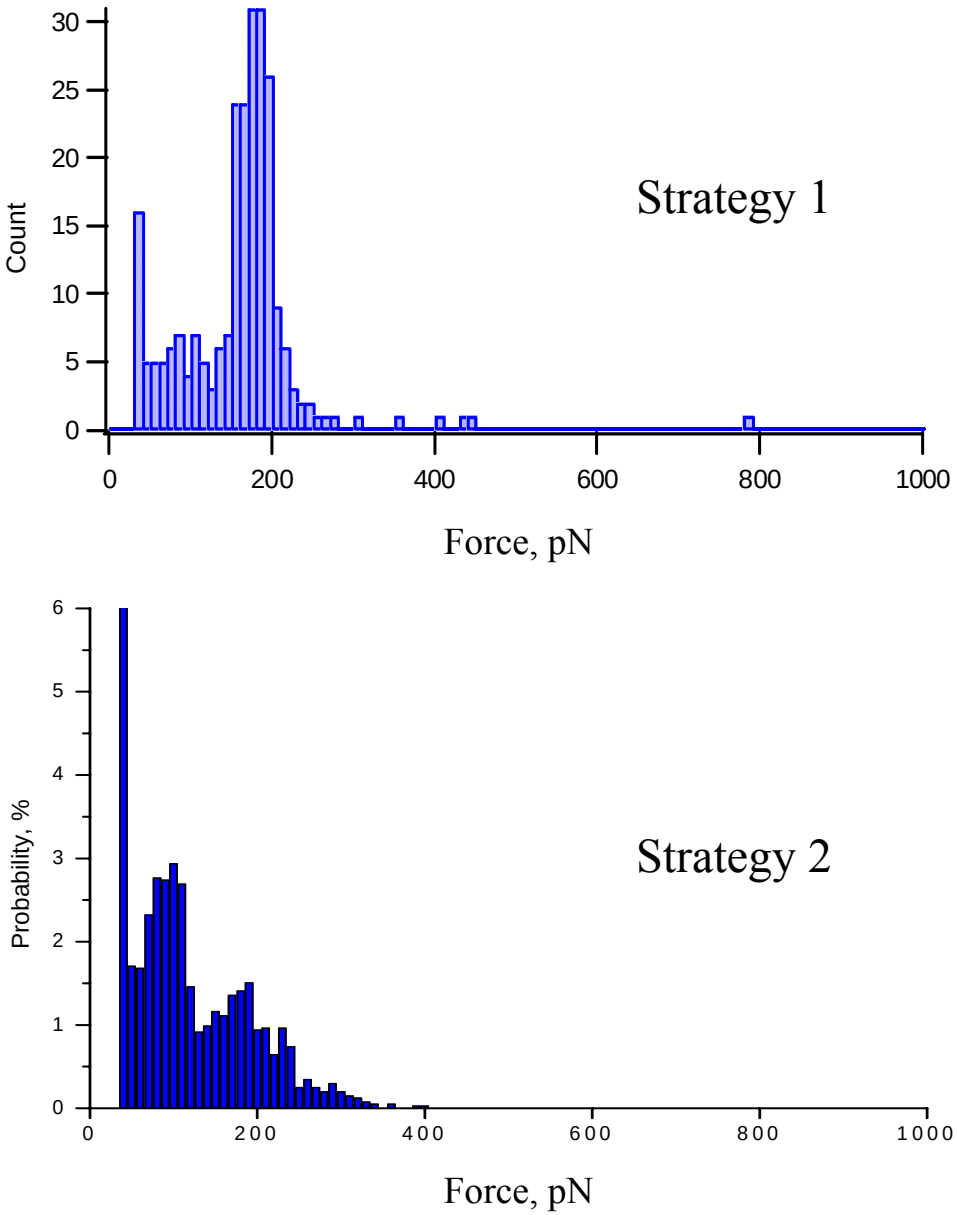

Figure 3.3 Histograms of the observed interactions between covalently immobilized desAB-NDSK on the AFM tip and fibrinogen on the substrate generated via the two Strategies.

nearly identical for both strategies, suggesting the multiple interactions were not the result of protein aggregates or the immobilization methods. Thus, it was concluded that the multiple interactions were more likely the result of complex, specific interactions between desAB-NDSK and fibrinogen. To elucidate which of the specific fibrin-fibrin interactions were contributing to the complex force curves, Strategy 2 was exclusively in subsequent studies with fibrinogen and its fragments.

3.3.3 Comparison of desA-NDSK and desAB-NDSK: Strategy 2. To determine if the multiple peaks in the force curves represented rupture events between "A-a" and "B-b" interactions, the forces between desA-NDSK on the AFM tip and fibrinogen on the substrate were examined. Since desA-NDSK contained only "A" active knobs, no "B-b" interactions were possible between desA-NDSK and fibrinogen. Figure 3.4 illustrates representative histograms comparing the interactions of either desAB-NDSK or desA-NDSK on the AFM tip and fibrinogen on both substrates. No differences were observed in the magnitude and appearance of events when both "A-a" and "B-b" interactions were possible compared to only "A-a" interactions, suggesting "B-b" knob-hole interactions did not contribute to the interactions observed between desAB-NDSK and fibrinogen.

3.3.4 Comparison of fibrinogen, D and DD fragment: Strategy 2. Since fibrinogen is a large, complex molecule with many potential sites for specific interactions, examining the interactions with fragments of fibrinogen may provide more detail as to the specific region of

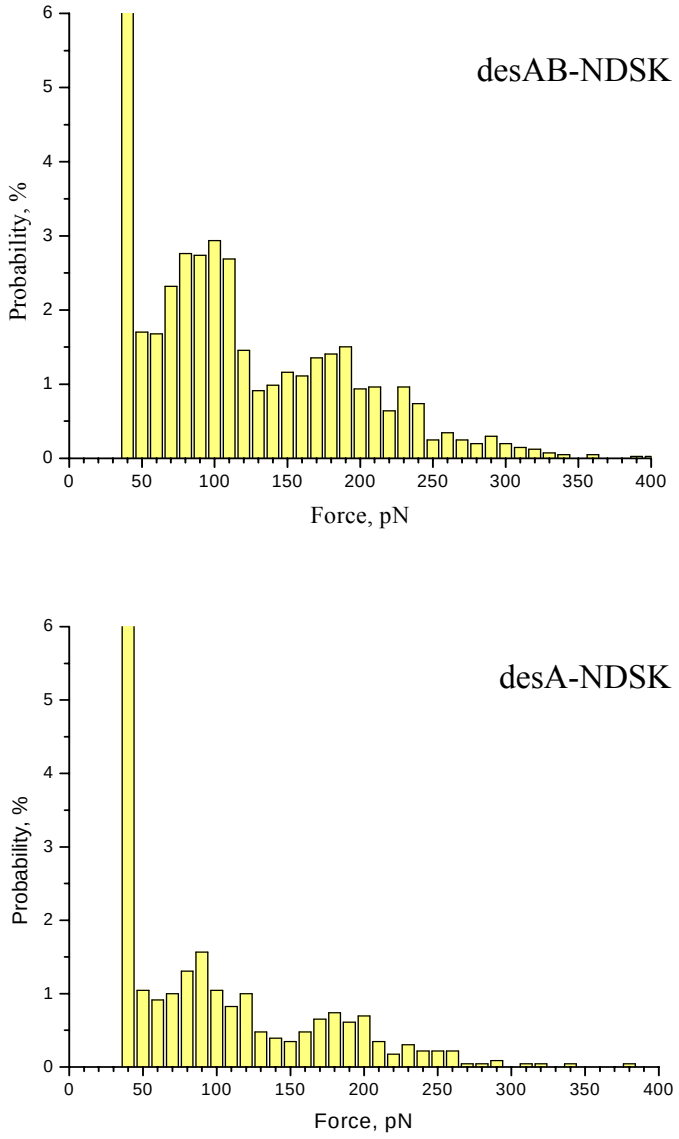

Figure 3.4 Histograms of the observed interactions between covalently immobilized desAB-NDSK (top) and desA-NDSK (bottom) on the AFM tip and fibrinogen on the substrates generated via Strategy 2.

the protein responsible for the multiple interactions. To elucidate whether the surface-bound fibrinogen's coiled-coils or E region were participating in the interaction between desAB-NDSK and fibrinogen, experiments were conducted with the D fragment of fibrinogen instead of the full-length molecule (data not shown). Yet again, no differences between desAB-NDSK interacting with fibrinogen compared to D fragment were observed.

To model "A-a" interactions occurring within protofibrils during fibrin formation, the interaction between desAB-NDSK and DD fragment were examined. Protofibrils are double-stranded, half-staggered polymers held together by interactions between the E regions (similar to desAB-NDSK) of one strand and the two D regions of adjacent molecules in the opposite strand during clotting (Fig. 1.4). The DD fragment is generated from a fully-formed, covalently cross-linked clot and represents the interface of two adjacent molecules within a protofibril. Since desAB-NDSK contains two "A" knobs per fragment, it is possible that an "A-a" bond could form between desAB-NDSK and each of the D regions contained in the DD fragment. To determine how the establishment of two parallel "A-a" interactions would manifest in the histograms generated by Strategy 2, the interaction between desAB-NDSK and DD fragment was examined. Figure 3.5 is a representative histogram of the interactions between desAB-NDSK and DD fragment. The observed interactions between desAB-NDSK and DD fragment did not contain two clearly pronounced populations of forces as was observed between desAB-NDSK and fibrinogen or D fragment. Instead, a broad distribution of forces was observed. Of note, forces significantly greater than 200 pN were not observed, suggesting the observed forces did not represent the rupture of two parallel "A-a" interactions. The implications of the differences observed between DD

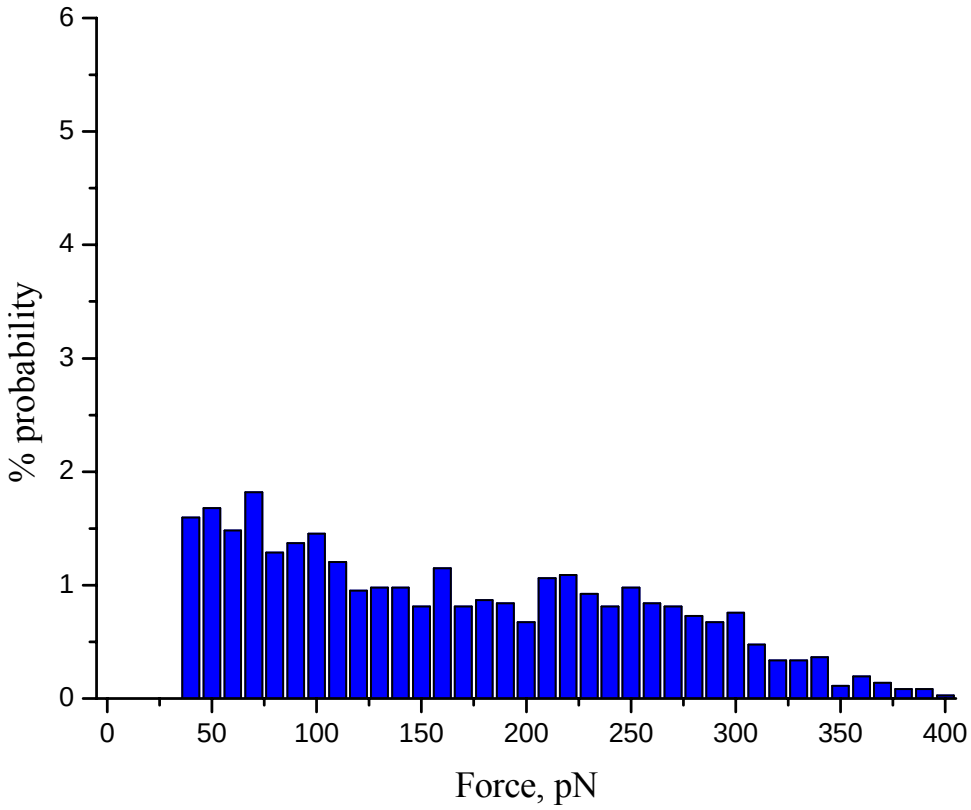

Figure 3.5 Histogram of the observed interactions between covalently immobilized desAB-NDSK on the AFM tip and DD fragment.

fragment and D fragment or fibrinogen were not realized until further along in the progression of this project and is described at the end of this chapter.

3.3.5 Specificity of fibrin(ogen)-fibrin interactions: Strategy 2. Since protein surfaces contain many charged and hydrophobic residues, the potential for non-specific interactions between any two proteins that come into contact with one another exists. As such, great care must be taken during AFM force measurements to both minimize non-specific interactions and to ensure observed events are specific to the biochemical phenomenon of interest. The AFM buffer developed by Dr. Gorkun containing 2 mg/mL BSA and 0.1% Triton X-100 essentially eliminated non-specific interactions between fibrinogen and its fragments in the force range of the specific interactions (> 50 pN). Nevertheless, a population of low magnitude forces (< 50 pN) was still frequently observed (Fig. 3.6 B,C). Figure 3.6 illustrates the interactions observed in the absence of active knobs (NDSK immobilized on the tip, fibrinogen on the substrate) and holes (desAB-NDSK on the tip and BSA on the substrate). The use of an "A-a" inhibitor, Gly-Pro-Arg-Pro-amide, quenched the observed interactions between desAB-NDSK and fibrinogen (Fig. 3.6), indicating the rupture events occurring > 50 pN were the result of specific fibrin-fibrin interactions.

To further illustrate the specificity of the observed interactions, fibrinogen was covalently immobilized to both the tip and substrate allowing the examination of fibrinogen-fibrinogen interactions (Fig. 3.7A). Next, the fibrinogen on the substrate was activated by thrombin to expose "A" and "B" knobs and the fibrinogen-fibrin interactions were examined. Hirudin was used to inhibit thrombin and prevent premature activation of the remaining fibrinogen

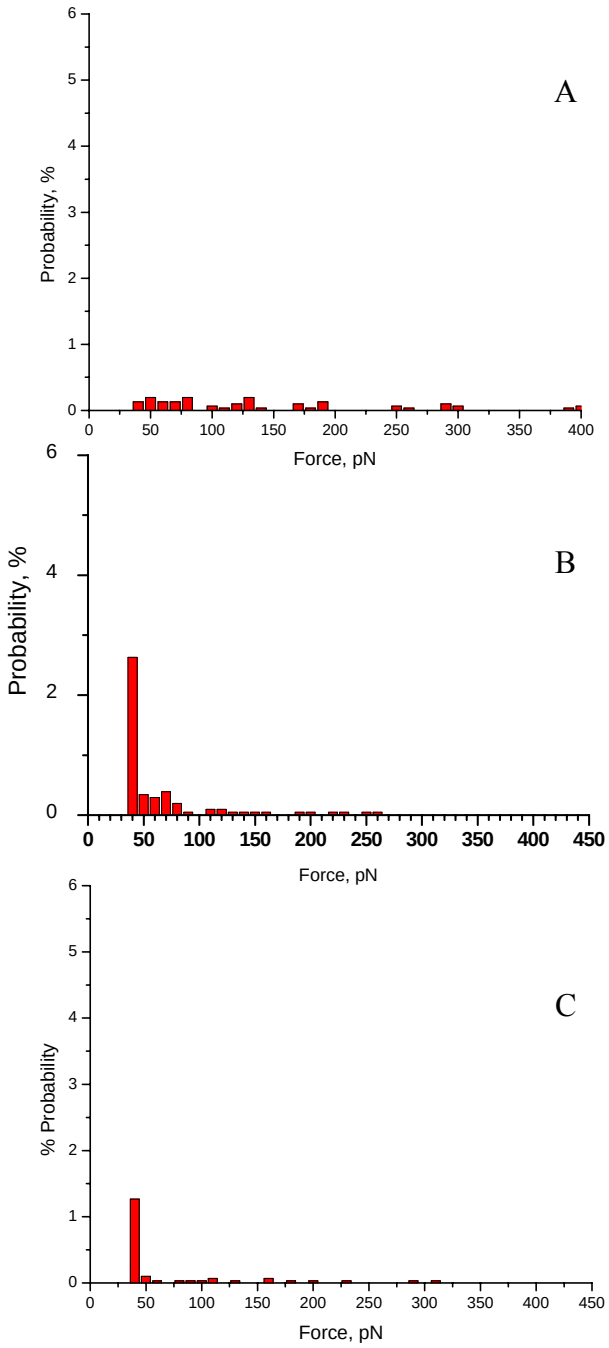

Figure 3.6 Histograms of the observed non-specific interactions between **A.** NDSK and fibrinogen, **B.** desAB-NDSK and BSA, and **C.** desAB-NDSK and fibrinogen in the presence of 2 mM Gly-Pro-Arg-Pro-amide, a specific "A-a" interaction inhibitor.

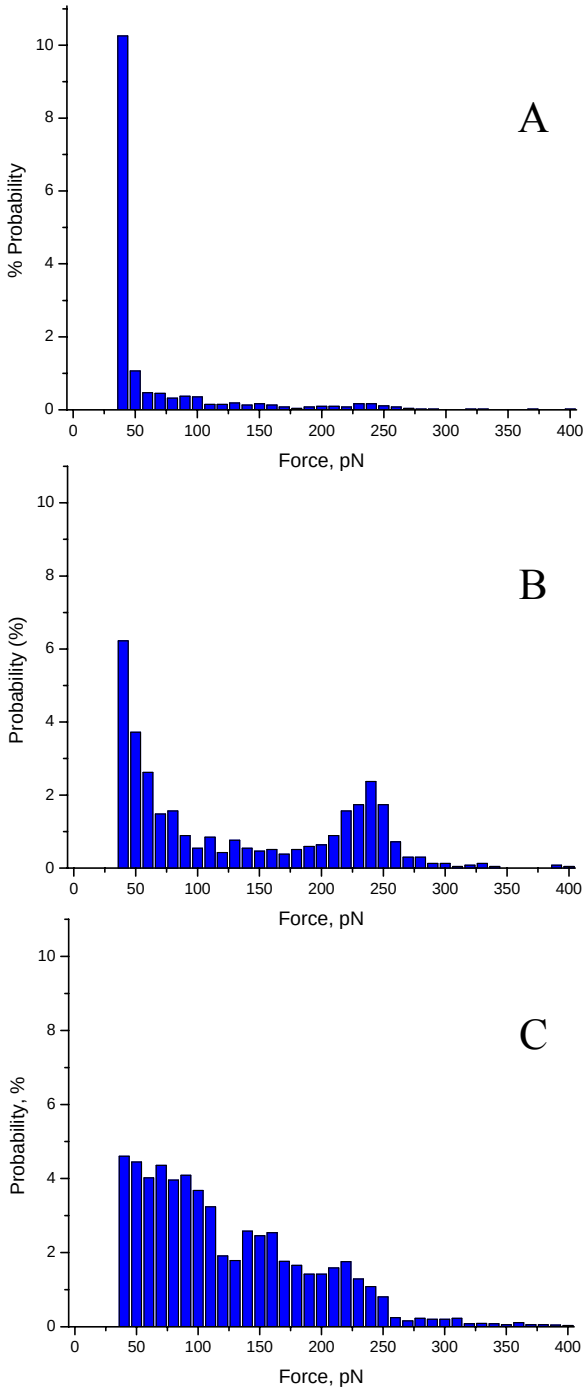

Figure 3.7 Histograms of the observed interactions between **A.** fibrinogen on both surfaces, **B.** fibrin on the substrate and fibrinogen on the tip, and **C.** fibrin on both surfaces.

surface. Finally, the fibrinogen on the tip was activated by thrombin to examine fibrin-fibrin interactions (Fig. 3.7C). As shown in Figure 3.7A, predominately events of low force (< 50 pN) were observed between fibrinogen and itself. Upon converting fibrinogen to fibrin, specific forces appeared and increased in probability as both surfaces were activated (Fig. 3.7B+C), suggesting the interactions were dependent upon the exposure of active knobs.

3.4 Conclusions

The interaction between fibrin(ogen)-fibrin was more complex than anticipated based on results from previous laser tweezers studies (1). To elucidate whether the multiple interactions observed were the result of a single interaction between multiple pairs of molecules (i.e. one "A-a bond between two fibrin-fibrinogen pairs) or multiple interactions between a single pair of molecules (i.e. one "A-a" and "B-b" bond between a single fibrin-fibrinogen pair), modifications were made to both the sample preparation and data collection methods. Since decreasing the amount of protein immobilized on the AFM surfaces only decreased the overall number of interactions and not their complexity, it was unlikely that a single interaction was occurring between multiple molecular pairs. The multiple events observed in the force curves were likely the result of a complex series of interactions between a single molecule on the AFM tip and a single molecule on the substrate. Several studies were completed to investigate potential sites of interactions such as "A-a" and "B-b" knob-hole interactions or αC-Bβ chain interactions.

DesA-NDSK and desAB-NDSK interacted similarly with fibrinogen and D fragment, suggesting "B-b" and αC-Bβ chain interactions were not participating in the interaction between desAB-NDSK and fibrinogen. Of note, the interactions between desAB-NDSK and

DD fragment were different than desAB-NDSK and fibrinogen, but the exact nature of the difference was indiscernible by the software generously written by Dr. Taylor. As a result of the major advances in protein immobilization and data collection, it became clear that the data analysis method was insufficient for examining the complex rupture patterns consistently observed between fibrin(ogen) and fibrin. To assist with data analysis, a formal collaboration with Dr. Boris Akhremitichev was established. Dr. Akhremetichev provided the Schoenfisch lab with custom MatLab v. 7.1 (MathWorks, Natick, MA) software designed to analyze complex ruptures more thoroughly (13). The new analysis method coupled with several additional experiments enabled an in-depth examination of fibrin-fibrin interactions. The final result was a complex and fascinating study elucidating the nature of the intricate interactions observed between desAB-NDSK and fibrinogen as discussed next.

3.5 Evolution of the Project

The majority of the work described in this chapter detailed the protein immobilization and data collection method development used to study fibrin-fibrin interactions by AFM. However, major collaborative advancements in data analysis subsequent to my independent contributions to this project, especially the custom software generously provided by Dr. Akhremitichev and analysis methods by Laurel Averett, enabled a thorough re-examination of the data presented in this chapter. Upon the re-examination of the data and several additional experiments by Laurel, a characteristic pattern of forces related to the rupture of the "A-a" knob-hole interaction emerged. Careful control experiments ruled out all known fibrin-fibrin interactions as the source of the complex characteristic pattern and the "A-a" bond was identified as the sole tether between desAB-NDSK on the tip and fibrinogen on the

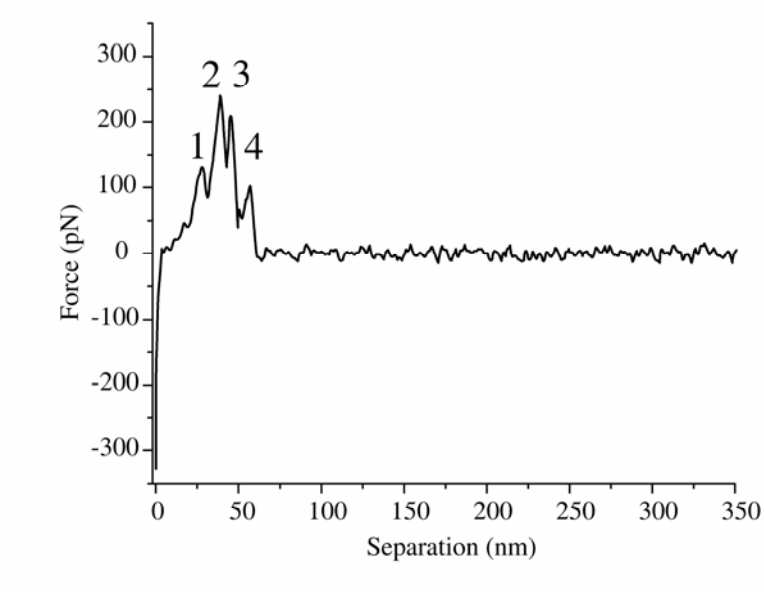

Figure 3.8 Representative force versus separation curve showing the prevalent pattern of the rupture of interactions between desAB-NDSK (tip) and fibrinogen (substrate). Curves with any combination of the 4 events shown here were identified as the characteristic pattern of rupture. All characteristic curves included the doublet of events above 200 pN (event 2 & 3).

substrate. The characteristic pattern of forces shown in Figure 3.8 illustrates the "signature" 4-event rupture pattern observed between desAB-NDSK and fibrinogen. The histogram resulting from the analysis of all events in the characteristic pattern is represented in Figure 3.9. Re-examination of the DD fragment data indicated the complexity of the characteristic pattern was due to structural changes within the D region of fibrinogen upon the rupture of the "A-a" bond. Since the DD fragment has a covalent cross-link and a large interfacial region between the two D fragments in the dimer (Fig. 3.1), the structure of this fragment is substantively more rigid than that of D fragment or fibrinogen's D region alone and deformations did not readily occur with this fragment (14).

In summary, this project was highly collaborative in nature and relied on the diverse expertise of several researchers with backgrounds in biochemistry, analytical chemistry, biophysics and physics. It represents the first comprehensive study of the complexity of the "A-a" knob-hole interaction measured by AFM.

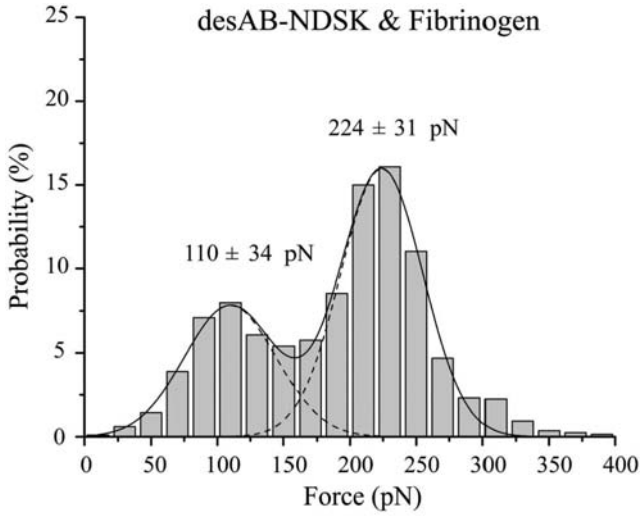

Figure 3.9 Distribution of forces observed between desAB-NDSK immobilized on the AFM tip and fibrinogen immobilized on the substrate. Bin size = 20 pN.

REFERENCES

(1) Litvinov, R. I.; Gorkun, O. V.; Owen, S. F.; Shuman, H.; Weisel, J. W. "Polymerization of fibrin: specificity, strength, and stability of knob-hole interactions studied at the single-molecule level." *Blood* 2005**,** *106*, 2944-2951.

(2) Litvinov, R. I.; Gorkun, O. V.; Galanakis, D. K.; Yakovlev, S.; Medved, L.; Shuman, H.; Weisel, J. W. "Polymerization of fibrin: Direct observation and quantification of individual B:b knob-hole interactions." *Blood* 2007**,** *109*, 130-138.

(3) Gorkun, O. V.; Litvinov, R. I.; Veklich, Y. I.; Weisel, J. W. "Interactions mediated by the N-terminus of fibrinogen's Bbeta chain." *Biochemistry* 2006**,** *45*, 14843-14852.

(4) Levy, R.; Maaloum, M. "Specific molecular interactions by force spectroscopy: From single bonds to collective properties." *Biophysical Chemistry* 2005**,** *117*, 233-237.

(5) Fisher, T. E.; Oberhauser, A. F.; Carrion-Vazquez, M.; Marszalek, P. E.; Fernandez, J. M. "The study of protein mechanics with the atomic force microscope." *Trends in Biochemical Sciences* 1999**,** *24*, 379-384.

(6) Clausen-Schaumann, H.; Seitz, M.; Krautbauer, R.; Gaub, H. E. "Force spectroscopy with single bio-molecules." *Current Opinion in Chemical Biology* 2000**,** *4*, 524-530.

(7) Heinz, W. F.; Hoh, J. H. "Spatially resolved force spectroscopy of biological surfaces using the atomic force microscope." *Trends in Biotechnology* 1999**,** *17*, 143-150.

(8) Zlatanova, J.; Lindsay, S. M.; Leuba, S. H. "Single molecule force spectroscopy in biology using the atomic force microscope." *Progress in Biophysics and Molecular Biology* 2000**,** *74*, 37-61.

(9) Okumura, N.; Gorkun, O. V.; Lord, S. T. "Severely impaired polymerization of recombinant fibrinogen gamma-364 Asp --> His, the substitution discovered in a heterozygous individual." *J Biol Chem* 1997**,** *272*, 29596-29601.

(10) Kostelansky, M. S.; Bolliger-Stucki, B.; Betts, L.; Gorkun, O. V.; Lord, S. T. "b-beta Glu397 and b-beta Asp398 but not b-beta Asp 432 are required for "B:b" interactions." *Biochemistry* 2004**,** *43*, 2465-2474.

(11) Kostelansky, M. S.; Betts, L.; Gorkun, O. V.; Lord, S. T. "2.8 A crystal structures of recombinant fibrinogen fragment D with and without two peptide ligands: GHRP binding to the "b" site disrupts its nearby calcium-binding site." *Biochemistry* 2002**,** *41*, 12124-12132.

(12) Evans-Nguyen, K. M.; Schoenfisch, M. H. "Fibrin proliferation at model surfaces: influence of surface properties." *Langmuir* 2005**,** *21*, 1691-1694.

(13) Hirayama, A.; Noronha-Dutra, A. A.; Gordge, M. P.; Neild, G. H.; Hothersall, J. S. "*S*-nitrosothiols are stored by platelets and released during platelet-neutrophil interactions." *Nitric Oxide* 1999**,** *3*, 95-104.

(14) Yang, Z.; Pandi, L.; Doolittle, R. F. "The crystal structure of fragment double-D from cross-linked lamprey fibrin reveals isopeptide linkages across an unexpected D-D interface." *Biochemistry* 2002**,** *41*, 15610-15617.

CHAPTER 4

INFLUENCE OF GLUTATHIONE AND ITS DERIVATIVES ON FIBRINOGEN POLYMERIZATION

4.1 Introduction

The complex relationship between glutathione species (GSX) found in the blood has been used to diagnose and monitor a number of disease states (1-4). For example, increased glutathione (GSH) found in the lungs have been associated with cystic fibrosis, chronic obstructive airway disease, and asthma (5). Conversely, the nitrosated analogue, *S*-nitrosoglutathione (GSNO), has been used as a treatment for a number of cardiovascular disorders due to its anti-platelet (6-11) and vasodilatory effects (12-15). As shown in Figure 4.1, endogenously GSH is converted to GSNO through nitrosative species (N_2O_3) and other redox mechanisms involving transition metal centers (16). In plasma, GSNO and other nitrosothiols react readily with protein thiols (e.g., free cysteine residues of serum albumin) to form stable protein-SNO complexes that serve as the ultimate sink for circulating NO (17, 18). The transfer of NO from low molecular weight thiols to proteins occurs via transnitrosation (direct transfer of NO from one thiol to another). Transnitrosation is responsible for much NO transport in vivo resulting in a dynamic relationship between the high concentrations of GSH (500 μM) and the transient RSNO species (2 μM) in blood (Figure 4.1). Moreover, GSH can directly decompose nitrosothiol donors to form disulfides (e.g., GSSG) and multiple NOx species (19, 20).

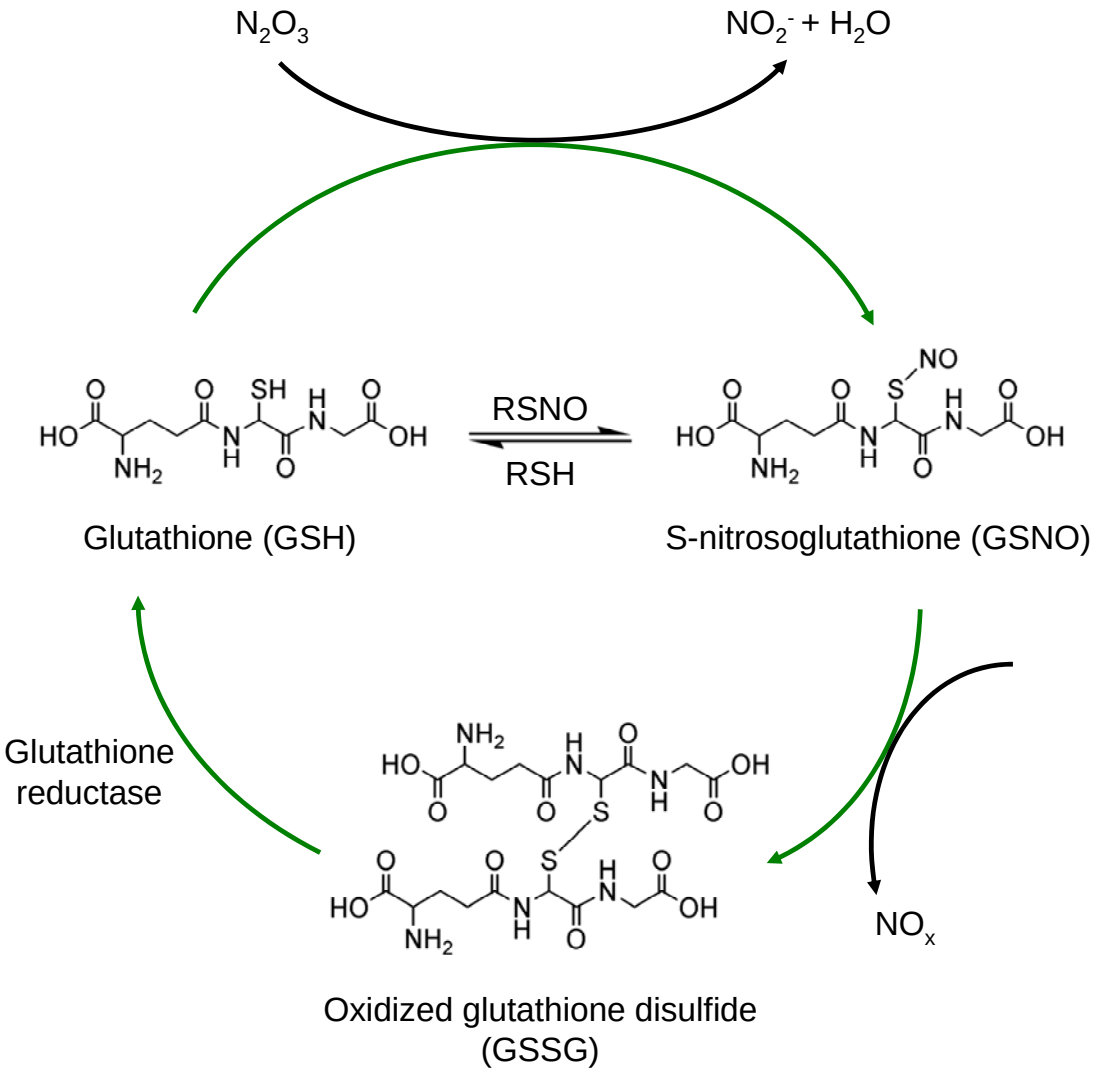

Figure 4.1. Schematic of the interconversion between GSH, GSSG and GSNO species.

In a number of cases transnitrosation reactions of GSNO have been shown to result in *S*-thiolation, forming mixed disulfides between proteins and glutathione (21). The most significant example is thiolation of protein disulfide isomerase (PDI) by GSNO on the surface of platelets (22-24). The NO released from glutathionylation of PDI diffuses across the plasma membrane and inhibits platelet activation via a guanylyl-cyclase dependent mechanism (6). The mixed disulfide also plays a role in inhibiting platelet aggregation by interfering with the enzymatic function of PDI (22-24). Due to GSNO's ability to mitigate platelet adhesion and aggregation, a number of animal and clinical studies have been conducted using GSNO and other nitrosothiols as novel anti-thrombotic agents (8-11). Since activated platelets initiate the coagulation cascade, platelets have been an excellent target for RSNO intervention. However, little emphasis has been placed on the effects of nitrosothiols and their decomposition products on subsequent aspects of thrombosis, specifically fibrinogen and fibrin formation.

Fibrinogen, a 340 kDa plasma protein, is composed of two copies each of three polypeptide chains, Aα, Bβ and γ (Fig. 1.1) (25). Fibrinogen polymerizes upon activation by the enzyme thrombin to form a fibrin clot. In vivo, fibrin serves as the structural scaffolding of the blood clot by stabilizing the initial platelet plug and localizing important wound healing and inflammation factors to the site of injury. The transformation of fibrinogen to fibrin occurs in a multi-step process (Fig 1.4). Thrombin cleaves fibrinopeptide A (FpA) from the N-terminus of fibrinogen's Aα chains, exposing a new amino acid sequence (the "A" knob) and generating fibrin monomer (25). The "A" knobs interact with holes "a" in other fibrin molecules to form double-stranded, half-staggard protofibrils. Thrombin also cleaves fibrinopeptide B (FpB) from the N-termini of the Bβ chains, exposing the "B" knobs

that interact with holes "b" to form "B-b" interactions. Upon removal of FpB, protofibrils lengthen, branch and laterally aggregate to form fibers. Protofibril lateral aggregation is thought to be mediated predominantly by "B-b" interactions and intermolecular αC-αC interactions between the C-termini of the Aα chains (26, 27).

Mutus and co-workers examined the effects of GSNO on the initial rates of fibrin formation and found 4.0 ± 1.0 μM GSNO was sufficient to inhibit the initial rate by 50% (28). GSNO-dependent structural changes in fibrinogen were studied using circular dichroism and tryptophan fluorescence spectroscopy. The authors concluded that the observed inhibition was due to conformational changes in the C-terminal region of fibrinogen's α chain induced by GSNO binding. In this chapter, the role of the reduced, oxidized and nitrosated derivatives of glutathione on the entire process of fibrin formation are examined with the goal to expand the previous work beyond the exploration of initial rates of fibrin formation. Lag time, V_{max}, and final optical densities (OD) were examined for fibrinogen solutions treated with each of the GSX species and compared to normal. Studies were also conducted to examine the rates of fibrinopeptide cleavage and the polymerization of a variant fibrinogen missing the αC domains to elucidate the mechanistic effects of nitrosothiols on fibrin formation.

4.2 Experimental Methods

4.2.1 Materials. Reagents were of analytical grade and purchased from Sigma (St. Louis, MO) unless noted otherwise. Human plasma fibrinogen (FIB 1) and α-thrombin (HT 2970PA) were purchased from Enzyme Research Laboratories (Southbend, IN). Fibrinogen was stored at -80 °C, thawed at 37 °C for 10 min and maintained at ambient temperature. The

buffer for all experiments was 20 mM HEPES, 150 mM NaCl, 1 mM $CaCl_2$, pH 7.4 (HBSC). Protein concentration was determined using an extinction coefficient of 1.51 or 1.6 at 280 nm for a 1 mg/mL solution of normal fibrinogen and Aα251 fibrinogen, respectively (29). Recombinant normal and Aα251 fibrinogen were prepared as described previously (29, 30). Thrombin aliquots were freshly thawed, diluted to 10 U/mL and stored on ice. Immediately prior to experiments, thrombin was diluted to 0.1 U/mL. Reduced and oxidized glutathione solutions, GSH and GSSG, respectively, were dissolved in HBSC and stored on ice.

4.2.2 Synthesis of S-nitroso-glutathione (GSNO). GSNO was synthesized according to a previously reported procedure (31). Briefly, 100 mg of GSH were dissolved in 10 mL of 2 M HCl at 0 °C and treated with a 2:1 molar excess of $NaNO_2$. After stirring for 30 min in the dark, 25 mL of acetone were added to the red solution and stirred for an additional 10 min on ice. The pink GSNO precipitate was recovered via filtration, washed with cold water (2 x 10 mL) and cold ether (2 x10 mL), dried under vacuum and stored at -20 ºC in the dark. To minimize thermal decomposition, GSNO was kept on ice in the dark and diluted immediately prior to use for each experiment.

4.2.3 Fibrinogen Polymerization Assays. Experiments were performed in triplicate using medium-binding 96-well microtiter plates. Fibrinogen (100 µl) and either GSH, GSNO or GSSG (100 µL) was added to each well and incubated at 37 ºC for 10 min. Next, thrombin (100 µl) was simultaneously added to each well to initiate fibrinogen polymerization. Changes in optical density (OD) were monitored at 405 nm using a SpectraMax plate reader. Final concentrations after all dilutions varied from 2-0.07 mg/mL (6-0.2 µM) fibrinogen and

500-0.03 μM GSH, GSSG or GSNO. A final thrombin concentration of 0.03 U/mL (0.3 nM) was used for all polymerizations.

4.2.4 Analysis of Polymerization Results. The maximum velocity of polymerization (V_{max}) was determined as the steepest part of the polymerization curve by finding the maximum value of the 1st derivative. Lag time was measured as the time of initial increase in optical density (OD) and the final OD was the turbidity value at the plateau in the polymerization curve. A p value of ≤ 0.05 was considered significant according to unpaired t-tests.

4.2.5 Fibrinopeptide Release. To initiate fibrinopeptide release, thrombin (10 μL of 1 U/mL) was added to fibrinogen (2 mL of 0.1 mg/mL), mixed by inversion and pipetted into 240 μL aliquots. All protein manipulations were completed within 1 min after thrombin addition. The reaction was quenched by placing each tube in boiling water for 15 min at 2, 5, 10, 20, 40, 80 or 120 min after thrombin addition. The boiled samples were stored on ice for the duration of the experiment. Fibrinogen (240 μL) not treated with thrombin and fibrinogen (240 μL) treated for 60 min with an excess of thrombin (1 μL of 2360 U/mL) served as controls for no fibrinopeptide release and complete fibrinopeptide release, respectively. Samples were spun for 10 min and the supernatant containing fibrinopeptides was stored at -80 ºC before detection by reverse-phase HPLC monitored at 210 nm as previously described (32). The percent of FpA and FpB released was calculated relative to the amount of FpA or FpB detected after excess thrombin treatment. The rates of FpA and FpB release were determined using kinetic equations described previously (33).

4.3 Results and Discussion

4.3.1 GSX Influence on Polymerization. The dose-dependent effects of GSNO were evaluated over the entire process of fibrinogen (0.07 mg/mL) polymerization. Similar to results by Mutus and co-workers, inhibition of fibrin formation was observed (maximum inhibition at 500 μM, Fig. 4.2). The effects of reduced glutathione (GSH), the physiological precursor to GSNO, on fibrin formation were also investigated. Unlike previously reported, the influence of GSH on fibrin formation was the same as GSNO. Similar behavior was observed for the exogenous RSNO donor *S*-nitroso-*N*-acetyl-DL-penicillamine (SNAP), the free thiol *N*-acetyl-DL-penicillamine (NAP), and the simplified derivative *N*-acetyl-DL-cysteine, suggesting a clear relationship between the presence of reactive thiols and the inhibition of fibrin formation (data not shown). The presence of *N*-acetyl-DL-serine (containing an alcohol moiety instead of a thiol) showed no effect on fibrin formation up to 600 μM, analogous to the effects of carboxymethylated GSH (containing a protected, unreactive thiol moiety) reported by Akhter et al..

Due to the abundance of GSH in plasma, the therapeutic utility of GSNO and the role of GSSG as a predicative marker for oxidative stress, the mechanistic effects of these species on fibrin formation were explored. The representative polymerization curves for normal fibrinogen and in the presence of 500 μM GSNO are shown in Figure 4.2. Relative to normal polymerization, glutathione and related derivatives delayed the fibrin formation, as evidenced by a reduced rise in turbidity and lower the final optical density (Fig. 4.2). Based on methods described previously, three parameters related to critical aspects of fibrin formation were obtained from the polymerization curves (34). The lag time, representative of the rate of protofibril formation (Fig. 4.2A), was measured when an increase in turbidity

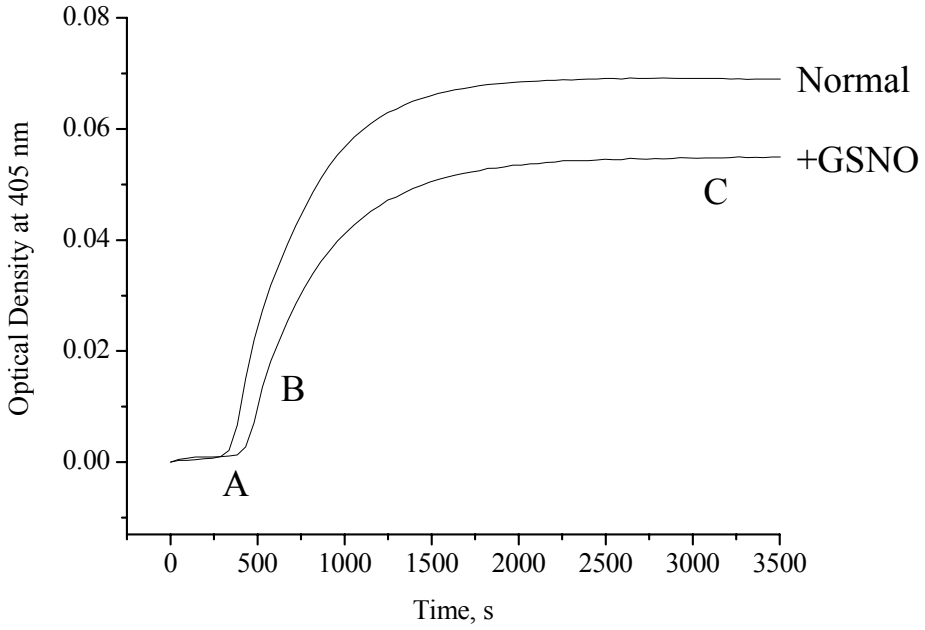

Figure 4.2 Turbidity curves monitored spectrophotometrically at 405 nm comparing the polymerization of 0.07 mg/mL fibrinogen and 0.03 U/mL thrombin with and without GSNO. The three phases of the polymerization curves are as follows: **A.** Lag time is the time at when an increase in optical density was observed, **B.** region of the polymerization curve corresponding to the lateral aggregation of protofibrils, **C.** Final optical density of the turbidity curves (proportional to fibrin fiber diameter).

was first detected. Factors that influence the lag time are the rate of FpA release and the ability of the activated fibrin monomers to interact with one another (34). In the subsequent phase of polymerization, the protofibrils laterally aggregate to form fibers, leading to an increase in optical density in the polymerization curve (Fig. 4.2B). Both FpB release (leading to "B-b" interactions) and αC-αC intermolecular interactions have been shown to influence lateral aggregation of protofibrils (26, 35). The maximum rate of lateral aggregation or V_{max} appears at the steepest part of the polymerization curve. The final optical density (Fig. 4.2C) is proportional to the average fibrin fiber diameter and may provide insight into the structure of the resulting clot (34). In general, clots formed from thicker fibers are more permeable and susceptible to lysis compared to clots formed from thinner fibers (36).

Figure 4.3 summarizes the three parameters of fibrinogen polymerization in the presence of GSH, GSSG and GSNO relative to normal conditions. For clarity the results are reported as percentages of normal. The addition of GSH, GSSG and GSNO caused a ~20% increase in lag time compared to normal; V_{max} was reduced. Compared to GSNO, the inhibition of V_{max} was less for GSH or GSSG, but this difference was not significant according to an unpaired t-test ($p = 0.11$ and $p = 0.16$, respectively). The addition of GSH or GSSG led to a ~30% reduction in turbidity, whereas only a ~20% reduction was observed with GSNO. The small difference in GSNO's influence on final OD was significant compared to GSH ($p = 0.05$) but not significant compared to GSSG ($p = 0.12$). As would be expected, the final optical densities of all the clots formed in the presence of glutathione and its derivatives were reduced compared to normal.

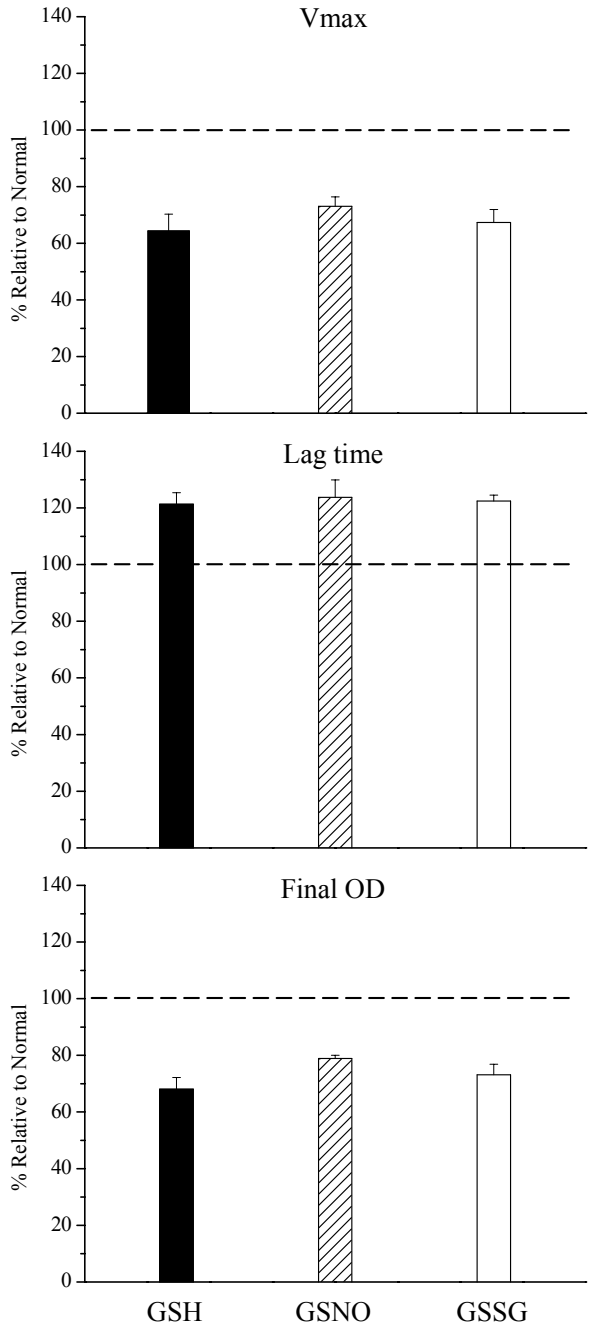

Figure 4.3 The maximum rate of lateral aggregation (V_{max}), clotting onset time (lag time) and final clot turbidity (OD) calculated relative to normal fibrin polymerization obtained from the turbidity curves in Figure 4.2. The values obtained for normal were defined as 100% and are denoted by the dashed lines.

Based on the results obtained from the polymerization curves, GSH, GSNO and GSSG influence fibrin formation to the same extent, contradicting a previous report that found GSNO but not GSSG influenced the initial rates of fibrin formation (28). The authors did not examine the effects of unmodified GSH on polymerization of fibrinogen. Importantly, two major differences between the experiments presented in this chapter and those reported previously exist. First, the polymerization assays described herein examined the entire polymerization process instead of the first 100 s. Second, the concentrations of fibrinogen and thrombin used in this study were lower compared to those used in the previous work. The lower concentration of thrombin was chosen to slowly polymerize fibrinogen to allow observation of early phases of fibrin formation that are difficult to observe at higher thrombin concentrations.

Since the concentration of GSH in blood is higher than GSSG and GSNO, the remainder of this chapter is focused on an in-depth analysis of fibrin formation in the presence of GSH. The work presented herein expands the significance of GSX's influence on fibrin formation and suggests a regulatory role of glutathione in blood on fibrin formation

4.3.2 Dose-Dependent Effect of GSH. The concentration of GSH in blood has been shown to fluctuate in response to numerous disease states (4, 37-40). For example, GSH levels increase in response to the oxidative stress induced by cigarette smoking (38, 39). Consequently, investigation of the concentration dependence of GSH's influence on fibrin polymerization may prove useful in understanding a broader impact of the up- or down-regulation of this important antioxidant.

The polymerization of 0.07 mg/mL fibrinogen was examined over a range of GSH concentrations (32 nM to 500 μM). Figure 4.4 summarizes the dose-dependent effects of GSH on each of the polymerization parameters obtained from the polymerization curves (data not shown). As expected, the greatest inhibition was observed at the largest GSH concentration (500 μM) where the lag time was prolonged by ~20% and the V_{max} slowed by 30%, indications that GSH impaired protofibril formation and lateral aggregation, respectively. Of note, 100 and 500 μM GSH had the same effect on fibrin formation, suggesting maximal inhibition was achieved. The three lowest concentrations of GSH (32, 160 and 800 nM) did not significantly affect fibrin formation. The dose-dependent influence of GSH on fibrinogen polymerization suggests changes in glutathione levels in response to oxidative stress or disease could also affect fibrin clot formation.

4.3.3 The Effect of GSH on Thrombin Activity. Prolonged lag times and decreased rates of lateral aggregation were observed for the polymerization of 0.07 mg/mL fibrinogen at GSH concentrations above 800 nM and 500 μM GSH using fibrinogen concentrations less than 0.25 mg/mL. Previous studies have demonstrated that lag time is affected by the rate of FpA release (e.g., thrombin's activity) and fibrin monomer assembly into protofibrils. Similarly, the rate of lateral aggregation is influenced by FpB release and/or the assembly of protofibrils into branched, thicker fibers. To determine if GSH impaired thrombin's ability to activate fibrinogen thrombin activity was assayed directly. The most common method used for assaying thrombin activity is based on a chromogenic substrate that undergoes a measurable absorption maximum shift upon cleavage by thrombin. The intensity of the color change is proportional to the concentration of cleaved substrate and can be related to the activity of

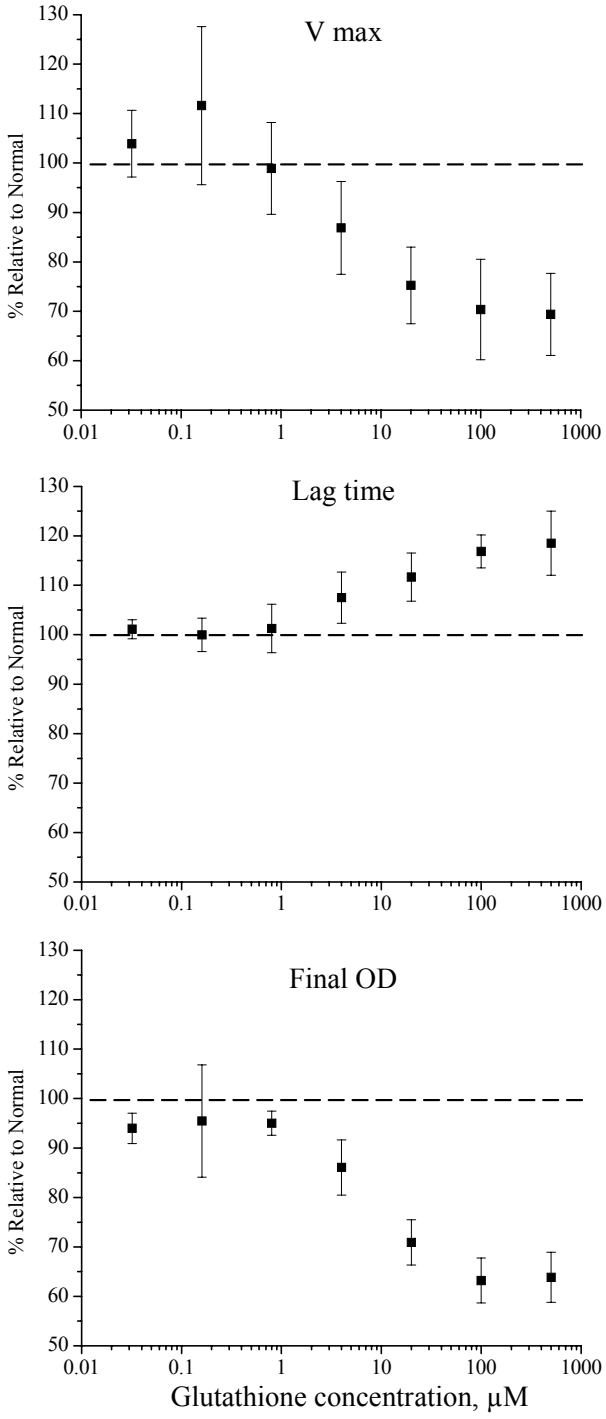

Figure 4.4 The V_{max}, lag time and final OD calculated relative to normal (no glutathione) fibrinogen polymerization of 0.07 mg/mL fibrinogen with 0.03 U/mL thrombin as a function of glutathione concentration. The values obtained for normal were defined as 100% and are denoted by the dashed lines.

thrombin. Unfortunately, the chromogenic assay only probes the function of thrombin's active site and not the enzyme's ability to bind fibrinogen and cleave fibrinopeptides. As an alternative approach to the chromogenic assay, thrombin's ability to cleave FpA and FpB from fibrinogen in the presence of GSH was measured directly via reverse-phase HPLC. Table 4.1 summarizes the kinetic constants for fibrinopeptide release with and without 500 μM GSH.

No significant difference in the rate of FpA or FpB release from fibrinogen was observed in the presence of GSH compared to the absence, indicating a minimal GSH influence on thrombin. Since fibrinopeptide release was normal under these conditions, the activation of fibrinogen to fibrin monomer and the release of FpB from protofibrils are assumed to be unaffected. As such, fibrinogen activation is not influenced by GSH. More likely, the effects of GSH on fibrinogen polymerization are the result of changes in the fibrinogen molecule that preclude its interaction with other fibrin molecules during fibrin formation.

4.3.4 Influence of Fibrinogen Concentration. The normal rates of fibrinopeptide cleavage observed in the presence of GSH suggest that structural changes in fibrinogen are responsible for the inhibited rates of protofibril formation/aggregation. To determine the influence of fibrinogen concentration, the concentration of fibrinogen was varied from 0.07 to 2 mg/mL in the presence of 500 μM GSH. The results of the polymerization curves and parameters of polymerization relative to the normal polymerization of fibrinogen at each concentration are shown in Figure 4.5. As the fibrinogen concentration increased from 0.07 mg/mL to 2.0 mg/mL, an inversion of GSH's effect on polymerization was observed at 0.25 mg/mL. At fibrinogen concentrations below 0.25 mg/mL, GSH appeared to slow protofibril formation

Table 4.1. Rate of thrombin-catalyzed FpA and FpB from normal and GSH-treated fibrinogen as detected by HPLC.

	Rate of FpA Release (10^{-2} $M^{-1}s^{-1}$)		Rate of FpB Release (10^{-2} $M^{-1}s^{-1}$)	
Experiment	-GSH	+ GSH	-GSH	+ GSH
1	2.10 ± .16	1.56 ± .12	1.57 ± .79	1.35 ± .07
2	1.66 ± .08	1.51 ± .05	1.23 ± .06	9.56 ± .04
3	1.68 ± .06	2.10 ± .10	1.42 ± .05	1.55 ± .08
Average	1.81 ± .25	1.72 ± .33	1.41 ± .17	1.29 ± .30

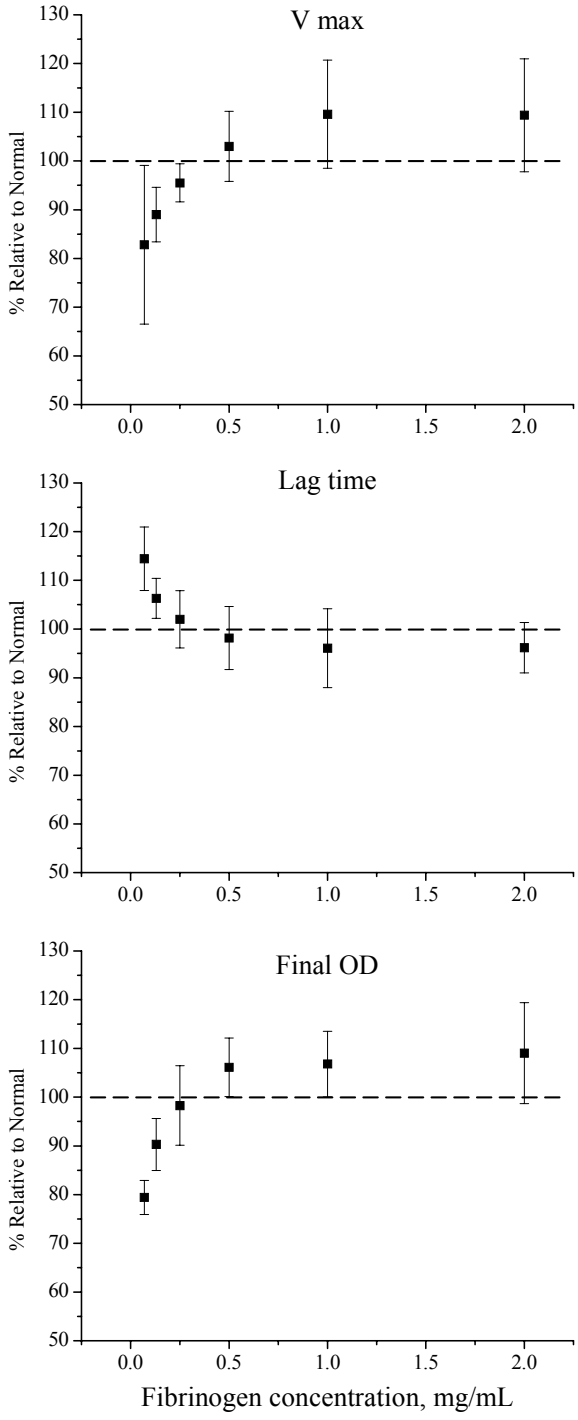

Figure 4.5 The V_{max}, lag time and final OD calculated relative to normal (no glutathione) fibrinogen polymerization for each fibrinogen concentration with 0.03 U/mL thrombin and 500 μM glutathione. The values obtained for normal were defined as 100% and are denoted by the dashed lines.

and lateral aggregation as evidenced by prolonged lag times and lower V_{max} values, respectively (Fig. 4.5). The final OD's of the resulting clots were also reduced with GSH compared to the normal clots at each concentration (Fig. 4.5). At fibrinogen concentrations above 0.25 mg/mL, GSH had the opposite effect: V_{max} was accelerated, the lag times were shorter, and the final ODs were larger compared normal clots at each concentration. GSH's influence on fibrin formation is thus dependent on fibrinogen concentration.

4.3.5 Mechanism of GSH's Effect on Fibrin Formation. Mutus and co-workers proposed several regions within the C-terminus of fibrinogen's α chain (e.g., αC regions) as potential sites of interaction with GSNO (28). Since no substantive differences were observed between the effects of GSNO, GSH and GSSG herein, the impairment of fibrin formation likely does not result from specific interactions between GSNO and aromatic residues within fibrinogen. Rather, GSH and its derivatives act on fibrinogen in a thiol-specific manner partially reducing disulfide bonds, leading to structural and functional alterations. Indeed, fibrinogen contains 29 disulfide bonds, two of which are located in the highly solvent-accessible αC regions of the molecule (Fig. 1.2). Due to their flexible structure and location (on the exterior of fibrinogen), the C-termini of the α chains are readily susceptible to reduction and/or degradation.

To determine if GSH alters fibrin formation via interaction with the αC regions, Aα251 recombinant fibrinogen was employed. Aα251 fibrinogen contains normal Bβ and γ chains, but only the first 251 residues of the Aα chain (29). In other words, Aα251 lacks the αC regions.

Aα251 polymerization as a function of GSH is shown in Figure 4.6. As evidenced by identical turbidity curves, GSH had no measurable effect on the polymerization of Aα251. Previous work has demonstrated the importance of αC regions in polymerization (26, 41, 42). Fibrin formation for fibrinogen mutants lacking αC regions were characterized by prolonged lag times and reduced V_{max} values, similar to the effects of exposure to GSH and its derivatives reported herein at low fibrinogen concentrations. It is reasonable to conclude that reductions in the disulfide bridge in the αC regions induced by GSH, GSNO or GSSG may lead to changes in fibrin formation similar to those observed when functional αC regions are not present.

4.4 Conclusions

The studies reported herein represent the first examination of the influence of reduced, oxidized and nitrosated glutathione on the entire process of fibrin formation. Based on turbidity measurements, each of the glutathione derivatives inhibited fibrin formation to the same degree according to turbidity measurements. While it is possible that GSH, GSSG, and GSNO interact via different mechanisms, a more likely explanation of the observed inhibition is that the glutathione species undergo thiolation reactions with fibrinogen. Studies using Aα251 recombinant fibrinogen indicate that the disulfides between Cys 442 and 472 located in the exposed, solvent-accessible αC regions are critical to the normal polymerization of fibrinogen. Understanding the interaction of glutathione and its derivatives with fibrinogen and their role in fibrin formation may provide a clearer picture of the physiological role of nitrosothiols and their decomposition products *in vivo*.

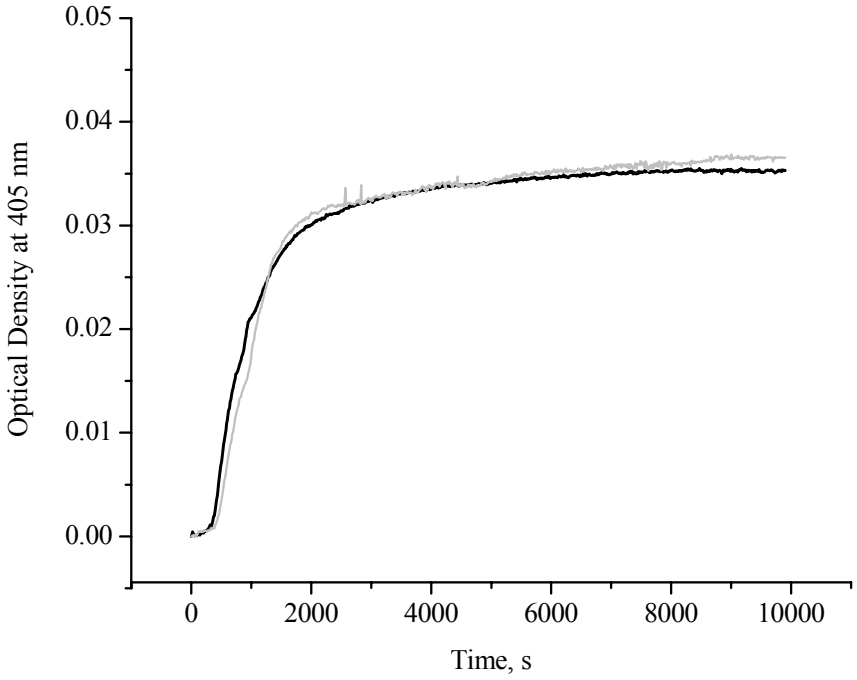

Figure 4.6 Turbidity curves monitored spectrophotometrically at 405 nm comparing the polymerization of 0.05 mg/mL Aα251 recombinant fibrinogen and 0.03 U/mL thrombin without gluathione (black trace) and 500 μM glutathione (grey trace).

REFERENCES

(1) Pastore, A.; Federici, G.; Bertini, E.; Piemonte, F. "Analysis of glutathione: implication in redox and detoxification." *Clinica Chimica Acta* 2003**,** *333*, 19-39.

(2) Reid, M.; Jahoor, F. "Glutathione and disease." *Curr. Opin. Clin. Nutr. Metabol. Care* 2001**,** *4*, 65-71.

(3) White, A. C.; Thannickal, V. J.; Fanburg, B. L. "Glutathione deficiency in human disease." *J. Nutr. Biochem.* 1994**,** *5*, 218-226.

(4) Rossi, R.; Dalle-Donne, I.; Milzani, A.; Giustarini, D. "Oxidized forms of glutathione in peripheral blood as biomarkers of oxidative stress." *Clin Chem* 2006**,** *52*, 1406-1414.

(5) Kelly, F. J. "Glutathione: in defence of the lung." *Food Chem. Toxicol.* 1999**,** *37*, 963-966.

(6) Mellion, B. T.; Ignarro, L. J.; Myers, C. B.; Ohlstein, E. H.; Ballot, B. A.; Hyman, A. L.; Kadowitz, P. J. "Inhibition of human platelet aggregation by S-nitrosothiols. Heme-dependent activation of soluble guanylate cyclase and stimulation of cyclic GMP accumulation." *Mol Pharmacol* 1983**,** *23*, 653-664.

(7) Radomski, M. W.; Rees, D. D.; Dutra, A.; Moncada, S. "S-nitroso-glutathione inhibits platelet activation in vitro and in vivo." *Br J Pharmacol* 1992**,** *107*, 745-749.

(8) de Belder, A. J.; MacAllister, R.; Radomski, M. W.; Moncada, S.; Vallance, P. J. T. "Effects of S-nitrosoglutathione in the human forearm circulation: evidence for selective inhibition of platelet activation." *Cardiovasc. Res.* 1994**,** *28*, 691-694.

(9) Radomski, M. W.; Moncada, S. "Regulation of platelet function by nitric oxide." *Adv. Molec. Cell Biol.* 1997**,** *18*, 367-381.

(10) Molloy, J.; Martin, J. F.; Baskerville, P. A.; Fraser, S. C. A.; Markus, H. S. "*S*-nitrosoglutathione reduces the rate of emolization in humans." *Circulation* 1998**,** *98*, 1372-1375.

(11) Salas, E.; Langford, E. J.; Marrinan, M. T.; Martin, J. F.; Moncada, S.; Debelder, A. J. "*S*-nitrosoglutathione inhibits platelet activation and deposition in coronary artery saphenous vein grats in vitro and in vivo." *Heart* 1998**,** *80*, 146-150.

(12) Ignarro, L. J.; Buga, G. M.; Wood, K. S.; Byrns, R. E.; Chaudhuri, G. "Endothelium-derived relaxing factor produced and released from artery and vein is nitric oxide." *Proc. Natl. Acad. Sci. U. S. A.* 1987**,** *84*, 9265-9269.

(13) Ignarro, L. J. "Nitric oxide: A unique endogenous signaling molecule in vascular biology." *Angew. Chem. Int. Ed.* 1999**,** *38*, 1882-1892.

(14) Ignarro, L. J. "Nitric oxide: A novel signal transduction mechanism for transcellular communication." *Hypertension* 1990**,** *16*, 477-483.

(15) Furchgott, R. F. "Endothelium-derived relaxing factor: discovery, early studies, and identification as nitric oxide." *Angew. Chem., Int. Ed.* 1999**,** *38*, 1870-1880.

(16) Hogg, N. "The biochemistry and physiology of *S*-nitrosothiols." *Annu. Rev. Pharmacol. Toxicol.* 2002**,** *42*, 585-600.

(17) Tyurin, V. A.; Tyurina, Y. Y.; Liu, S.-X.; Bayir, H.; Hubel, C. A.; Kagan, V. E. "Quantification of *S*-nitrosothiols in cells and biological fluids." *Methods in Enzymol.* 2002**,** *352*, 347-360.

(18) Stamler, J. S. "*S*-nitrosothiols in the blood." *Circ. Res.* 2004**,** *94*, 414-417.

(19) Singh, R. J.; Hogg, N.; Joseph, J.; Kalyanaraman, B. "Mechanism of nitric oxide release from S-nitrosothiols." *J. Biol. Chem.* 1996**,** *271*, 18596-18603.

(20) Xu, A.; Vita, J. A.; Keaney, J. F., Jr. "Ascorbic acid and glutathione modulate the biological activity of S-nitrosoglutathione." *Hypertension* 2000**,** *36*, 291-295.

(21) Ghezzi, P. "Regulation of protein function by glutathionylation." *Free Radic Res* 2005**,** *39*, 573-580.

(22) Walsh, G. M.; Leane, D.; Moran, N.; Keyes, T. E.; Forster, R. J.; Kenny, D.; O'Neill, S. "*S*-nitrosylation of platelet $\alpha_{IIb}\beta_3$ as revealed by raman spectroscopy." *Biochemistry* 2007**,** *46*, 6429-6436.

(23) Root, P.; Sliskovic, I.; Mutus, B. "Platelet cell-surface protein disulphide-isomerase mediated *S*-nitrosoglutathione consumption." *Biochem. J.* 2004**,** *382*, 575-580.

(24) Bell, S. E.; Shah, C. M.; Gordge, M. P. "Protein disulfide-isomerase mediates delivery of nitric oxide redox derivatives into platelets." *Biochem J* 2007**,** *403*, 283-288.

(25) Weisel, J. W. "Fibrinogen and fibrin." *Adv Protein Chem* 2005**,** *70*, 247-299.

(26) Weisel, J. W.; Medved, L. "The structure and function of the alpha C domains of fibrinogen." *Ann N Y Acad Sci* 2001**,** *936*, 312-327.

(27) Weisel, J. W.; Veklich, Y.; Gorkun, O. "The sequence of cleavage of fibrinopeptides from fibrinogen is important for protofibril formation and enhancement of lateral aggregation in fibrin clots." *J Mol Biol* 1993**,** *232*, 285-297.

(28) Akhter, S.; Vignini, A.; Wen, Z.; English, A.; Wang, P. G.; Mutus, B. "Evidence for S-nitrosothiol-dependent changes in fibrinogen that do not involve transnitrosation or thiolation." *Proc Natl Acad Sci U S A* 2002**,** *99*, 9172-9177.

(29) Gorkun, O. V.; Henschen-Edman, A. H.; Ping, L. F.; Lord, S. T. "Analysis of A alpha 251 fibrinogen: the alpha C domain has a role in polymerization, albeit more subtle than anticipated from the analogous proteolytic fragment X." *Biochemistry* 1998**,** *37*, 15434-15441.

(30) Lord, S. T.; Binnie, C. G.; Hettasch, J. M.; Strickland, E. "Purification and characterization of recombinant human fibrinogen." *Blood Coagul Fibrinolysis* 1993**,** *4*, 55-59.

(31) Hart, T. W. "Some observations concerning the S-nitroso and S-phenylsulfonyl derivatives of L-cysteine and gluathione." *Tet. Lett.* 1985**,** *26*, 2013-2016.

(32) Lord, S. T.; Strickland, E.; Jayjock, E. "Strategy for recombinant multichain protein synthesis: fibrinogen B beta-chain variants as thrombin substrates." *Biochemistry* 1996**,** *35*, 2342-2348.

(33) Higgins, D. L.; Lewis, S. D.; Shafer, J. A. "Steady state kinetic parameters for the thrombin-catalyzed conversion of human fibrinogen to fibrin." *J Biol Chem* 1983**,** *258*, 9276-9282.

(34) Weisel, J. W.; Nagaswami, C. "Computer modeling of fibrin polymerization kinetics correlated with electron microscope and turbidity observations: clot structure and assembly are kinetically controlled." *Biophys J* 1992**,** *63*, 111-128.

(35) Weisel, J. W. "Fibrin assembly. Lateral aggregation and the role of the two pairs of fibrinopeptides." *Biophys J* 1986**,** *50*, 1079-1093.

(36) Wolberg, A. S. "Thrombin generation and fibrin clot structure." *Blood Rev* 2007**,** *21*, 131-142.

(37) Uhlig, S.; Wendel, A. "The physiological consequences of glutathione variations." *Life Sci* 1992**,** *51*, 1083-1094.

(38) Toth, K. M.; Berger, E. M.; Beehler, C. J.; Repine, J. E. "Erythrocytes from cigarette smokers contain more glutathione and catalase and protect endothelial cells from hydrogen peroxide better than do erythrocytes from nonsmokers." *Am Rev Respir Dis* 1986**,** *134*, 281-284.

(39) Lane, J. D.; Opara, E. C.; Rose, J. E.; Behm, F. "Quitting smoking raises whole blood glutathione." *Physiol Behav* 1996**,** *60*, 1379-1381.

(40) Anderson, M. E.; Meister, A. "Dynamic state of glutathione in blood plasma." *J Biol Chem* 1980**,** *255*, 9530-9533.

(41) Gorkun, O. V.; Veklich, Y. I.; Medved, L. V.; Henschen, A. H.; Weisel, J. W. "Role of the alpha C domains of fibrin in clot formation." *Biochemistry* 1994**,** *33*, 6986-6997.

(42) Medved, L. V.; Gorkun, O. V.; Manyakov, V. F.; Belitser, V. A. "The role of fibrinogen alpha C-domains in the fibrin assembly process." *FEBS Lett* 1985**,** *181*, 109-112.

CHAPTER 5

SURFACE-DEPENDENT FIBRINOPEPTIDE A ACCESSIBILITY TO THROMBIN

5.1 Introduction

Inadequate biocompatibility continues to limit the utility of blood-contacting medical devices such as stents and catheters (*1*). One severe consequence of poor biocompatibility is surface induced thrombosis, or the undesirable formation of a blood clot at the blood/material interface. Clots formed at the blood/material interface may occlude blood flow to/past the implant, impair proper function of the device, and/or dislodge from the surface and cause thrombotic embolism. Much research has been devoted to understanding surface-induced thrombosis and its dependence on the surface properties of the underlying substrate (*2, 3*). However, few studies have examined the influence of surface properties on the mechanism of surface-induced thrombosis.

When an implanted material contacts blood, a series of pathologic responses involved in the coagulation cascade is triggered ultimately leading to thrombosis. The initial event in the cascade is plasma protein adsorption, a process that mediates subsequent cellular interactions between cells and the surface of the material (*4*). Of all plasma proteins, fibrinogen is of particular importance in thrombosis because of its dual role in modulating platelet adhesion and fibrin polymer formation (*5*). Fibrinogen is a 340 kDa plasma protein composed of two copies each of three polypeptide chains (Aα, Bβ and γ) forming a trinodular structure (*6-8*).

As shown in Figure 5.1, the N-termini of all six chains are located in the center globular E region, while the C-termini of all six chains extend outward from the center forming two coiled-coil structures that terminate in a globular D region formed by the Bβ and γ chains (Fig. 5.1A). Fibrinogen polymerization is initiated when the enzyme thrombin proteolytically cleaves the first 16 residues of the Aα chain, known as fibrinopeptide A (FpA). After removal of FpA, fibrinogen is referred to as desA-fibrin monomer (Fig. 5.1B). The newly exposed N-terminus of the α chain forms an active site "A" that is able to bind to a corresponding polymerization hole "a" found in the D region of other fibrin monomers. The fibrin monomers spontaneously align via "A-a" interactions to form double-stranded, half-staggered protofibrils (Fig. 5.1C). Subsequently, thrombin cleaves the first 14 residues of the Bβ chain, fibrinopeptide B (FpB), exposing a "B" active site which binds to a corresponding polymerization hole "b" in the D region, allowing for "B-b" interactions. Ultimately, protofibrils lengthen and laterally aggregate forming highly branched, cable-like fibers that serve as the structural backbone of a clot.

Previous studies have examined the influence of surface properties on fibrinogen adsorption and fibrin formation (*9*-*13*). Evans-Nguyen et al. studied fibrinogen adsorption to self-assembled monolayers (SAMs) on gold presenting diverse terminal functional groups via surface plasmon resonance (SPR). Similar amounts of fibrinogen were found to adsorb to hydrophobic and negatively-charged interfaces, yet the subsequent fibrin networks formed from the corresponding fibrinogen layers resulted in dramatically different clot structures (*9*). Fibrin formed at the hydrophobic surface was highly branched and contained a dense network while fibrin at the negatively-charged surface was sparse with few branch points. Sit

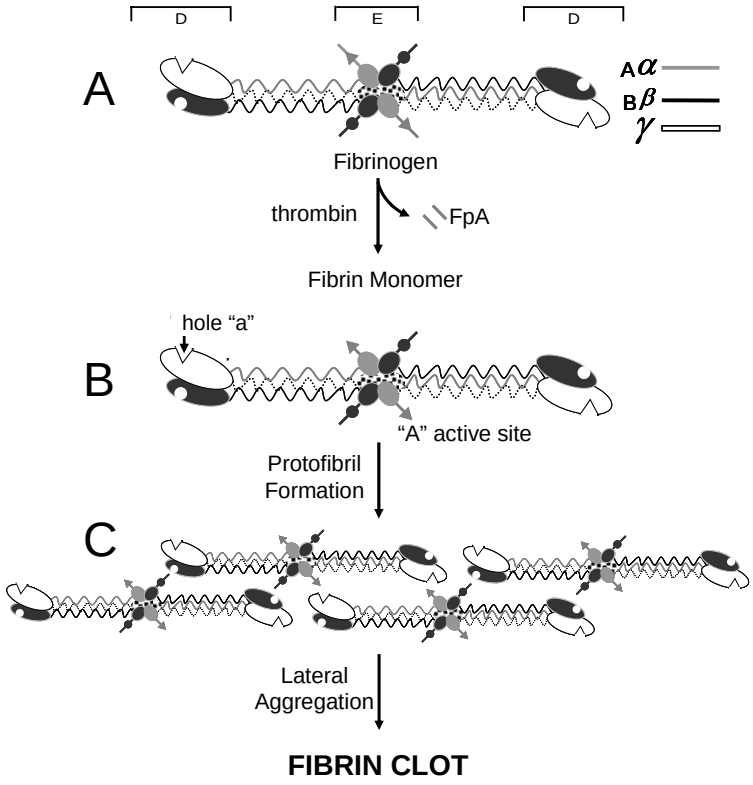

Figure adapted from (18).

Figure 5.1 **A.** Structure illustrating fibrinogen's D and E regions and FpA location in the center of the molecule and the color code for the three polypeptide chains. **B.** Fibrin monomer formation upon thrombin cleavage of FpA. **C.** Spontaneous alignment of fibrin monomers forming characteristic half-staggard, double stranded protofibrils via "A:a" intermolecular interactions.

and Marchant observed similar trends when comparing fibrinogen polymerization at hydrophobic graphite to negatively-charged mica using atomic force microscopy (*10*). Fibrin polymerization at surfaces appears to be highly dependent on surface charge and hydrophobicity.

To better understand the influence of surface properties on fibrin formation, Evans-Nguyen et al. characterized the thrombin-catalyzed FpA cleavage from fibrinogen adsorbed to both hydrophobic and negatively-charged SAMs (*12*). Unlike the fibrinogen adsorption characteristics, both the kinetics and quantities of FpA released were found to be significantly different, despite relatively similar amounts of fibrinogen adsorbed at the hydrophobic and negatively-charged SAMs. Significantly less FpA was released at a slower rate from fibrinogen adsorbed to negatively charged (0.9 ± 0.2 pmol/cm^2 and 0.071 ± 0.003 min^{-1}, respectively) versus hydrophobic SAMs (2.7 ± 0.4 pmol/cm^2 and 0.17 ± 0.05 min^{-1}, respectively) (*12*). Of note, the mechanism explaining the observed differences in amount and rate of FpA cleavage has yet to be elucidated.

In this chapter, FpA accessibility studies for adsorbed fibrinogen were conducted to elucidate the mechanism by which surface properties influence thrombin-catalyzed fibrinopeptide release and fibrin formation. The amount of accessible FpA on fibrinogen adsorbed to both hydrophobic and negatively-charged SAMs was quantified using polyclonal anti-FpA IgG binding in surface plasmon resonance (SPR) studies. In addition, the susceptibility of FpA to thrombin-catalyzed fibrinopeptide cleavage from adsorbed fibrinogen was investigated to verify that available FpA was removed by thrombin.

5.2 Experimental Methods

5.2.1 Materials. Dodecanethiol (HS-$(CH_2)_{11}CH_3$) and 11-mercaptoundecanoic acid (HS-$(CH_2)_{11}COOH$) were purchased from Sigma Scientific (St. Louis, MO) and used as received. Plasminogen-depleted human fibrinogen (FIB 1), human α-thrombin (HT 2970PA), sheep anti-human FpA purified IgG (SAFPA-IG 110) and non-immune sheep purified IgG (NIS-IG 120) were purchased from Enzyme Research Laboratory (Southbend, IN). HEPES-buffered saline with calcium (HBSC), [0.02 M HEPES, 0.15 M NaCl, and 1 mM $CaCl_2$ (pH 7.4)] was used to both prepare protein solutions and as the buffer for all experiments. The anti-FpA IgG was dialyzed against HBSC for 24 h prior to aliquot preparation and freezing. Fibrinogen and thrombin aliquots were stored at -80 °C while antibody aliquots were stored at -20 °C. A fresh fibrinogen aliquot was thawed daily at 37 °C and kept at room temperature. Fresh thrombin and antibody aliquots were thawed and kept on ice. Water was purified using a Milli-Q A10 gradient UV system (Millipore Corp., Billerica, MA) to a final resistivity of 18.2 MΩ•cm and a total organic content of < 6 ppb.

5.2.2 Preparation of gold substrates. Gold substrates were prepared according to the method previously described by Evans-Nguyen et al (*11*). Briefly, glass microscope coverslips (Electron Microscopy Sciences, Washington, PA) were cleaned in piranha solution (1:3 v/v 30 % hydrogen peroxide: concentrated sulfuric acid) and rinsed thoroughly. The coverslips were coated with a 3 nm chromium adhesion layer followed by a 45 nm gold layer. Upon removal, the gold-coated coverslips were stored in absolute ethanol until used. Thiol solutions of methyl- and carboxylic acid-terminated self-assembled monolayers were generated by immersing the gold-coated substrates in dodecanethiol and 11-

mercaptoundecanoic acid solution (2 mM in absolute ethanol), respectively, overnight immediately prior to use in experiments.

5.2.3 Surface plasmon resonance. All SPR experiments were conducted using a BIAcore X instrument (Biacore, Inc., Uppsala, Sweden) and repeated in triplicate. Gold-coated coverslips were removed from the thiol solutions and rinsed copiously with ethanol and Milli-Q water. The sensorchips were dried under a gentle stream of nitrogen before placement into the SPR instrument. The HBSC flow rate was adjusted to 10 µl/min and maintained through the instrument at all times. After a stable baseline (<1 response unit/min) was achieved, 1 mg/mL fibrinogen was injected over the sensorchip surface for 600 s to allow fibrinogen adsorption. The adsorbed fibrinogen layer was then washed with HBSC for 300 s, and rinsed three times with buffer using Biacore's software "wash" command over a second 300 s period prior to any additional injections.

5.2.4 FpA accessibility studies. A 40 nM anti-FpA solution was introduced for 600 s over fibrinogen adsorbed to the hydrophobic and negatively-charged interfaces. The relative amount of FpA available on fibrinogen at each surface was determined by monitoring the antibody association and dissociation profiles for 600 s each. A competitive enzyme-linked immunosorbent assay (ELISA) was performed to determine the concentration of free FpA sufficient to block antibody binding to FpA on adsorbed fibrinogen (data not shown). Based on the ELISA results, 240 nM free FpA was used to inhibit 40 nM anti-FpA and determine the non-specific antibody binding to fibrinogen at both surfaces. The antibody/inhibitor solution was incubated for 1 h and then introduced to the adsorbed fibrinogen layer. Non-

specific association and dissociation were monitored for 600 s each and subtracted from the association and dissociation curves obtained when 40 nM anti-FpA alone was injected over the adsorbed fibrinogen to yield specific anti-FpA binding responses. The specific antibody association and dissociation profiles were also normalized with respect to the amount of fibrinogen adsorbed during each experiment by dividing each antibody binding profile by the net fibrinogen response (difference in response immediately prior to antibody injection and prior to fibrinogen injection.)

5.2.5 *Fibrinopeptide A susceptibility to thrombin cleavage.* 1 mg/mL fibrinogen was deposited on each surface for 600 s followed by 600 s of rinsing with HBSC. Thrombin-catalyzed fibrinopeptide cleavage was initiated by flowing 5 U/mL thrombin over fibrinogen adsorbed to both the hydrophobic and negatively-charged surfaces for 600 s. To prevent thrombin carry-over, a 600 s injection of 40 U/mL hirudin, a thrombin inhibitor (*14, 15*), was performed prior to the antibody injection. A 40 nM anti-FpA solution was then introduced over the thrombin-treated fibrinogen layers while monitoring antibody association and dissociation profiles. Antibody signals were normalized to the amount of fibrinogen deposited at each surface in the same manner as described above. After each experiment, the SPR flow cells were rinsed with 10 mg/mL pepsin (20 mM citrate buffer; pH 3, 300 s) followed by 0.5 % (w/v) sodium dodecyl sulphate (SDS) solution (300 s) to remove residual thrombin and possible fibrin and to prevent blockage of the SPR flow cells. The flow cells were rinsed several times with HBSC to remove remaining SDS prior to additional experiments.

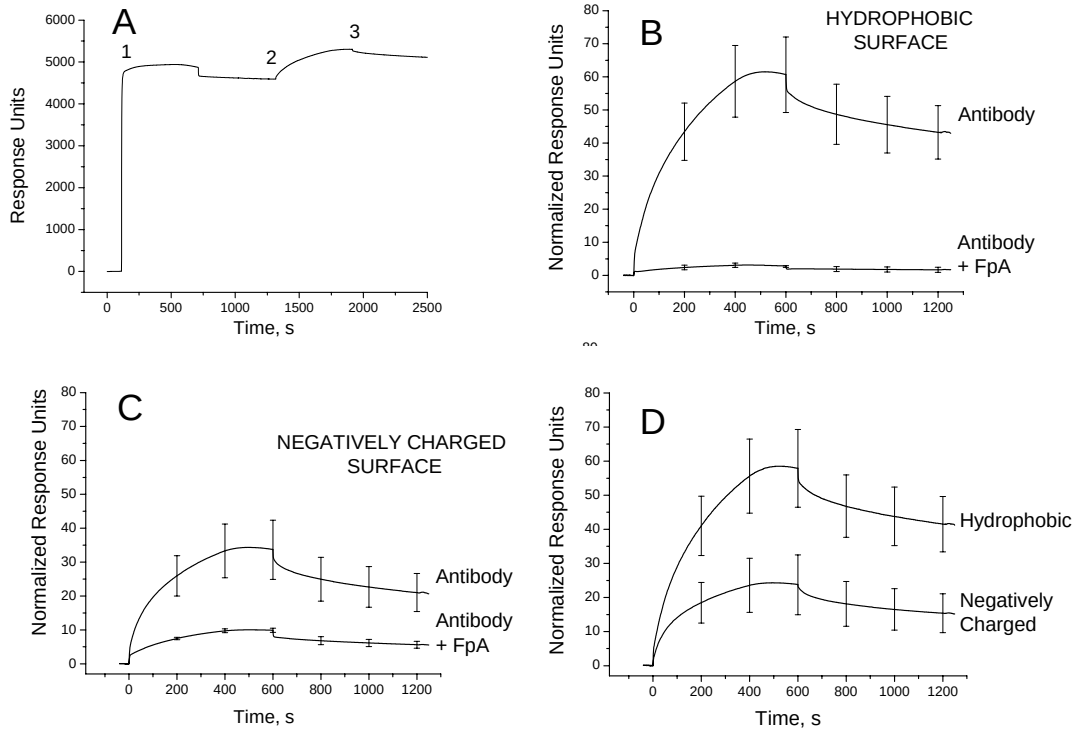

Figure 5.2 **A.** Representative SPR sensorgram of response unit changes observed during (1) injection of fibrinogen, (2) injection of anti-FpA and (3) partial anti-FpA dissociation upon restoration of buffer flow for a hydrophobic surface. **B.** 40 nM anti-FpA with and without 240 nM free FpA binding to fibrinogen adsorbed to the hydrophobic SAM as determined by SPR. The antibody binding curve was obtained by zeroing time and response axes at point 2 in Figure 5.2A and normalizing for the amount of fibrinogen at each surface. **C.** 40 nM anti-FpA with and without 240 nM free FpA binding to fibrinogen adsorbed to the negatively charged SAM as determined by SPR. The antibody binding curve was obtained by zeroing time and response axes at point 2 in Figure 5.2A and normalizing for the amount of fibrinogen at each surface. **D.** Specific anti-FpA binding to fibrinogen adsorbed to the hydrophobic and negatively charged surface. Specific antibody binding was calculated as the difference between SPR signals measured for antibody and antibody inhibited with 240 nM FpA binding to fibrinogen at each surface. Error bars depicted every 200 s in panels B-D represent the standard deviation of antibody binding responses obtained from three separate experiments.

5.3 Results

5.3.1 *Fibrinopeptide A accessibility.* Fibrinopeptide A accessibility was measured as anti-FpA binding to adsorbed fibrinogen using surface plasmon resonance. A representative SPR sensorgram is shown in Figure 5.2A. Upon addition of 1 mg/mL fibrinogen to the flow cell, rapid increase in SPR response was observed corresponding to fibrinogen adsorption to the surface (i.e., SAM-modified interface) (Fig. 5.2A, 1). The amount of irreversibly adsorbed fibrinogen at the hydrophobic and negatively-charged surfaces (5531 ± 738 response units and 5255 ± 413 response units, respectively) was comparable 20 min after initial fibrinogen adsorption. The fibrinogen adsorption signals observed for both the hydrophobic and negatively-charged surfaces correlated well with previous reports using similar conditions and instrumentation (*11, 13*).

An increase in instrument response was observed upon introduction of the antibody to the SPR flow cells (Fig. 5.2A, 2), indicating association of the antibody with accessible FpA. After the antibody injection was complete and buffer flow restored, partial dissociation of the antibody from the adsorbed fibrinogen was noted (Fig. 5.2A, 3) suggesting the antibody's interaction with fibrinogen was partly reversible over the course of our experiments. Due to the non-selective sensing principles of SPR, all antibody binding near the surface would elicit an instrument response, regardless of the interaction's specificity. Thus, the SPR response includes both specific and non-specific binding signals. To correlate anti-FpA binding to FpA availability on fibrinogen at both surfaces, only the specific anti-FpA interaction with FpA on fibrinogen should be considered. Non-specific anti-FpA binding to fibrinogen was consequently quantified for both surfaces using a competitive binding assay where 240 nM free FpA was present during the antibody injection.

The antibody binding profiles normalized for fibrinogen adsorption at both surfaces are shown in Figure 5.2B-C. Following anti-FpA injection, an increase in SPR response was observed indicating antibody association with fibrinogen at both surfaces (Figure 5.2B-C, upper curves). Upon completion of the injection at 600 s, buffer flow resumed over the adsorbed fibrinogen for an additional 600 s and a decrease in SPR response indicating partial dissociation of bound antibody was observed. In the case of anti-FpA in the presence of excess FpA (Fig. 5.2B-C, lower curves), a smaller increase in SPR response was observed upon injection of the inhibited antibody for both the hydrophobic and negatively charged surfaces. The smaller but detectable binding responses observed for the inhibited antibody injections at both surfaces indicated that non-specific interactions contribute to the total antibody binding signal (Table 5.1). Anti-FpA binding was greater at the hydrophobic surface compared to the negatively-charged surface (Fig. 5.2B-C) indicating less anti-FpA bound to fibrinogen at the negatively charged surface. In contrast, there were fewer non-specific interactions at the hydrophobic surface (relative to the negatively-charged surface) as indicated by the reduced binding of inhibited antibody.

Figure 5.2D illustrates the clear contrast between specific anti-FpA binding to fibrinogen at the hydrophobic and negatively-charged surfaces. Indeed, a greater amount anti-FpA associated with fibrinogen adsorbed on a hydrophobic surface compared to a negatively-charged surface. Specific anti-FpA binding was 2.7 times higher to fibrinogen adsorbed on the hydrophobic surface compared to the negatively charged surface 20 min after the initial antibody injection, indicating greater FpA availability on the hydrophobic SAM (Table 5.1).

Table 5.1 Anti-FpA Binding to Immobilized Fibrinogen as measured via surface plasmon resonance 1200 s after anti-FpA injections, normalized as described in methods.

Surface	Anti-FpA alone	Anti-FpA and FpA	Anti-FpA after thrombin	Specific anti-FpA binding
Hydrophobic	43.2 ± 8.1	1.7 ± 0.8	2.0 ± 1.2	41.5 ± 8.1
Negatively Charged	21.1 ± 5.6	5.6 ± 1.0	6.2 ± 2.4	15.4 ± 5.7

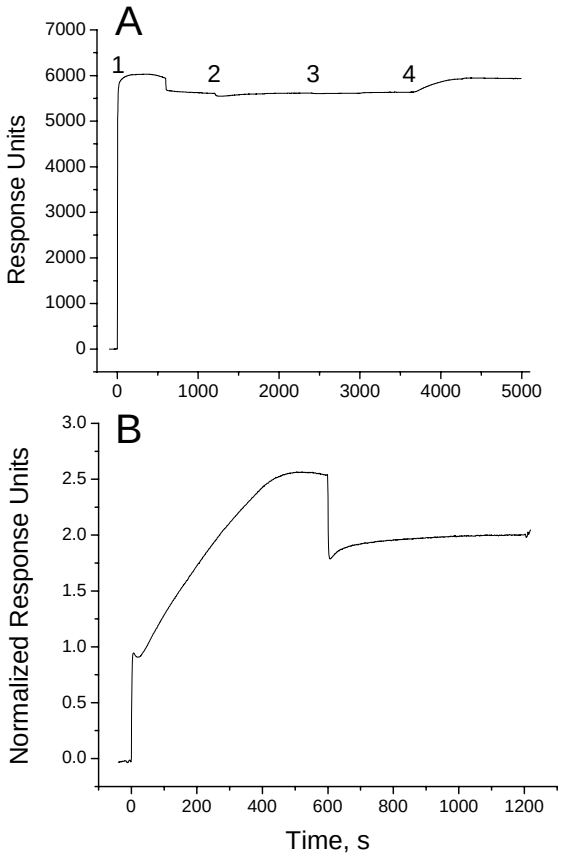

Figure 5.3 **A.** Representative SPR sensorgram of response unit changes observed during injection of (1) fibrinogen, (2) thrombin (3) hirudin, and (4) anti-FpA for the hydrophobic surface. **B.** 40 nM anti-FpA binding to thrombin-treated fibrinogen. The normalized antibody binding curve was obtained by zeroing time and response axes at point 4 in Figure 5.3A and normalizing for the amount of fibrinogen deposited at point 1 in Figure 5.3A for the hydrophobic surface.

5.3.2 Fibrinopeptide A susceptibility to thrombin cleavage. To investigate thrombin's ability to cleave available FpA on adsorbed fibrinogen, SPR was employed to measure anti-FpA binding to fibrinogen after thrombin-catalyzed FpA cleavage. As shown in Figure 5.3A, the initial increase in SPR response showed fibrinogen adsorption to the surface (Fig. 5.3A, 1). Upon injection of thrombin, a decrease in SPR response due to cleavage of fibrinopeptides A and B was observed. The response correlated well with previously published SPR data for thrombin cleavage (*12*). Hirudin was introduced to inhibit residual thrombin (*14*), and thebinding of anti-FpA assessed the remaining available FpA. The SPR response was normalized to the amount of fibrinogen remaining on the surface just prior to anti-FpA injection and a representative binding curve is shown in Figure 5.3B. The normalized SPR responses for anti-FpA bound to thrombin-treated fibrinogen 1200 s after antibody injection were 2.0 ± 1.2 and 6.2 ± 2.4 at the hydrophobic and negatively-charged surfaces, respectively. Antibody binding after thrombin-catalyzed fibrinopeptide cleavage correlated well with the level of non-specific antibody interaction observed for each surface with anti-FpA in the presence of 240 nM FpA (Table 5.1). This indicates that all available FpA was susceptible to thrombin cleavage, as expected. Of note, a significantly higher level of non-specific interaction was observed at the negatively-charged (compared to the hydrophobic) surface under both conditions; i.e., thrombin exposure and inhibition with FpA (Table 5.1). Our results indicate all FpA recognized by the antibody is cleaved by thrombin and only non-specific interactions contribute to the observed antibody binding signal after thrombin exposure.

5.4 Discussion

The accessibility and susceptibility of FpA to thrombin-catalyzed fibrinopeptide cleavage from adsorbed fibrinogen at hydrophobic and negatively-charged surfaces were evaluated. As determined by specific anti-FpA binding assays, roughly 2.7 times more FpA was available at hydrophobic versus negatively-charged interfaces (Table 5.1), indicating the amount of FpA available for thrombin cleavage is highly dependent on the properties of the underlying surface. These results correlate well with studies by Evans-Nguyen et al. that reported three times more FpA is released from fibrinogen adsorbed to a hydrophobic surface relative to a negatively-charged surface (*12*). Our findings provide the mechanistic basis (i.e., FpA availability) of surface-dependent FpA release reported previously (*12*).

The results also explain the reduced fibrin formation observed by Sit and Marchant at negatively-charged mica relative to hydrophobic graphite (*10*). Sit and Marchant proposed several hypotheses for reduced fibrin formation at mica including altered fibrinogen conformation, electrostatic interferences and thrombin inactivity (*10*). While adsorbed fibrinogen conformation and orientation has been shown to vary as a function of underlying surface properties (*16, 17*), the accessibility of polymerization sites such as FpA has not been previously evaluated. The increased FpA availability at the hydrophobic SAM suggests fibrinogen exists in a favorable orientation more suitable for thrombin-catalyzed fibrinopeptide A cleavage. However, available FpA was removed upon thrombin exposure to fibrinogen at both the hydrophobic and negatively-charged surfaces. Therefore, all accessible FpA was equally susceptible to thrombin cleavage and thrombin activity was not influenced by the underlying surface chemistry. Based on our data, reduced fibrin formation at the negatively-charged interface is the result of FpA availability. Consequently, if FpA is

unavailable, thrombin is not able to expose the "A" active site (Fig. 4.1B) and fibrin formation will not occur.

Although previous studies have shown reduced FpA release and fibrin formation at negatively-charged surfaces, the explanation for these observations remained unclear (*10, 12*). Our findings provide key insight into the surface-dependent behavior of fibrin formation of adsorbed fibrinogen. The results suggest negatively-charged surfaces may be useful in minimizing surface-induced thrombosis, and thus aid in the development of more biocompatible blood-contacting devices.

REFERENCES

(1) Anderson, J. M., Biological responses to materials. *Annu. Rev. Mater. Res.* 2001; *31*, 81-110.

(2) Gorbet, M. B., and Sefton, M. V., Biomaterial-associated thrombosis: roles of coagulation factors, complement, platelets and leukocytes. *Biomaterials* 2004; *25*, 5681-5703.

(3) Tang, L., and Hu, W.-J., Molecular determinants of biocompatibility. *Expert Rev. Med. Devices 2* 2005; 493-500.

(4) Brash, J. L., and Horbett, T. A., Proteins at interfaces: An overview, in *Proteins at interfaces II* (Brash, J. L., and Horbett, T. A., Eds.) 1995; pp 1-23, American Chemical Society, Washington DC.

(5) Feng, L., and Andrade, J. D., Structure and adsorption properties of fibrinogen, in *Proteins at Interfaces II:Fundamentals and applications* (Brash, J. L., and Horbett, T. A., Eds.) 1995; pp 66-79, American Chemical Society, Washington DC.

(6) Blomback, B., Fibrinogen: Evolution of the structure-function concept. *Ann. N.Y. Acad. Sci.* 2001; *936*, 1-10.

(7) Mosesson, M., Siebenlist, K. R., and Meh, D. A., The structure and biological features of fibrinogen and fibrin. *Ann. N.Y. Acad. Sci.* 2001; *936*, 11-30.

(8) Weisel, J. W., Fibrinogen and fibrin. *Adv. Protein Chem.* 2005; *70*, 247-299.

(9) Evans-Nguyen, K., and Schoenfisch, M. H., Fibrin proliferation at model surfaces: Influence of surface properties. *Langmuir* 2005; *21*, 1691-1694.

(10) Sit, P. S., and Marchant, R. E., Surface-dependent differences in fibrin assembly visualized by atomic force microscopy. *Surf. Sci.* 2001; *491*, 421-432.

(11) Evans-Nguyen, K., Fuierer, R. R., Fitchett, B. D., Tolles, L. R., Conboy, J. C., and Schoenfisch, M. H., Changes in adsorbed fibrinogen upon conversion to fibrin. *Langmuir* 2006; *22*, 5115-5121.

(12) Evans-Nguyen, K. M., Tolles, L. R., Gorkun, O. V., Lord, S. T., and Schoenfisch, M. H., Interactions of thrombin with fibrinogen adsorbed on methyl-, hydroxyl-, amine-, and carboxyl-terminated self-assembled monolayers. *Biochemistry* 2005; *44*, 15561-15568.

(13) Ostuni, E., Yan, L., and Whitesides, G. M., The interaction of proteins and cells with self-assembed monolayers of alkanethiolates on gold and silver. *Colloids and Surfaces, B: Biointerfaces* 1999; *15*, 3-30.

(14) Markwardt, F., Sturzebecher, J., and Walsmann, P., The hirudin standard. *Thromb. Res.* 1990; *59*, 395-400.

(15) Lundblad, R. L., Kingdon, H. S., and Mann, K. G., Thrombin. *Methods in Enzymol.* 1976; *45*, 156-176.

(16) Sit, P. S., and Marchant, R. E., Surface-dependent conformations of human fibrinogen observed by atomic force microscopy under aqueous conditions. *Thromb. Haemostasis* 1999; *82*, 1053-1060.

(17) Marchin, K. L., and Berrie, C. L., Conformational changes in the plasma protein fibrinogen upon adsorption to graphite and mica investigated by atomic force microscopy. *Langmuir* 2003; *19*, 9883-9888.

(18) Cote, H. C. F., Lord, S. T., and Pratt, K. P., Gamma-chain dysfibrinogenemias: Molecular structure-function relationships of naturally occurring mutations in the gamma chain of human fibrinogen. *Blood* 1998; *92*, 2195-2212.

CHAPTER 6

SUMMARY AND FUTURE DIRECTIONS OF THIS RESEARCH

6.1 Summary

The work detailed in this dissertation combines the technologies of surface-based analytical methods and biochemistry to deepen the current understanding of the mechanism of fibrin formation in solution and at interfaces. In Chapter 2, surface plasmon resonance was used to detect both "A-a" and "B-b" knob-hole interactions occurring between desAB-NDSK and fibrinogen. Equilibrium dissociation constants of 5.8 ± 1.1 and 3.7 ± 0.7 μM were measured for desA- and desAB-NDSK, respectively binding to adsorbed fibrinogen. Peptide inhibition studies showed desAB-NDSK binding to fibrinogen was reduced by both "A-a" and "B-b" interaction inhibitors, providing evidence that "B-b" interactions may occur alongside "A-a" interactions. These experiments demonstrate "B-b" interactions may have a more substantive role in protofibril formation than previously thought.

In Chapter 3, protein immobilization and data collection strategies were optimized to develop an atomic force microscopy method to measure the mechanical properties of the bonds that rupture upon the dissociation of fibrin-fibrinogen interactions. This method was used to investigate the complexity of the "A-a" knob-hole interaction and found molecular deformations occur within fibrinogen upon the forced rupture of the "A-a" bond. In Chapter 4, the effects of *S*-nitrosoglutathione and glutathione (oxidized and reduced) on the mechanism of fibrin formation were investigated using turbidity measurements. GSNO,

GSH and GSSG each led to slower rates of protofibril assembly and lateral aggregation. The final turbidities of clots formed in the presence of GSNO, GSH and GSSG were significantly reduced compared to normal. While previous reports have examined the influence of GSNO on the initial rate of polymerization, this research represents the first examination of GSNO, GSH and GSSG on the entire fibrin formation process and a previously unreported role of GSH. In Chapter 5, surface plasmon resonance studies were used to demonstrate that fibrinopeptide A was ~ 2.7 times more available for thrombin cleavage on fibrinogen adsorbed at a model hydrophobic surface compared to negatively charged surface, providing an explanation for reduced fibrin formation observed at negatively charged substrates.

6.2 Future Directions of this Research

Despite a deeper understanding of the mechanism of fibrin formation in solution and at surfaces provided by this research, many unanswered questions remain. The utility of surface-based analytical methods such as surface plasmon resonance (SPR) and atomic force microscopy (AFM) has been clearly established in the literature and this dissertation (1-8). However, the instrumental techniques (SPR and AFM) alone are insufficient at answering mechanistic questions regarding complex biological processes. Combining the capabilities of surface-based analytical methods with relevant biological reagents (e.g., recombinant fibrinogens or cells) has the power to enable future researchers to probe critical aspects of fibrin formation and other important systems.

6.2.1 SPR investigation of role of "B-b" interactions in protofibril formation. In Chapter 2, "B-b" interactions were detected via selective "B-b" interaction inhibitors. However, "B-

b" interactions were only measured in conjunction with "A-a" interactions. The individual contribution of "B-b" interactions to the binding affinity of desAB-NDSK for fibrinogen remains unclear. To further investigate the role of "B-b" interactions in protofibril formation in the absence of "A-a" interactions, experiments with a recombinant fibrinogen having impaired holes "a" could prove very useful. Specifically, γD364H fibrinogen containing non-functional holes "a" (9) could be adsorbed on the hydrophobic SAM. The interactions of desAB-NDSK and desA-NDSK with the mutants would be assessed in the same manner as described in Chapter 2. Since γD364H can not support "A-a" interactions, any binding of desAB-NDSK to this mutant would arise from "B-b" or "A-b" interactions. DesA-NDSK could be used to determine the extent of "A-b" interactions since desA-NDSK only has "A" knobs available; "B-b" interactions are not possible with this fragment. By comparing the binding of desAB-NDSK and desA-NDSK to γD364H, a measure of the affinity of "B-b" interactions independent of "A-a" interactions would be possible. The direct measurement of the affinity of "B-b" interactions would provide a clearer picture of the role of "B-b" interactions in the early phases of polymerization (i.e., protofibril formation).

6.2.2 DesAB-NDSK and desA-NDSK interaction with DD fragment. During fibrin formation, the molecules align end-to-end within a protofibril and one E region interacts with two D regions on the opposite strand of the protofibril (Fig. 1.4). Therefore, both "A" knobs in fibrin's E region interact each with holes "a" located in the D regions of two adjacent fibrin molecules (i.e., one desA- or desAB-NDSK binding to two D regions). The SPR experiments described in this dissertation involved fibrinogen adsorbed to a surface and the interaction of one desA- or desAB-NDSK with one of the two D regions within fibrinogen.

To better model "A-a" and "B-b" knob-hole interactions occurring within a protofibril, SPR studies quantifying desAB-NDSK and desA-NDSK interactions with DD fragment would be useful. The DD fragment contains two D regions "fixed" as they would be within a protofibril by FXIII, an enzyme that cross-links specific residues in fibrin (10). By examining the interaction of desA- or desAB-NDSK with DD fragment, the synergistic effect on the affinity of multiple knob-hole interactions (e.g., two "A-a" or two "A-a" and "B-b" interactions) could be directly measured for the first time. The measurement of the affinity of knob-hole interactions occurring between fibrin molecules as they exist in protofibrils would provide useful information in understanding the interactions responsible for protofibril formation and provide deeper understanding of the mechanism of the early steps in fibrin formation.

6.2.3 Effects of surface properties on desAB-NDSK binding to fibrinogen. Previous studies have demonstrated impaired fibrin formation at negatively charged substrates compared to hydrophobic surfaces (11-13). Evans-Nguyen et al. found thrombin cleaved ~ 3 times more FpA from fibrinogen adsorbed at a hydrophobic surface compared to a negatively charged surface (12). The work in Chapter 5 showed FpA is ~ 3 times more accessible to thrombin on fibrinogen adsorbed at the hydrophobic compared to the negatively charged surface, providing an explanation for Evans-Nguyen et al. results. However, the influence of surface properties on subsequent phases of fibrin formation, such as fibrin (desAB-NDSK) binding to fibrinogen has not been fully studied. The work detailed in Chapter 2 characterized desA- and desAB-NDSK binding to fibrinogen adsorbed at a hydrophobic surface. Investigating desA- and desAB-NDSK binding to fibrinogen adsorbed at model

hydrophilic, positively charged and negatively charged surfaces could provide crucial insight into additional mechanisms by which surface properties influence fibrin formation. One study has previously examined the influence of surface properties on the binding of fibrinogen to adsorbed fibrin monomers (desAB-fibrin) (14). Only "A-a" with "B-b" interactions were examined since thrombin activation was used exclusively. The influence of surface properties on "A-a" interactions alone in addition to "A-a" with "B-b" interactions were not examined. Differences in thrombin's ability to cleave fibrinopeptides from fibrinogen at different surfaces were not considered. Evans-Nguyen reported that thrombin interactions with adsorbed fibrinogen were highly dependent on the underlying substrate (12). The alternative approach described herein would avoid introducing surface-dependent differences in the adsorbed fibrin layers because the fibrin source would be soluble desA- or desAB-NDSK. The interactions between soluble desA-or desAB-fibrin fragments and fibrinogen adsorbed at a hydrophilic, hydrophobic, positively and negatively charged surfaces would allow for comparison of "A-a" with "B-b" and "A-a" interactions alone as a function of surface properties. Fully understanding the extent of the influence of surface properties on the mechanism of fibrin formation could be useful in developing materials to prevent or control surface-induced thrombosis.

6.2.4 Application of the AFM method to study fibrinogen-platelet interactions. The development of a robust, reliable AFM method in combination with sophisticated data analyses for measuring the forces of rupture for fibrin-fibrin interactions enables future researchers to apply the same method, with minor modifications, to investigate numerous biological systems. For example, the interaction between fibrin(ogen) and the platelet

integrin $\alpha_{IIb}\beta_3$, the protein responsible for the aggregation of platelets via fibrinogen bridging, could be studied using the methods developed in Chapter 3. Previous work has examined the forces of interaction between fibrinogen and purified $\alpha_{IIb}\beta_3$ or $\alpha_{IIb}\beta_3$ bound to a synthetic membrane (15-17). However, no AFM studies have examined the forces of interaction between fibrinogen and $\alpha_{IIb}\beta_3$ located within the platelet membrane due to complications associated with rupture data convoluted with molecular and/or cellular deformations. The methods and data analyses developed herein to investigate complex fibrin-fibrin interactions may be capable of distinguishing specific interactions between fibrinogen and $\alpha_{IIb}\beta_3$ within the platelet membrane from those related to molecular or cellular deformations. A monoclonal antibody specific to $\alpha_{IIb}\beta_3$ could be used to examine the molecular and cellular deformations that result from an applied force to the $\alpha_{IIb}\beta_3$ integrin, independent of specific fibrinogen-integrin interactions. Unmodified AFM tips could be used to characterize the deformability of the platelets upon compression.

In addition to fundamentally characterizing the physical properties of the interactions between fibrinogen and $\alpha_{IIb}\beta_3$ within a platelet membrane, the AFM may allow the study of the distribution of $\alpha_{IIb}\beta_3$ integrins over the surface of the platelet. Only activated platelets present the active form of the fibrinogen receptor ($\alpha_{IIb}\beta_3$) on their surface. Since platelets (upon activation) can be up to 10 μm in diameter (much larger than the diameter of the AFM tip), the distribution of fibrinogen receptors on the platelet surface could be "mapped" by collecting an array of force versus separation distance curves across the surface of a single platelet. Once the fibrinogen- $\alpha_{IIb}\beta_3$ rupture "signature" has been identified, the surface of the cell could be screened for specific interactions that could easily be distinguished from non-specific fibrinogen-platelet interactions. The cell could then be imaged with the AFM probe

or the AFM could be coupled to an inverted microscope, and the location/magnitude of the specific $\alpha_{IIb}\beta_3$ interactions with fibrinogen could be overlaid with the platelet image. The distribution of $\alpha_{IIb}\beta_3$ over the platelet surface, as well as information regarding the strength and mechanical properties of the interaction between fibrinogen and $\alpha_{IIb}\beta_3$ could be obtained from a single experiment. Since $\alpha_{IIb}\beta_3$ would be located in its natural environment (e.g., bound to the platelet membrane) the results may enable a deeper understanding of platelet-fibrinogen interactions critical to thrombosis. It would also be interesting to compare the distribution and function of $\alpha_{IIb}\beta_3$ activated via different methods of platelet stimulation (e.g., thrombin or other agonists) since the mechanism of activation could influence the distribution of $\alpha_{IIb}\beta_3$ on the platelet surface. Previous studies have quantified fibrinogen binding to platelets (18), but information regarding the distribution of bound fibrinogen on the platelet surface has not been reported using AFM.

To investigate factors that may influence the interactions between fibrinogen and $\alpha_{IIb}\beta_3$, force measurements could be acquired as a function of NO-exposure via small molecule NO donors (e.g., *S*-nitrosothiols). These studies are particularly interesting since NO has been shown to affect platelet aggregation (19-23). The relationship between NO exposure the mechanical properties of the fibrinogen and $\alpha_{IIb}\beta_3$ interaction have not been reported. Investigation of the NO-dependent effects on the fibrinogen-$\alpha_{IIb}\beta_3$ interaction could provide unique information regarding the mechanism of reduced platelet aggregation due to NO exposure.

6.2.4 Application of the AFM method to study fibrinogen-bacteria interactions. Similar to fibrinogen-platelet interactions, fibrinogen-bacterium interactions could be investigated using

the method developed in Chapter 3. *Staphylococci* have been shown to bind fibrinogen via several membrane-bound receptors (24, 25). Yet, the distribution of the fibrinogen-specific receptors on the surface of the bacterial cell has not been thoroughly investigated. The AFM method developed in Chapter 3 could be used to investigate both the intricacies of the fibrinogen-fibrinogen receptor interactions in their natural state (e.g., bound within the cell membrane) and the location of these interactions on the cell surface. Although previous studies have examined the adhesion strength of bacterial cells to fibrinogen-coated surfaces or the interaction between fibrinogen and purified fibrinogen receptors (e.g., clumping factor A and fibronectin binding protein), the force of interaction between fibrinogen and the fibrinogen receptors on a living cell has not been reported.

Once the characteristic interaction between fibrinogen and the fibrinogen-specific receptors on the cell surface has been elucidated, numerous investigations relevant to biomedical infection could be completed. For example, the interactions between fibrinogen and membrane proteins on the bacterial cell surface could be examined as a function of adhesion time or underlying substrate surface properties. Investigating the distribution of fibrinogen receptors on bacterial cells adhered to a variety of biomaterials or nitric oxide (NO)-releasing films could provide key insight into the mechanism of implant-associated infections *in vivo*. Numerous reports from the Schoenfisch lab have detailed the antimicrobial effects of NO and reduced adhesion of bacteria to NO-releasing surfaces (26-31). Additionally, the effects of NO on fibrinogen-mediated adhesion have been examined. Bacterial adhesion to fibrinogen-coated NO-release surfaces was reduced compared to control surfaces incapable of NO release (32).

However, the mechanism by which NO reduces fibrinogen-mediated adhesion has not been examined. The AFM method developed in Chapter 3 is well-suited to make significant strides in understanding NO's effect on specific fibrinogen-fibrinogen receptor interactions. For example, fibrinogen could be covalently attached to the AFM tip and *S. aureus* could be adhered to an NO-releasing xerogel. The interactions between the fibrinogen-modified tip and the bacterial cell adhered to an NO-releasing surface could be examined as a function of time and/or NO-release properties (e.g., flux of NO, total NO concentration, and xerogel composition). If the interaction between fibrinogen and the fibrinogen receptors is unaffected by NO exposure, then researchers can conclude NO does not reduce fibrinogen-mediated bacterial adhesion by disrupting the specific fibrinogen-receptor interactions but more likely affects bacterial cell adhesion via a fibrinogen-independent mechanism.

6.2.5 AFM investigations of reactive species and fibrin(ogen)-fibrin interactions. In addition to investigating the influence of NO on fibrinogen-bacteria interactions, the AFM could be used to investigate the influence of NO or *S*-nitrosothiols on fibrin(ogen)-fibrin interactions. Chapter 4 demonstrated glutathione and its derivatives influence several aspects of fibrin formation via prolonged lag times, slower rates of lateral aggregation and lower final turbidities. The effect of glutathione and its derivatives on fibrinogen has not been examined at the single molecule level. Investigating alterations in fibrinogen function using the AFM method developed in Chapter 3 could provide unique information not measurable using other techniques. It would be interesting to investigate whether NO or *S*-nitrosothiols influence both the magnitude of the rupture and the deformation pattern observed upon the dissociation of the "A-a" knob-hole interaction. Understanding the consequences of NO or

nitrosothiol exposure to fibrinogen at the single molecule level could provide insight into fibrinogen's structure and/or function that is not measurable in global turbidity assays. For example, Chapter 4 found glutathione likely reduces a critical disulfide in the αC domains of fibrinogen, leading to impaired polymerization. If additional disulfides are reduced, the turbidity curve may not be affected but further modifications may be manifested at the single molecule level. AFM would be useful for assessing modifications to fibrinogen's structure that may affect mechanical properties but not lead to measurable changes in turbidity.

REFERENCES

(1) Jandt, K. D. "Atomic force microscopy of biomaterials surfaces and interfaces." *Surf. Sci.* 2001**,** *491*, 303-332.

(2) Schuck, P. "Reliable determination of binding affinity and kinetics using surface plasmon resonance biosensors." *Curr. Opin. Biotechnol.* 1997**,** *8*, 498-502.

(3) Schuck, P. "Use of Surface Plasmon Resonance to Probe the equilibrium and dynamic aspects of interactions between biological macromolecules." *Annu. Rev. Biophys. Biomol. Struct.* 1997**,** *26*, 541-566.

(4) Siedlecki, C. A.; Marchant, R. E. "Atomic force microscopy for characterization of the biomaterial interface." *Biomaterials* 1998**,** *19*, 441-454.

(5) Marchant, R. E.; Kang, I.; Sit, P. S.; Zhou, Y.; Todd, B. A.; Eppell, S. J.; Lee, I. "Molecular views and measurements of hemostatic processes using atomic force microscopy." *Current Protein and Peptide Science* 2002**,** *3*, 249-274.

(6) Fisher, T. E.; Oberhauser, A. F.; Carrion-Vazquez, M.; Marszalek, P. E.; Fernandez, J. M. "The study of protein mechanics with the atomic force microscope." *Trends in Biochemical Sciences* 1999**,** *24*, 379-384.

(7) Zlatanova, J.; Lindsay, S. M.; Leuba, S. H. "Single molecule force spectroscopy in biology using the atomic force microscope." *Progress in Biophysics and Molecular Biology* 2000**,** *74*, 37-61.

(8) Santos, N. C.; Castanho, M. A. "An overview of the biophysical applications of atomic force microscopy." *Biophys Chem* 2004**,** *107*, 133-149.

(9) Okumura, N.; Gorkun, O. V.; Lord, S. T. "Severely impaired polymerization of recombinant fibrinogen gamma-364 Asp --> His, the substitution discovered in a heterozygous individual." *J Biol Chem* 1997**,** *272*, 29596-29601.

(10) Yang, Z.; Pandi, L.; Doolittle, R. F. "The crystal structure of fragment double-D from cross-linked lamprey fibrin reveals isopeptide linkages across an unexpected D-D interface." *Biochemistry* 2002**,** *41*, 15610-15617.

(11) Evans-Nguyen, K.; Schoenfisch, M. H. "Fibrin proliferation at model surfaces: Influence of surface properties." *Langmuir* 2005**,** *21*, 1691-1694.

(12) Evans-Nguyen, K. M.; Tolles, L. R.; Gorkun, O. V.; Lord, S. T.; Schoenfisch, M. H. "Interactions of thrombin with fibrinogen adsorbed on methyl-, hydroxyl-, amine, and carboxyl-terminated self-assembled monolayers." *Biochemistry* 2005**,** *44*, 15561-15568.

(13) Sit, P. S.; Marchant, R. E. "Surface-dependent differences in fibrin assembly visualized by atomic force microscopy." *Surf. Sci.* 2001**,** *491*, 421-432.

(14) Wang, H.; Ratner, B., D.; Sage, H. E.; Jiang, S. "Stepwise assembly of fibrin bilayers on self-assembled monolayers of alkanethiolates: influence of surface chemistry." *J Phys Chem C* 2007**,** *111*, 8504-8508.

(15) Litvinov, R. I.; Vilaire, G.; Li, W.; DeGrado, W. F.; Weisel, J. W.; Bennett, J. S. "Activation of individual alphaIIbbeta3 integrin molecules by disruption of transmembrane domain interactions in the absence of clustering." *Biochemistry* 2006**,** *45*, 4957-4964.

(16) Hussain, M. A.; Agnihotri, A.; Siedlecki, C. A. "AFM imaging of ligand binding to platelet integrin alphaIIbbeta3 receptors reconstituted into planar lipid bilayers." *Langmuir* 2005**,** *21*, 6979-6986.

(17) Hussain, M. A.; Siedlecki, C. A. "The platelet integrin alpha(IIb) beta(3) imaged by atomic force microscopy on model surfaces." *Micron* 2004**,** *35*, 565-573.

(18) Endenburg, S. C.; Hantgan, R. R.; Sixma, J. J.; de Groot, P. G.; Zwaginga, J. J. "Platelet adhesion to fibrin(ogen)." *Blood Coagul Fibrinolysis* 1993**,** *4*, 139-142.

(19) Radomski, M. W.; Palmer, R. M. J.; Moncada, S. "The role of nitric oxide and cGMP in platelet adhesion to vascular endothelium." *Biochem. Biophys. Res. Commun.* 1987**,** *148*, 1482-1489.

(20) Shahbazi, T.; Jones, N.; Radomski, M. W.; Moro, M. A.; Gingell, D. "Nitric oxide donors inhibit platelet spreading on surfaces coated with fibrinogen but not with fibronectin." *Thrombosis Research* 1994**,** *75*, 631-642.

(21) Simon, D. I.; Stamler, J. S.; Jaraki, O.; Keaney, J. F.; Osborne, J. A.; Francis, S. A.; Singel, D. J.; Loscalzo, J. "Antiplatelet properties of protein S-nitrosothiols derived from nitric oxide and endothelium-derived relaxing factor." *Arterioscler Thromb* 1993**,** *13*, 791-799.

(22) Gordge, M. P.; Hothersall, J. S.; Noronha-Dutra, A. A. "Evidence for a cyclic GMP-independent mechanism in the anti-platelet action of S-nitrosoglutathione." *Br J Pharmacol* 1998**,** *124*, 141-148.

(23) Radomski, M. W.; Rees, D. D.; Dutra, A.; Moncada, S. "S-nitroso-glutathione inhibits platelet activation in vitro and in vivo." *Br J Pharmacol* 1992**,** *107*, 745-749.

(24) Hartford, O. M.; Wann, E. R.; Hook, M.; Foster, T. J. "Identification of residues in the Staphylococcus aureus fibrinogen-binding MSCRAMM clumping factor A (ClfA) that are important for ligand binding." *J Biol Chem* 2001**,** *276*, 2466-2473.

(25) Arciola, C. R.; Campoccia, D.; Gamberini, S.; Donati, M. E.; Montanaro, L. "Presence of fibrinogen-binding adhesin gene in *Staphylococcus epidermidis* isolates from central venous catheters-associated and orthopaedic implant-associated infections." *Biomaterials* 2004**,** *25*, 4825-4829.

(26) Dobmeier, K. P.; Schoenfisch, M. H. "Antibacterial properties of nitric oxide-releasing sol-gel microarrays." *Biomacromolecules* 2004**,** *5*, 2493-2495.

(27) Hetrick, E. M.; Schoenfisch, M. H. "Reducing implant-related infections: active release strategies." *Chem Soc Rev* 2006**,** *35*, 780-789.

(28) Hetrick, E. M.; Schoenfisch, M. H. "Antibacterial nitric oxide-releasing xerogels: cell viability and parallel plate flow cell adhesion studies." *Biomaterials* 2007**,** *28*, 1948-1956.

(29) Nablo, B. J.; Chen, T. Y.; Schoenfisch, M. H. "Sol-gel derived nitric-oxide releasing materials that reduce bacterial adhesion." *J Am Chem Soc* 2001**,** *123*, 9712-9713.

(30) Nablo, B. J.; Rothrock, A. R.; Schoenfisch, M. H. "Nitric oxide-releasing sol-gels as antibacterial coatings for orthopedic implants." *Biomaterials* 2005**,** *26*, 917-924.

(31) Nablo, B. J.; Schoenfisch, M. H. "Antibacterial properties of nitric oxide-releasing sol-gels." *J Biomed Mater Res A* 2003**,** *67*, 1276-1283.

(32) Charville, G.; Hetrick, E. M.; Geer, C. B.; Schoenfisch, M. H. "Reduced Escherichia coli, Staphylococcus aureus, and Staphylococcus epidermidis adhesion via polymeric nitric oxide release." *In preparation* 2007.